
Influence of repair proteins and chromatin modifiers on mobility of DNA double-strand breaks induced by heavy ion irradiation

Einflüsse von Reparaturproteinen und Chromatinmodifikationen auf die Bewegung von DNA Doppelstrangbrüchen nach Schwerionenbestrahlung

Zur Erlangung des akademischen Grades eines Doctor rerum naturalium genehmigte
Dissertation von Diplom Biologin Linda Carmen Annabelle Becker

Darmstadt, März 2014



TECHNISCHE
UNIVERSITÄT
DARMSTADT



Influence of repair proteins and chromatin modifiers on mobility of DNA double-strand breaks induced by heavy ion irradiation

Einflüsse von Reparaturproteinen und Chromatinmodifikationen auf die Bewegung von DNA Doppelstrangbrüchen nach Schwerionenbestrahlung

Vom Fachbereich Biologie der Technischen Universität Darmstadt

zur

Erlangung des akademischen Grades

eines Doctor rerum naturalium

genehmigte

Dissertation von

Diplom Biologin Linda Carmen Annabelle Becker

aus Darmstadt

1. Referent: Prof. Dr. Marco Durante

2. Referent: Prof. Dr. Gerhard Thiel

Tag der Einreichung: 28.03.2014

Tag der mündlichen Prüfung: 16.05.2014

Darmstadt 2014

D 17

Contents

Abbreviations	1
Summary / Summary in German	2
Publications of this work	6
Motivation	7
1. Introduction	10
1.1. Physical properties of ionizing radiation.....	10
1.2. Biological effects of ionizing radiation.....	14
1.3. Chromatin organization in the context of DNA damage.....	16
1.4. DNA repair factors and pathways	17
1.5. Nuclear matrix – Composition and cellular function	24
2. Material and methods	27
2.1. Cellular and biochemical methods.....	27
2.1.1. Cell culture and cell lines	27
2.1.2. siRNA mediated knockdowns	27
2.1.3. Cell lysates and western blot analyses	28
2.1.4. Protein inhibition	28
2.1.5. Nuclear matrix extraction	29
2.2. Irradiation with x-rays and heavy ions.....	29
2.3. Microscopy and mobility analyses	30
2.3.1. Immunofluorescence microscopy	30
2.3.2. Live cell microscopy	32
2.3.3. Analyses of IRIF mobility	32
3. Results	34
3.1. Mobility of DSBs after heavy ion irradiation	34
3.2. Mobility characteristics of DSBs after X-ray and heavy ion irradiation	39
3.2.1. Experimental setup	39
3.2.2. Mobility of 53BP1 and NBS1 foci after X-ray irradiation	42
3.2.3. Dynamic behavior of IRIF	43
3.2.4. Depletion of ATP	46

3.3.	Poly-ADP-ribosylation and the chromatin remodeler ACF1	47
3.3.1.	ACF1 does not influence chromatin mobility	47
3.3.2.	Chromatin mobility is not altered by poly-ADP-ribosylation	48
3.4.	Inhibition of ATM confines mobility of broken chromatin sites	50
3.4.1.	ATM alters mobility of high LET induced DSBs	50
3.4.2.	Effect of ATM inhibition after X-ray irradiation	53
3.5.	Tethering of DNA strands by Cohesin or the MRN complex	54
3.5.1.	Cell cycle analyses	56
3.6.	Interplay between nuclear matrix proteins and IRIF mobility	58
3.7.	Nuclear matrix interactions with repair proteins	60
4.	Discussion	66
4.1.	Characteristics of DSB mobility	67
4.2.	Role of repair proteins and chromatin modifiers on DSB mobility.....	69
4.2.1.	Chromatin modifications	69
4.2.2.	Tethering of DNA strands	71
4.2.3.	Repair proteins Ku80 and ATM	74
4.3.	Interactions between the nuclear matrix and DSBs.....	78
4.3.1.	Nuclear matrix proteins influence DSB mobility	78
4.3.2.	Nuclear extractions reveal interactions of repair proteins with the nuclear matrix	80
5.	Conclusions and outlook	83
	Bibliography	84
	Appendix	I
	Supplementary Figures.....	I
	List of Figures	I
	List of Tables.....	II
	Danksagung	III
	Lebenslauf.....	IV
	Ehrenwörtliche Erklärung	V

Abbreviations

53BP1 (p53-binding protein 1)
ACF1 (ATP-dependent chromatin assembly factor)
ATM (ataxia telangiectasia mutated protein)
ATP (adenosine triphosphate)
ATR (ataxia telangiectasia and Rad3-related protein)
DNA-PK (DNA-dependent protein kinase)
DSB (double strand break)
GFP (green fluorescent protein)
Gy (gray)
hnRNPs (heterogeneous nuclear ribonucleoproteins)
HR (homologous recombination)
IRIF (ionizing radiation induced foci)
kd (knockdown)
LET (linear energy transfer)
MAR (matrix attachment region)
MDC1 (Mediator of DNA damage checkpoint protein 1)
MEF (mouse embryonic fibroblasts)
MRE11 (meiotic recombination 11 homolog)
MSD (mean square displacement)
NBS1 (nijmegen breakage syndrome 1)
NHEJ (non homologous end joining)
NIPBL (nipped-B like protein)
NuMA (nuclear mitotic apparatus protein)
PAR (poly-ADP-ribose)
PARG (poly-ADP-ribose glycohydrolase)
PARP (poly-ADP-ribose polymerase)
PFA (paraformaldehyde)
RPA (replication protein A)
siRNA (small interfering ribonucleic acid)
SMC1 (structural maintenance of chromosomes protein 1)
SSB (single strand break)
U2OS (human osteosarcoma cell line)

Summary / Summary in German

Ionizing radiation induces DNA double strand breaks (DSBs) in cell nuclei which represent the most dangerous type of DNA lesions. Through error prone repair mechanisms they can lead to the formation of chromosome rearrangements, favoring genomic instability and the development of cancer. Movement of DSBs and surrounding chromatin domains is expected to influence DSB repair and promote the formation of chromosomal translocations. Addressing this expectation, DSB mobility was analyzed after heavy ion irradiation. To gain insight into influences of chromatin organization and repair related factors on the dynamic behavior of DSB sites, knockdown or inhibition of repair proteins and chromatin modifying proteins was used. Occurring changes in irradiation induced foci (IRIF) mobility were examined either by immunofluorescent analysis of fixed samples or by live cell microscopy.

Different mammalian cell lines deficient for the repair proteins Ku80, ATM and RAD50 were irradiated with charged particles under a low angle to induce DSBs in a linear track which can then be visualized by the accumulation of repair proteins. The dispersion of distinct focal accumulations of repair proteins was determined in fixed samples over time points up to 18 hours. No spreading of repair proteins from the linear track, exceeding a distance of 1 or 2 μm could be observed in all cell lines. These studies confirmed published results of a high positional stability of DSBs in mammalian nuclei and moreover showed an independency of mobility on those repair proteins on a μm scale.

To visualize changes in DSB mobility on a sub-micron range confocal live cell microscopy was applied. Human U2OS cells stably expressing 53BP1-GFP as a surrogate marker of DSBs were used. DSB mobility was expected to be influenced by a local decondensation of surrounding chromatin. Therefore advantage was taken from low angle charged particle irradiation, known to trigger a pronounced chromatin decondensation together with the induction of multiple complex DSBs in a μm range, depending on the linear energy transfer (LET) of the used ion. Tracking of IRIF was performed over two hours determining a diffusional mobility of DSB containing chromatin in a range below 1 μm per hour. Diffusion kinetics could be described by models of subdiffusion or confined diffusion.

Depletion of ATP, the main source of energy in a cell system, was shown to reduce the observed foci mobility around 65 %. The results validate the chosen setup to determine small scale changes in DSB mobility by disturbances in the cellular system. Moreover, a strong energy dependence of chromatin mobility was shown. Knockdown studies were used to determine the influence of chromatin modifying proteins like the chromatin remodeler ACF1 which acts in the DNA damage response. No influence on mobility was observed by knockdown of ACF1. Furthermore, influences of poly-ADP-ribosylation, mediated by PARP and degraded by PARG were determined. Poly-ADP-ribosylation is known to be involved in several DSB dependent signaling cascades, leading to a local decondensation. Mobility of DSBs was found to be unchanged by knockdown or inhibition of either PARP or PARG. It can be

expected that the chromatin structure in the surrounding of DSBs is altered only in the range of a few nucleosomes (composing few nm) but that these changes do not influence mobility of DSB in a sub-micron range as observed by this system.

Inhibition of ATM, a key component of DSB induced signaling cascades, resulted in a pronounced confinement of DSB mobility reducing the sampled volume of foci around 3 fold from $\sim 5 \mu\text{m}^3$ in controls to $\sim 1.5 \mu\text{m}^3$. This confinement following ATM inhibition was confirmed using X-rays, proving that the effect is not LET dependent and not restricted to densely ionizing radiation. It will be difficult to pinpoint the applied mechanism as ATM phosphorylates several hundreds of substrates but it might be attributed to a diminished radiation induced decondensation as ATM is known to act in decondensation of heterochromatic areas by phosphorylation of Kap1.

Tethering of broken DNA ends at the break site as well as connections with further DNA strands by Cohesin or the MRN complex were expected to stabilize DSBs. However, knockdown of MRE11, an essential component of the MRN complex, as well as diminishing the Cohesin complex by knockdown of SMC1 or NIPBL, the loading factor which mediates an interaction between Cohesin and DNA, did not change kinetics of DSB mobility. This implies an independency of DSB mobility on DNA tethering complexes in the observed spatial scale. As the Cohesin complex is known to act in sister chromatid cohesion of HR repair during S and G2 phase, a U2OS cell line expressing a cell cycle marker was used to determine variations in mobility dependent of the cell cycle phase. Statistics need to be improved but preliminary results marked a trend of an enhanced mobility in G2 compared to S/G1 phase in controls but no differences in mobility regarding the cell cycle phase were obtained in cells diminished of the Cohesin complex.

Knockdown of the nuclear matrix protein NuMA enhanced DSB mobility and an even stronger increase in mobility (72 %) was seen after knockdown of Lamin A/C, the main structural components of the nuclear matrix and lamina. Anchoring sites of the nuclear matrix for chromatin and DNA as well as a matrix mediated structural organization of the nucleus are thought to act in stabilizing chromatin. It needs to be determined if an enhanced DSB mobility arises from a nuclear wide enhancement of chromatin mobility or is restricted to DSBs. To investigate interactions between the nuclear matrix and repair proteins at sites of DSBs nuclear extractions were performed. The extraction removes DNA, soluble proteins and chromatin from the cell nucleus, revealing proteins bound to the structural components of the nuclear matrix. Immunofluorescent staining of repair proteins after X-ray irradiation indicated the extraction of most repair proteins. However, MRE11 foci persist in the nucleus, pointing to a direct interaction with nuclear matrix proteins.

This study discovered that DSB mobility can be enhanced or restricted by loss of single proteins like ATM or Lamin A/C and future experiments will further investigate the interplay between DSB mobility, repair related proteins and the nuclear matrix, addressing possible relations of mobility to repair defects and the formation of chromosome rearrangements.

Zusammenfassung

Durch ionisierende Strahlung entstehen DNA Doppelstrangbrüche (DSB) im Zellkern, die den gefährlichsten Typ von DNA Schäden darstellen. Durch fehlerbehaftete Reparaturmechanismen können sie zu Chromosomenaustauschen führen, die genomische Instabilität und die Entstehung von Krebs zur Folge haben können. Es wird angenommen, dass die Bewegung der DSB und der darum liegenden Chromatindomänen die Reparatur beeinflusst und die Entstehung von chromosomalen Translokationen begünstigt. Um diese Vermutung zu überprüfen wurde die Mobilität von DSB nach Schwerionenbestrahlung untersucht. Zur Analyse, wie Reparaturproteine oder die Struktur von Chromatin sich auf die Bewegung von DSB auswirken, wurden Reparaturproteine und Chromatin modifizierende Proteine genetisch herunterreguliert oder inhibiert. Resultierende Änderungen der DSB Bewegung wurden durch Immunfluoreszenz Analysen in fixierten Zellen und durch Lebendzellmikroskopie bestimmt.

Unterschiedliche Säuger-Zelllinien denen Reparaturproteine wie Ku80, ATM oder RAD50 fehlen, wurden mit Schwerionen unter einem niedrigen Winkel bestrahlt, wodurch DSB entlang einer linearen Spur erzeugt werden. Durch Bindung von Reparaturproteinen in Form von „Foci“ können diese anschließend sichtbar gemacht werden. Die lineare Anordnung der DSB wurde in fixierten Proben über einen Zeitraum von 18 Stunden beobachtet wobei keine Ausbreitung von DSB beobachtet werden konnte die über eine Distanz von 1 bis 2 μm hinausging. Damit konnte eine hohe positionsbezogene Stabilität von DSB bestätigt werden die unabhängig der erwähnten Reparaturproteine ist.

Mit Hilfe von konfokaler Lebendzellmikroskopie konnten Änderungen der DSB Mobilität in einem Sub-Mikrometer Bereich analysiert werden. Stabil in humane U2OS Zellen transfiziertes 53BP1-GFP agierte dabei als DSB Marker. Die Bestrahlung mit Schwerionen induziert viele komplexe DSB innerhalb weniger μm und ruft eine starke Dekondensation hervor, die die DSB Mobilität beeinflussen könnte. Über einen Zeitraum von zwei Stunden wurde die Bewegung der DSB analysiert und eine Diffusionsbewegung im Bereich von $<1 \mu\text{m}$ pro Stunde festgestellt. Die Diffusionsbewegung konnte durch Modelle von Subdiffusion oder Eingeschränkter Diffusion (confined diffusion) beschrieben werden. Eine Verminderung des ATP Levels, dem Haupt-Energielieferanten der Zelle, verringerte die DSB Mobilität um 65 %. Dieses Ergebnis zeigt, dass der Experimentaufbau minimale Änderungen in der Bewegung von DSB, die durch Störungen der Zellintegrität hervorgerufen werden, sichtbar machen kann. Zudem zeigt das Ergebnis eine starke Energieabhängigkeit der Chromatin Bewegung. Der Einfluss von Chromatin modifizierenden Proteinen wie dem Chromatin „Remodeler“ ACF1, der in der Schadensantwort nach DSB Induktion wirkt, wurde mittels „Protein Knockdown“ untersucht. Herunterregulierung des Proteins hatte keine Auswirkungen auf die DSB Mobilität. Weitere die Chromatinstruktur beeinflussende Effekte, wie die Poly-ADP-Ribosylierung durch PARP, wurden untersucht. Poly-ADP-Ribosylierung führt über Signalkaskaden ebenfalls zu einer lokalen

Dekondensation und wird anschließend durch PARG abgebaut. Die Mobilität von DSB blieb unverändert nach jeweiligem Knockdown oder Inhibition von PARP und PARG. Erwartete Strukturveränderungen könnten möglicherweise im Bereich von nur wenigen Nukleosomen (wenige nm) liegen, und damit keinen Einfluss auf DSB Mobilität im gemessenen submikrometer Bereich ausüben.

Inhibition von ATM, hauptverantwortlich für die Signalweiterleitung als Schadensantwort, verursachte eine starke Einschränkung der Mobilität. Dadurch würde das Volumen in dem sich ein Focus bewegt um das dreifache gesenkt werden von $\sim 5 \mu\text{m}^3$ in Kontroll-Zellen auf $\sim 1.5 \mu\text{m}^3$. Eine reduzierte Bewegung nach ATM Inhibition wurde auch nach Röntgenbestrahlung bestätigt, wodurch eine LET-Abhängigkeit ausgeschlossen werden konnte. Den verantwortlichen Mechanismus zu erfassen ist schwierig, da ATM mehrere hundert Proteine phosphoryliert. Jedoch könnte der Effekt auf einer reduzierten Dekondensation beruhen, da bekannt ist, dass ATM über Phosphorylierung von Kap1 eine Dekondensation heterochromatischer Bereiche bewirkt.

Der Verbindung von DNA Strängen durch den Cohesin oder MRN Komplex wird eine Stabilisierung von DSB zugeschrieben. Stränge können direkt durch Überbrückung der DNA Enden stabilisiert werden oder durch Vernetzungen mit anderen DNA Strängen zusammen gehalten werden. Herunterregulierung von MRE11, einer essentiellen Komponente des MRN Komplexes oder von Komponenten des Cohesin Komplexes wie SMC1 oder NIPBL, hatte keine Auswirkungen auf die DSB Mobilität. Diese scheint unabhängig von dieser Art der Verknüpfungen von DNA Strängen zu fungieren. Da Cohesin während der Homologen Rekombination in der S und G2 Phase Schwesterchromatide zusammenhält, wurde eine Zellzyklusabhängigkeit der Mobilität untersucht. Dazu wurde eine Zelllinie mit integriertem Zellzyklusmarker verwendet. In ersten Ergebnissen, die durch weitere Experimente bestätigt werden müssen, war ein Trend erkennbar, dass generell die DSB Mobilität in der G2 Phase gegenüber der S/G1 Phase erhöht ist. In Zellen bei denen der Cohesin Komplex nicht funktional ist wurde jedoch keine Abhängigkeit vom Zellzyklus festgestellt.

Die Herunterregulierung des Kernmatrix Proteins NuMA erhöhte die Mobilität von DSB. Einen noch größeren Anstieg der Mobilität (72 %) erzeugte der Knockdown von Lamin A/C, den Hauptkomponenten der Kernmatrix und nuklearen Lamina. Um genauere Interaktionen zwischen Kernmatrix- und Reparaturproteinen zu untersuchen wurden Zellen extrahiert. Diese „Nukleare Extraktion“ entfernt DNA, lösliche Proteine und Chromatin aus dem Zellkern und setzt die Kernmatrix frei. Durch Immunfluoreszenzfärbung von Reparaturproteinen nach Röntgenbestrahlung konnte die Extraktion der meisten Reparaturproteine beobachtet werden. MRE11 hingegen blieb in Form von Foci im Kern bestehen. Dieses deutet auf eine direkte Bindung von MRE11 an Kernproteine hin.

In dieser Arbeit konnte eine Abhängigkeit der DSB Mobilität von einzelnen Proteinen, wie ATM oder Lamin A/C gezeigt werden und zukünftige Experimente sollen das Zusammenspiel von DSB Bewegung, Reparaturproteinen und der Kernmatrix in Bezug auf die Ausbildung chromosomaler Translokationen und anderen Reparaturdefekten genauer untersuchen.

Publications of this work

Publications

A. Becker, M. Durante, G. Taucher-Scholz, B. Jakob (2014)
„ATM Alters the Otherwise Robust Chromatin Mobility at Sites of DNA Double-Strand Breaks (DSBs) in Human Cells”
PloS One 9(3): e92640

A. Becker, B. Jakob, R. Khan, A. L. Leifke, G. Becker, M. Durante, G. Taucher-Scholz (2012)
“Influence of the chromatin remodeler ACF1 on the dynamic behaviour of 53BP1 foci after heavy ion irradiation”
GSI Scientific Report (2012) S. 430

A. Becker, B. Jakob, A.L. Leifke, G. Becker, M. Durante and G. Taucher-Scholz (2011)
„Influence of PARP on irradiation induced foci dynamics”
GSI Scientific Report (2011) S. 495

Conference contributions

A. Becker, M. Durante, G. Taucher-Scholz, B. Jakob (2013)
“Influence of DNA repair proteins on DSB mobility after high LET irradiation.” Poster presentation
EMBO meeting Nuclear Structure and Dynamics, France

A. Becker, M. Durante, G. Taucher-Scholz, B. Jakob (2013)
“Mobility of DSB containing chromatin domains after high LET irradiation.” Poster presentation
16th Annual GBS Meeting, Germany

A. Becker, M. Durante, G. Taucher-Scholz, B. Jakob (2013)
“Characteristics of the dynamic behavior of radiation induced foci after high LET irradiation.” Poster presentation
Heavy ion in Therapy and Space Radiation Symposium (HITSRS), Japan

A. Becker, M. Durante, G. Taucher-Scholz, B. Jakob (2012)
“Influence of repair proteins on the dynamic behavior of radiation induced foci after high LET irradiation.” Oral presentation.
12th Biennial DGDR Meeting / 15th Annual GBS Meeting, Germany

A. Becker, M. Durante, G. Taucher-Scholz, B. Jakob (2011)
“Influence of poly-ADP ribosylation and protein kinases on the dynamic behavior of radiation induced foci after high LET radiation.” Poster presentation
12th international workshop on radiation damage to DNA, Czech Republic

Motivation

The organization of DNA and proteins in chromatin and its dynamics affect many biological processes like cell division, gene regulation or DNA repair. The regulation of various cellular functions, mediated by structural changes in chromatin represents a hot topic in a variety of biological studies. In the context of DNA damage repair chromatin organization as well as damage induced modifications can influence repair processes and repair kinetics are strongly dependent on chromatin compaction (Goodarzi et al., 2008; Shi and Oberdoerffer, 2012).

DNA double strand breaks (DSBs) represent one of the most dangerous types of DNA lesions. They arise from natural cellular processes as well as from external damaging agents like ionizing radiation. Upon induction of DSBs a complex signal cascade leads to the recruitment of repair factors and mediator proteins. The damage response includes chromatin alterations surrounding the break sites, regulation of cell cycle arrest or as a last consequence the induction of apoptosis (Lukas et al., 2011b; Sulli et al., 2012). Repair of DSBs is essential for cell survival and failure or incorrect repair can lead to genomic instability and the development of cancer.

Homologous recombination (HR) and non homologous end joining (NHEJ) are two major classical pathways of DSB repair. Whereas in HR DSBs are repaired by the use of an undamaged homologous sequence as a template, in NHEJ a ligation of broken DNA ends takes place. Especially if multiple breaks are present, NHEJ can lead to the formation of chromosome exchanges. It is yet unclear what promotes the choice for DSB ends to be joined, but proximity and mobility of the ends are considered to play an important role (Dion and Gasser, 2013). In yeast an aimed movement of individual DSBs can be observed as DSBs move to the nuclear periphery and form repair centers in order to be repaired (Lisby et al., 2003; Nagai et al., 2008; Oza et al., 2009). Moreover, a general enhanced chromosome mobility was observed after ionizing radiation, enlarging the roaming volume of DSBs. This enhanced mobility is expected to facilitate homology search as HR is the predominant pathway of repair in budding yeast (Miné-Hattab and Rothstein, 2012).

In mammalian cells early investigations found a Brownian movement of chromatin in living cells (Marshall et al., 1997). More recent work confirmed a diffusion on a small spatial scale and point out a relatively stable position of DSB containing chromatin domains (Girst et al., 2013; Jakob et al., 2009a; Soutoglou et al., 2007). In this context however movement of chromatin was found to be slightly enhanced by the induction of DSBs and a local expansion of chromatin is seen after DNA damage (Falk et al., 2007; Krawczyk et al., 2012; Kruhlak et al., 2006). This local decondensation of chromatin was observed in the vicinity of DSBs induced by X-rays (Falk et al., 2007) and even more pronounced after charged particle irradiation (Jakob et al., 2011; Müller et al., 2013) and might contribute to the enhanced mobility of broken chromatin.

Analyzing dynamics of individual break ends, induced by restriction enzymes, revealed a dependency on Ku80 to the ability of break ends to locally diffuse (Soutoglou et al., 2007). In a study on uncapped telomeres further influences of repair proteins on chromatin mobility were shown. Uncapped telomeres represent a very special form of damage that can be considered a sort of one ended DSB and is processed accordingly (De Lange, 2005). A reduction in mobility of uncapped telomeres could be observed in 53BP1 and ATM deficient cells compared to controls (Dimitrova et al., 2008). So far not much is known about the physiological consequences or factors involved in radiation induced chromatin dynamics.

Mobility of DSBs is considered to influence the frequency of chromosome rearrangements, especially in the context of multiple DSBs in close proximity as induced by densely ionizing charged particles, used for example in cancer treatment, creating a potentially important factor in carcinogenesis.

This study therefore addresses the role of repair factors and chromatin modifiers on mobility of DSB containing chromatin domains. System of choice for analyses of mobility was a live cell approach with human U2OS cells, expressing fluorescently tagged repair proteins. SiRNA mediated knockdown or inhibition of repair proteins or chromatin modifying proteins was used to elucidate influences on DSB mobility. For induction of DSBs advantage could be taken from the local dose deposition of low energy charged particles generated at the heavy ion accelerator facility of GSI (Helmholtzzentrum für Schwerionenforschung). Substantial local decondensation as well as a high number of complex DSBs in close proximity can be expected by this type of irradiation. By irradiation in a low angle, DSBs can be visualized along the ion traversals of nuclei and mobility of DSBs can be tracked over several hours (Jakob et al., 2003, 2009b).

Parts of the findings of this PhD thesis and according figures are published in (Becker et al., 2014).

1. Introduction

1.1. Physical properties of ionizing radiation

Ionizing radiation is a form of radiation that carries enough energy to interact with an atom or molecule and thereby liberate tightly bound electrons from the outer shell, causing the atom to become positively charged (ionized). The characteristic of this ionization process is the local release of a large amount of energy. Covalent bonds can be broken by the ionization process, leading to a disintegration of molecules like DNA thus potentially creating severe biological damage. Moreover, ions and electrons are produced which can lead to subsequent interaction processes creating further damage. A more detailed overview about ionizing radiation and particle interactions with matter can be found e.g. in (Alpen, 1990; Hall and Giaccia, 2006; Stabin, 2007a).

The energy deposited in matter is termed the dose (D). It is defined as the mean absorbed energy (ΔE_{abs}) per mass unit (Δm) with the unit Gray (Gy).

$$D = \frac{\Delta E_{abs}}{\Delta m} \left[Gy = \frac{J}{kg} \right] \quad (\text{eq.1})$$

Ionizing radiation can be divided into sparsely ionizing radiation like photon irradiation (X-rays or gamma rays) and densely ionizing radiation like particle irradiation (neutrons, alpha particles or heavy ions).

Photon radiation is a form of electromagnetic radiation and mainly indirectly ionizing. Through interaction processes of photons and matter electrons are released which can induce chemical and biological damage to molecules by secondary ionizations. Photons do not contain any mass or electric charge. Their energy is dependent on their wavelength λ or frequency ν by

$$E = h\nu = \frac{hc}{\lambda} \quad (\text{eq.2})$$

h being the Planck constant and c the speed of light.

The interaction processes of photons with matter (Figure 1) are depending on their energy. At energies below 60 keV the photoelectric effect is the most common interaction. At higher energies the Compton Effect becomes more likely until the pair production predominates at energies higher than 10 MeV. By the photoelectric effect the complete energy of the photon is transferred to the electron which is then released from the atom. In contrast, by the Compton Effect a photon with high energy is scattered at

an electron and transfers only part of its energy onto the electron which gets released from the atom. Due to the loss of energy the photon is redirected from its original trajectory with a higher wavelength so that the overall energy and momentum of the system is conserved. The scattered photon can then interact with further electrons. Pair production only takes place at high energies. In this process an initial energy exceeding 1.02 MeV is needed (twice the rest energy of an electron) as the photon is converted into an electron and a positron.

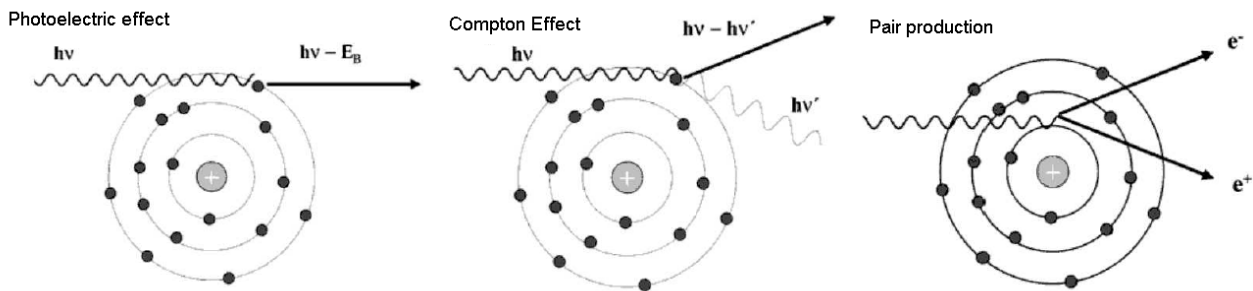


Figure 1 – Physical interaction processes of photons with matter.

$h\nu$ = energy of the photon, represented by sinuous lines, E_B = binding energy of the electron, $h\nu'$ = photon energy after interaction, e^- = electron, e^+ = positron. Solid line represents the track of electrons. Figure according to (Kiefer and Kiefer, 2003).

Electrons which are released from the atom by the processes described above can further interact with matter and if the energy is high enough also induce ionization events. X-rays and γ -rays are commonly used photons in radiation biology and differ only in their origin not in its physical properties. In sparsely ionizing radiation, ionization events are evenly distributed on a μm scale whereas by densely ionizing radiation, like heavy ions or low energy protons, atoms and molecules are mostly ionized locally along the ion track. Protons, neutrons and heavy ion charged particles are an important component of space radiation and exhibit drastic damage to DNA.

The dose deposition decreases from the center of the ion track proportionally to the square of the radius ($1/r^2$). For the same applied dose, the dose distribution pattern in matter differs for photons and charged particles and is moreover dependent on the energy of the ion (Figure 2).

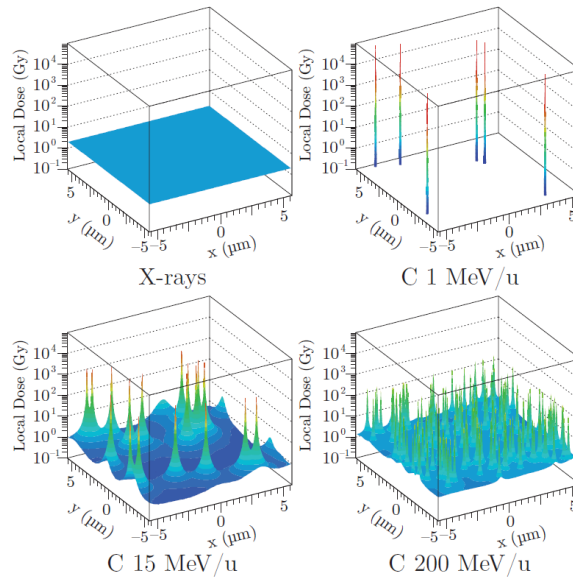


Figure 2 – Dose distribution of X-rays and carbon ions of different energies.

A mean dose of 2 Gy is deposited in each scheme. Whereas for X-rays a homogenous dose distribution can be observed, carbon ions deposit energy locally around the ion track. The dose maximum decreases with increasing energy and a higher fluence of particles is needed to reach the same dose of 2 Gy at higher energies (Scholz, 2003).

The path length of an ion in matter is dependent on its energy. For high energy charged particles like heavy ions, many interactions are necessary to stop the particle. Each interaction leads to a deposition of energy and the velocity of the particle is decreased. The most common interaction process is electronic stopping through inelastic Coulomb interactions. The majority of the energy loss is usually through δ -electrons which are released by interactions of atoms with the particle. Most δ -electrons have a low energy and therefore deposit their energy within a few nanometers surrounding the primary ion thus creating a highly localized dose deposition along the ion track. The deposited energy E per path length x is defined as the linear energy transfer (LET) which is proportional to the square of the effective particle charge Z_{eff} and its relativistic velocity $\beta = v/c$ (Bethe, 1930; Bloch, 1930).

$$LET = \frac{dE}{dx} \propto \frac{Z_{\text{eff}}^2}{\beta^2} \quad (\text{eq.3})$$

The interactions are dependent on the velocity of the particle. When high energy charged particles enter matter they interact rarely while the interactions increase with reduced velocity and energy. The reduced velocity after energy deposition enables a longer subsequent interaction and thus greater energy deposition. After a certain distance within the medium a drastic reduction of velocity and ion energy is observed leading to a strong increase of the LET until the point of maximum dose deposition,

termed the *Bragg-peak* (Figure 3). At the end of the track the particle starts to pick up electrons whereby the effective charge decreases and the particle stops. The location of the sharp peak of energy deposition is dependent on the energy of the ion, as ions with higher energy can penetrate further until the final loss of energy (Figure 3).

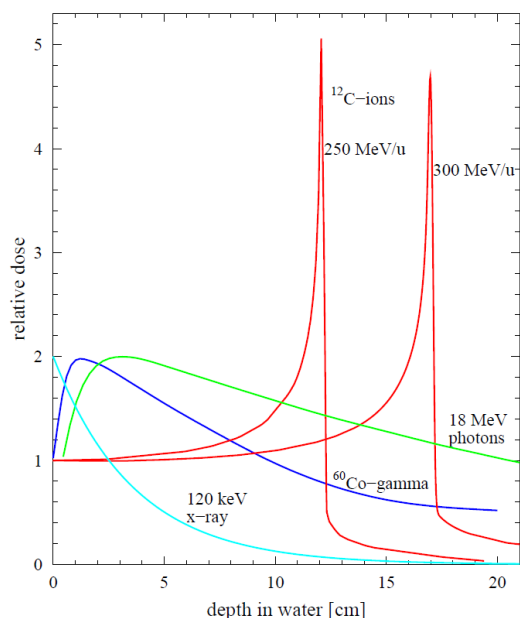


Figure 3 – Depth dose profiles of particles and photon irradiation at different energies in water.

Heavy ions like carbon show an enhanced dose deposition at the end of its track, the so called Bragg-Peak whose depth is dependent on the ion energy. Photons exhibit a shallow peak followed by exponential decrease of energy deposition in matter (Kraft, 2008).

Charged particles with different energies are used in cancer radiotherapy to achieve a dose deposition in the desired depth. Normal tissue at the entrance site of the ion can be spared due to low energy deposition and the maximum dose deposited at the Bragg-peak can be located to the tumor inside the body.

The dose which is deposited in matter by charged particles depends on the LET, the fluence F of particles and the density ρ of the target material. As biological material like cells or tissue consists mostly of water, the density of water is typically used for dose calculations.

$$D(\text{Gy}) = 1.602 * 10^{-9} \left(\frac{\mu\text{m} \cdot \text{g} \cdot \text{J}}{\text{keV} \cdot \text{cm} \cdot \text{kg}} \right) * F \left(\frac{1}{\text{cm}^2} \right) * LET \left(\frac{\text{keV}}{\mu\text{m}} \right) * \frac{1}{\rho} \left(\frac{\text{cm}^3}{\text{g}} \right) \quad (\text{eq. 4})$$

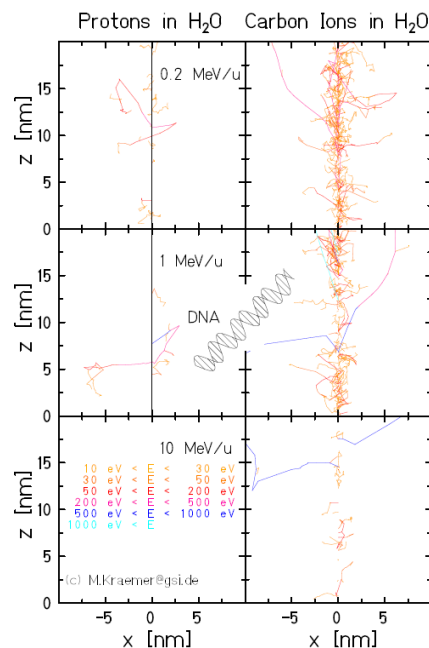
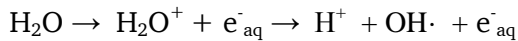


Figure 4 – Track structures of protons and carbon ions of different energies in water.

Simulations of ions in matter show that at lower energies more δ -electrons are produced, enhancing the density of ionization events around the ion traversal. A sketch of the DNA provides a comparison of size. (Image courtesy of M. Krämer, GSI.)

1.2. Biological effects of ionizing radiation

Ionizing radiation causes atoms and molecules to become ionized which can break or modulate chemical bonds between molecules like the DNA or proteins. As the cell consists mostly of water, it leads moreover to the production of highly reactive free radicals ($O_2\cdot$, H_2O^+ , $OH\cdot$) through a dissociation of water molecules:



Free radical species and hydrated electrons undergo further reactions with each other and molecules creating a large variety of radical species and by-products with a longer lifetime like H_2O_2 that can possibly damage DNA. The time window of the initial ionization process is 10^{-15} s and radicals mostly have a lifetime of $\sim 10^{-10}$ s to 10^{-5} seconds. While ionization processes of electrons can damage DNA directly the induction of secondary damages by radicals is conferred to as an indirect action of ionizing radiation (Figure 5) and further information of both processes can be found in (Hall and Giaccia, 2006; Stabin, 2007b).

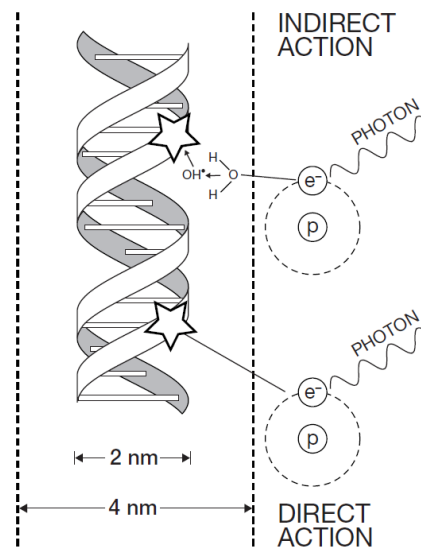


Figure 5 – Direct and indirect effects of ionizing radiation on DNA

Photons can directly interact with target material like DNA or molecules and induce ionizations or excitations which can alter the biological integrity. Indirect damage is created when a photon interacts with other molecules in the cell, like water, and creates reactive radicals which then damage the DNA (Hall and Giaccia, 2006).

In biological systems the DNA is the most critical target for radiation as it contains the genetic code for cell survival and proliferation and is needed for cell integrity. Damaged proteins or RNA on the other hand are available in multiple copies in a cell and undergo a turnover where they can be replaced.

Ionizing radiation can produce a variety of damage to DNA strands like base damage, single strand breaks (SSBs) or double strand breaks (DSBs) where the latter are the most critical for cell survival. To keep their integrity cells have evolved several mechanisms to repair DNA damage.

Ionizing radiation effects on DNA vary with irradiation quality and LET (Asaithamby and Chen, 2011; Hirayama et al., 2009). In photon irradiation around 70% of DNA damage comes from indirect reactions thus mostly leading to SSB induction and base damage. In contrast, high LET radiation creates a large amount (around 80 %) of direct damage and due to the physical properties of charged particles many clustered DSBs are produced in close proximity.

The biological effectiveness of irradiation can be compared by cell survival assays. Irradiated with the same dose cells show a higher survival rate after X-ray irradiation compared to high LET irradiation (Figure 6). A quantitative parameter to describe the biological effect of different radiation qualities is the relative biological effectiveness (RBE). It is defined as the ratio between the dose of a reference radiation (D_{ref}) (mostly X-rays) and the dose of an irradiation to be tested (D_{test}) that yields the same biological effect (isoeffect).

$$RBE_{iso} = \frac{D_{ref}}{D_{test}} \quad (\text{eq. 5})$$

In survival studies a RBE of >1 would result from a higher efficiency in cell killing for the test irradiation, in case of Figure 6 carbon ions, compared to X-rays. However, for cell survival the RBE depends on many parameters like dose, LET, cell type, fractionation or oxygen level (Alpen, 1990).

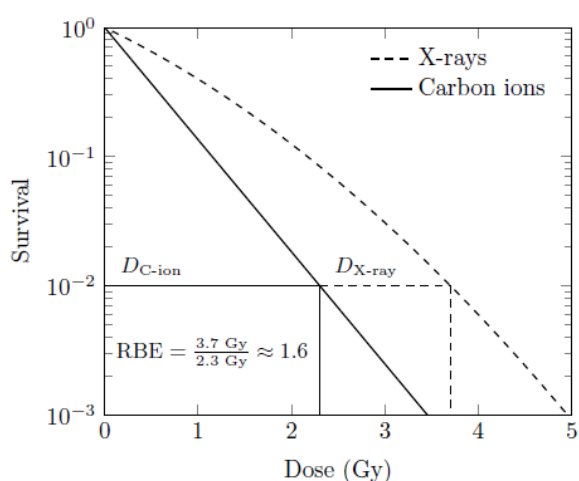


Figure 6 – RBE measurement of carbon ions compared to X-rays

Cell survival after irradiation with X-rays and carbon ions of different doses is plotted and the RBE for cell survival is calculated. Modified from (Schardt et al., 2010).

Densely ionizing particles like heavy ions typically have a higher RBE than X-rays and show a more linear survival curve compared to the linear quadratic curve of sparsely ionizing irradiation like X-rays. The linear quadratic model of the survival (S) consists of a linear term (α) and a quadratic term (β) and describes the survival at a given dose (D) (Hall and Giaccia, 2006).

$$S = e^{-\alpha D - \beta D^2} \quad (\text{eq. 6})$$

The linear term describes the initial slope which follows an exponential decrease as seen for densely ionizing radiation. The quadratic term accounts for the bending of the curve and is dependent on the repair capability of cells. The idea of the model evolved following results of chromosome aberration studies. Induced DSB can be repaired incorrectly (described in more detail in the following section) and result in chromosome exchanges like dicentric chromosomes which are lethal for the cell. The probability of those exchanges was found to be proportional to the square of the dose.

Models of the linear quadratic term consider that the linear term comes from single lethal events which rise proportional to the dose while in the quadratic term two lesions are needed to produce a lethal damage. DNA repair deficient cell lines and irradiation with densely ionizing radiation both enhance the quadratic term of cell survival. The α/β ratio describes the dose at which linear and quadratic components of cell killing are equal. It represents an important quantity in radiotherapy to determine the radio-sensitivity of a tissue type. Due to their physical and biological properties, leading to increased cell killing abilities, heavy ions have proven to be an effective tool for radiotherapy (Durante and Loeffler, 2010; Fowler, 1989).

1.3. Chromatin organization in the context of DNA damage

DNA in eukaryotic cells is highly organized. It is associated with proteins, mostly histones, building a highly structured nucleoprotein complex called chromatin. Chromatin structure and DNA packing regulate a number of essential cellular processes like transcription, cell division, differentiation or DNA repair (Woodcock and Ghosh, 2010).

One main unit of the chromatin is the nucleosome, an octameric complex consisting of two molecules of each of the core histones H2A, H2B, H3 and H4 (Luger et al., 1997). 146 bp of DNA is wrapped around the nucleosome in approximately 1.7 turns. A DNA linker sequence of variable length between each nucleosome connects the nucleosomes to a “beads on a string” conformation (Olins and Olins, 1974). For higher compaction the nucleosomes are then packed into chromatin fibers of 10 nm, 30 nm or higher order structures. The most condensed state of chromatin is found during mitosis or meiosis

when the individual chromosomes become visible. Packing density of chromatin is variable and in interphase it can be divided into two main groups, the densely packed heterochromatin which contains a low gene density and the more open, transcriptionally active chromatin areas of the euchromatin which constitute around 75 % of the mammalian chromatin (Xu and Price, 2011). Alterations in packing density are mediated by linker length, histone variants and posttranscriptional modifications like acetylation, phosphorylation or methylation. Those modifications lead to the recruitment of chromatin remodeling enzymes which act in nucleosome sliding, ejection or restructuring to control condensation and relaxation of chromatin (Clapier and Cairns, 2009).

One of the best described radiation induced chromatin modifications is phosphorylation of the histone H2AX (a subtype of H2A) at serin 139 (Rogakou et al., 1999). Referred to as γ H2AX, it serves as a reliable DSB marker (Rothkamm and Löbrich, 2003) and acts in the recruitment of repair proteins and checkpoint control (Rothkamm and Horn, 2009).

Upon induction of DSBs, posttranscriptional protein modifications like methylation or acetylation also lead to changes in the chromatin structure. Chromatin remodelers are recruited and act in DNA damage response and signaling. The most intense structural change observed after DSB induction is a local decondensation at sites of DSBs, which is supposed to facilitate recruitment and binding of repair factors (Gontijo et al., 2003; Jakob et al., 2011; Müller et al., 2013).

1.4. DNA repair factors and pathways

Exposed to ionizing radiation cells acquire DNA damage. DNA double strand breaks (DSBs) are considered the most serious damage as genetic information can be lost at the break site. Due to misrepair chromosome exchanges can occur, possibly leading to cell death, genetic instability and cancer induction. However, cells developed several repair mechanisms to respond to DNA damage. Two mayor DSB repair pathways are homologous recombination (HR) and non homologous end joining (NHEJ) (Figure 7). NHEJ can be performed throughout the cell cycle whereas HR requires homologous sister chromatids and is therefore only possible in S and G2 phase when the DNA is duplicated.

Repair by NHEJ is initiated by binding of the Ku70/Ku80 heterodimer to break ends, which has potential roles in stabilizing DNA ends. It protects against degradation of the ends and recruits the DNA-dependent protein kinase catalytic subunit DNA-PKcs. Binding of DNA-PKcs to the DNA-Ku complex results in activation of DNA-PKcs kinase activity which functions as a regulatory component for further recruitment of repair and end processing proteins. Before ligation of ends most breaks are processed by Artemis and other nucleases. Ligation of both strands is then mediated by Ligase IV while

XLF and XRCC4 stimulate the ligation activity. This repair mechanism is the preferred one in all cell cycle phases even though it is error prone. At the break site nucleotides can be lost during NHEJ repair and fusion of wrong DNA ends is possible, leading to aberrations like deletions or chromosome exchanges. NHEJ repair is reviewed in (Davis and Chen, 2013; Goodarzi and Jeggo, 2013; Misteli and Soutoglou, 2009).

In contrast HR is error free as it uses sequence information from its homologue sister chromatid. The MRN complex, formed by MRE11, RAD50 and NBS1, binds to the DSB and activates ATM kinase which phosphorylates H2AX in an area of several mega base pairs, generating γ H2AX. The mediator protein MDC1 binds to γ H2AX and recruits additional copies of MRN and ATM, acting in signal amplification and spreading. ATM then activates CtIP, a nuclease which enables extensive resection. Resected single stranded ends are bound by RPA which is afterwards replaced with RAD51 by BRCA2. RAD51 and RAD52 mediate strand invasion into the homologous template where the DNA sequence is renewed by DNA synthesis. HR repair is reviewed in (Brandsma and Gent, 2012; Chapman et al., 2012; Misteli and Soutoglou, 2009).

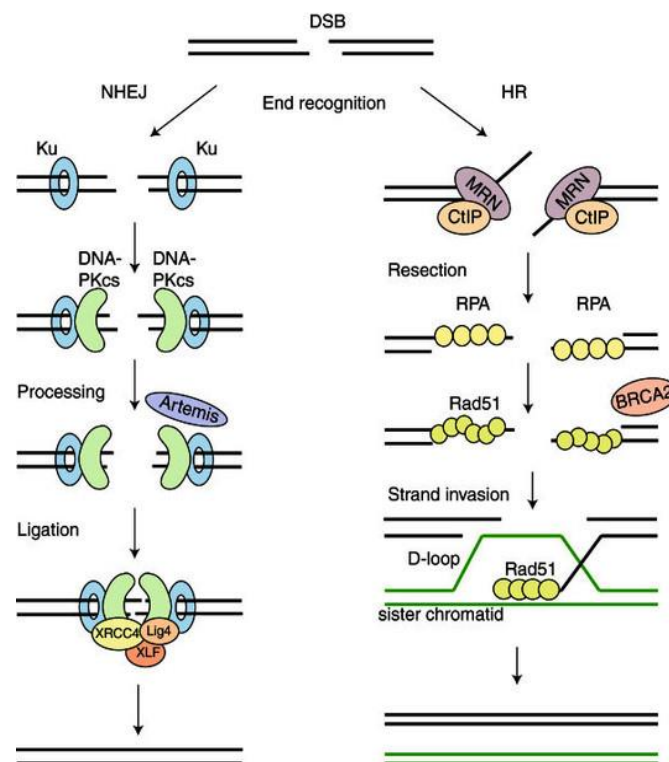


Figure 7 – NHEJ and HR, two major DNA repair pathways in mammals

Non homologous end joining (NHEJ) requires binding of Ku70/80 to DSB ends and phosphorylation by the kinase DNA-PKcs as a signal cascade in which other repair proteins can process the DNA ends before Ligase IV fuses both ends together. In homologous recombination (HR) the MRN complex binds to DNA ends and induces a signal cascade in which nucleases like CtIP resect both strands. Strand invasion into a homologue sister chromatid, mediated by RAD51, ensures correct repair without loss of genetic information (Brandsma and Gent, 2012).

A multiplicity of repair factors and mediator proteins work together in DNA repair to maintain cell integrity. DNA damage signaling can also result in cell cycle arrests to prevent damaged DNA from duplication and the transfer to the daughter cells (Bartek and Lukas, 2007). If a cell received too much damage to be repaired cell death can be induced as a DNA damage response (Surova and Zhivotovsky, 2013).

Upstream and downstream of DNA repair pathways several factors contribute to DSB recognition, signaling and repair. In the following section selected proteins, which play major roles in experiments of this PhD thesis are described in more detail. As chromatin organization has a strong effect on DNA repair not only repair proteins but also chromatin modifying proteins are addressed in this section.

ATM (Ataxia telangiectasia mutated)

Named after the human genetic disorder ataxia telangiectasia (AT) the protein ATM was identified to cause various diseases known as “genomic instability syndromes”. AT is characterized by cerebella degeneration, leading to neuromotoric dysfunctions (ataxia), small dilated blood vessels (telangiectasia), immunodeficiency, genomic instability and extreme sensitivity to ionizing radiation and DSB-inducing agents (Shiloh, 2003).

ATM belongs to the phosphatidylinositol 3-kinase-like protein kinases (PIKK) family, which includes ATR (ataxia telangiectasia and Rad3 related) and DNA-PK_{CS} (catalytic subunit of the DNA-dependent protein kinase) and has a major role in DNA repair. Initiated by binding of the MRN complex, composing of MRE11, RAD50 and NBS1, ATM kinase is recruited to the break site where autophosphorylation of serine 1981 leads to the activation of ATM from an inactive dimer to an active monomer (Bakkenist and Kastan, 2003). As a DNA damage response active ATM then phosphorylates tremendous numbers of substrates, acting in cell-cycle arrest, apoptosis and DNA repair (Matsuoka et al., 2007; Stracker et al., 2013). After X-ray irradiation most DSBs are repaired independently of ATM but deficiency of ATM results in 10 – 25 % non repaired, persisting DSBs after 24 hours which correspond to heterochromatic areas (Deckbar et al., 2007; Riballo et al., 2004). In those heterochromatic areas ATM is involved in a local relaxation of chromatin after induction of DSB through phosphorylation of KAP1 (Geuting et al., 2013; Goodarzi and Jeggo, 2012; Goodarzi et al., 2008). This is assumed to facilitate recruitment of repair proteins and ongoing repair.

53BP1 (Tumor suppressor p53-binding protein 1)

53BP1 is a large (350 kD) multi-domain protein with binding affinity to the tumor suppressor p53. It plays a key role in DNA damage response as it serves as a mediator protein in DSB signaling and pathway choice.

Upon induction of DSB 53BP1 accumulates at sites of lesions and forms large foci, colocalizing with γ H2AX and persisting during ongoing repair (Noon and Goodarzi, 2011). Its role in DNA repair is shown by knockout studies in mice where deficiency of 53BP1 results in hypersensitivity to irradiation, genomic instability and a defect in DNA repair (Ward et al., 2003). 53BP1 acts downstream of ATM and γ H2AX and gets phosphorylated by ATM and ATR, which is necessary for DNA repair but not required for the recruitment of 53BP1 to DSBs (Goodarzi and Jeggo, 2013). The major factor required for 53BP1 recruitment and binding is methylation of histone 4 (H4K20me2) (Botuyan et al., 2006). Moreover the MRN complex, MDC1 and RNF168 contribute to the recruitment and retention of 53BP1 at the break site (Doil et al., 2009; Noon and Goodarzi, 2011). 53BP1 was long known to have a role in damage signaling and also in G2/M checkpoint arrest after low dose radiation but the mayor impact on DNA repair seems to result from defining DSB repair pathway choice. It blocks end resection by restraining CtIP activity, inhibits end processing and promotes NHEJ (Zimmermann and De Lange, 2013). However, in G2 phase of heterochromatic DSBs it was also found to promote HR by interaction with Kap1 (Kakarougkas et al., 2013). Moreover it shows interactions with chromatin, influencing mobility of dysfunctional telomeres. Deprotection of telomeres by deletion of TRF2 increases mobility of telomeres, however, in the absence of 53BP1 this mobility is strongly decreased (Dimitrova et al., 2008).

MRN complex (MRE11, RAD50 and NBS1)

The MRN complex, consisting of MRE11, RAD50 and NBS1 is one of the initial DSB sensors and acts in end processing and tethering of DNA strands as well as signal transduction. It mediates recruitment and activation of ATM resulting in phosphorylation and spreading of γ H2AX (Figure 8).

The head domain of the complex is formed by a MRE11 dimer and two RAD50 ABC-ATPase domains (MR complex) and exhibits DNA binding activity. MRE11 has endonuclease as well as 3'→5' exonuclease activity and interacts with further nucleases like CtIP generating single stranded DNA overhangs for strand invasion during HR repair (Paull and Gellert, 1998; Yun and Hiom, 2009). RAD50 is a protein displaying both sequence and structural homology to structural maintenance of chromosome (SMC) family members. Two long coiled coil domains of RAD50 with apical zinc-hook dimerization motifs reach out of the complex and form a molecular clamp. Through binding and hydrolyses of ATP at the RAD50 subunits a conformational change of the MR complex is generated which opens and closes the clamp formation. In an ATP bound state the molecular bridges of RAD50 are closed and enable tethering of DNA strands and chromosomes (Figure 9) (Hopfner et al., 2002; Lobachev et al., 2004a). Additionally the ATP driven conformation change increases DNA binding activity and is essential for activation of ATM (Lammens et al., 2011; Lee et al., 2013).

The third component of the MRN complex is NBS1 which stimulates DNA binding, unwinding of double strands and MRE11 nuclease activity (Paull and Gellert, 1999). Moreover NBS1 is essential for localization of the MRN complex to the nucleus and to DSBs (Desai-Mehta et al., 2001). Without possession of own enzymatic activity but through protein interactions, like phosphorylation by ATM, it serves as a mediator protein for the recruitment of repair proteins to DSBs (Lamarche et al., 2010).

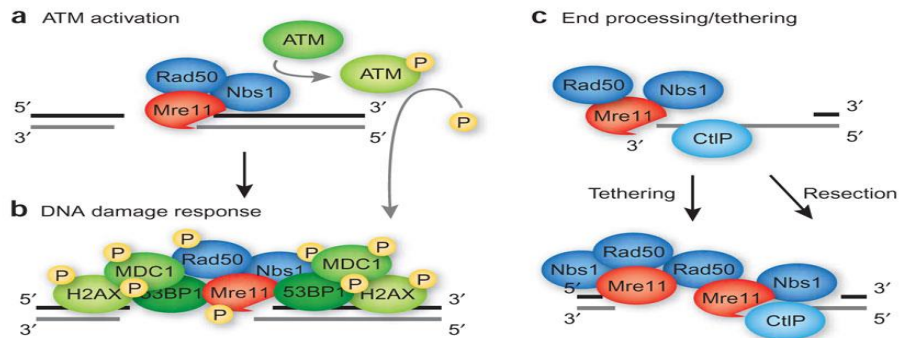


Figure 8 – Functions of the MRN complex in DNA repair

A, B) The MRN complex, formed by MRE11, RAD50 and NBS1 recruits and activates ATM after induction of DSBs to induce a signal cascade for the recruitment of repair proteins. C) By its nuclease activity and interaction with CtIP, MRN acts in strand resection and end processing. Tethering of DNA strands or sister chromatids is accomplished by RAD50 coiled coils and can keep broken strands in proximity to facilitate repair (Zha et al., 2009a).

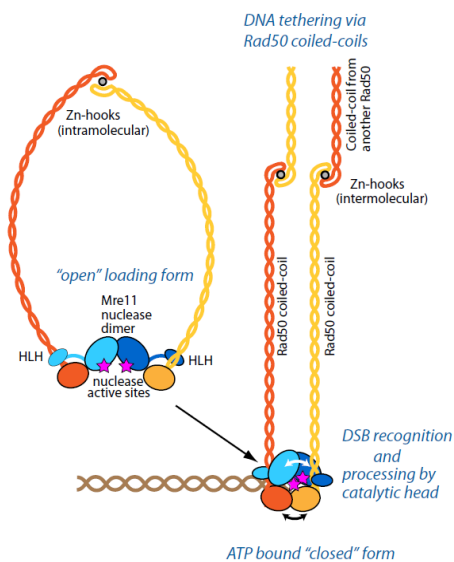


Figure 9 – MRE11 and RAD50 acting as an ATP driven molecular clamp

A MRE11 dimer and two RAD50 proteins with long coiled coil domains form a molecular clamp which can tether broken DNA or chromosomes in its closed conformation. ATP binding at the RAD50 subunit induces a conformational switch of the complex from an open to a closed form (Lammens et al., 2011).

PARP / PARG (poly-ADP-ribose polymerase and poly-ADP-ribose glycosylase)

The human PARP superfamily consists of 17 members from which PARP1 has been most extensively studied (Schreiber et al., 2006). PARP proteins are involved in many cellular processes like DNA synthesis and repair, epigenetic and transcriptional regulations, inflammatory or immune response or chromatin remodeling (Masutani and Fujimori, 2013). The characteristic enzymatic action is the poly-ADP-ribosylation of various proteins as a signal cascade. Branched poly-ADP-ribose (PAR) chains are synthesized by covalently attaching units of ADP-ribose hydrolyzed from nicotinamid adenine nucleotid (NAD^+) to itself, acceptor proteins or existing PAR chains (Figure 10) (D'Amours et al., 1999).

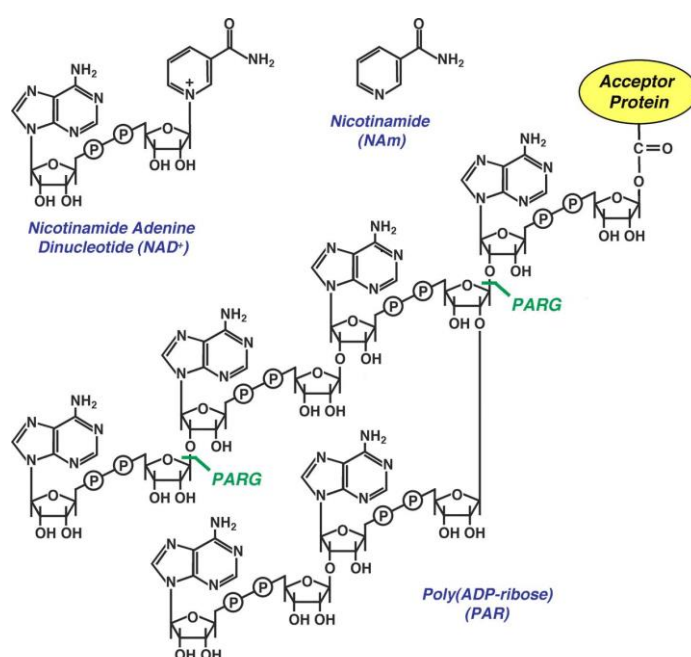


Figure 10 – Chemical structure of a poly-ADP-ribose chain

Poly-ADP-ribose (PAR) is synthesized using NAD^+ (nicotinamid adenine nucleotid) as a donor of ADP-ribose units creating NAM (nicotinamide) as a by-product. Glutamic acids residues of proteins function as covalent attachment sites of PAR. Hydrolysis by PARG degrades the PAR chains afterwards. Varied from (Kim et al., 2005).

A PAR chain can reach up to 200 units with an average branch length of 20–25 residues and as PAR holds twice the negative charge of DNA or RNA the branches create an electrorepulsive environment leading to an opening of the chromatin structure (Thomas and Tulin, 2013). PAR chains are degraded by poly-ADP-ribose glycohydrolase (PARG) and the dynamic turnover of PAR is essential for the maintenance of genomic integrity (Gagné et al., 2008). Deficiency of PARG was shown to be lethal in mice and downregulation by inhibition or siRNA treatment leads to an accumulation of PAR, resulting in apoptosis and hypersensitivity to ionizing radiation (Cortes et al., 2004; Slade et al., 2011). In

various pathways of carcinogenesis poly-ADP-ribosylation is acting in tumor suppression and inhibition of PARP1 is commonly used during cancer treatment (Masutani and Fujimori, 2013).

Involved in different repair mechanisms like SSB repair and alternative (or backup) endjoining-pathways of DSB repair (Hochegger et al., 2006; Mansour et al., 2010; Schreiber et al., 2006) PARP1 is one of the first proteins accumulating at sites of broken DNA (Haince et al., 2008). In the context of DNA repair PARP1 is moreover involved in a decondensation of chromatin through interactions with histones, electrostatic interactions and the recruitment of chromatin remodeling enzymes like the NuRD complex or ALC1 (Ahel et al., 2009; Chou et al., 2010; Kim et al., 2004; Thomas and Tulin, 2013).

ACF1 (ATP-utilizing chromatin assembly and remodeling factor 1)

The ACF complex of the ISWI family of chromatin remodelers consists of two subunits, ACF1 and the ATPase SNF2H. Similar to the other ACF1 containing complex, CHRAC, it promotes nucleosome sliding, catalyzes the deposition of histones and the relaxation of chromatin structure (Ito et al., 1999). In densely packed heterochromatic areas this remodeling ensures correct replication and transcription (Collins et al., 2002). ACF1 is conserved in many species, highly regulated during development and performs specific tasks to ensure cell integrity. During development of *Drosophila* ACF1 (also known as BAZ1A in mammals) was found to play a role in chromatin-mediated gene repression and the regulation of chromatin structures like the formation of heterochromatin (Chioda et al., 2010). In mammalian cells, besides its role in heterochromatic replication, ACF1 accumulates at *Scel* or laser induced DNA damage sites and directly interacts with the repair protein Ku70 promoting DNA repair (Lan et al., 2010). Moreover knockouts of ACF1 show enhanced sensitivity to ionizing radiation, a compromised G2/M checkpoint and high apoptosis rates (Sánchez-Molina et al., 2011), proving a direct involvement of ACF1 in DNA repair. The exact mechanism by which ACF1 provokes DNA repair and checkpoint control is still unclear but its function in nucleosome assembly and spacing seems to be required for NHEJ and HR in human cells (Lan et al., 2010).

Cohesin complex (SMC1 and NIPBL)

The Cohesin protein complex regulates cohesion and separation of sister chromatids during cell divisions like mitosis or meiosis and during HR repair of DSBs. The complex contains the SMC (structural maintenance of chromosomes) proteins SMC1 and SMC3 associated with SCC1, SCC3 and other accessory factors. SMC proteins contain an ATPase domain and two coiled-coil stretches, separated by a central hinge domain to form a ring structure which entraps sister chromatids by ATP driven dimerization of the SMC proteins (Figure 11) (Dorsett and Ström, 2012). During the whole cell

cycle progression different stably or dynamically bound nuclear Cohesin pools exist (Gerlich et al., 2006) but for association with DNA the mammalian SCC2 analogue NIPBL (nipped-B-like protein) is required to load Cohesin onto DNA (Bermudez et al., 2012). Cohesion regulates many cellular functions like chromosome condensation, transcription and gene regulation, centromere organization and even has an impact on DNA repair (Hagstrom and Meyer, 2003; Rudra and Skibbens, 2013). After induction of DSBs Cohesin is recruited to break sites to assist repair by locally stabilizing sister chromatids and facilitating homology search during HR in S/G2 phase (Wu and Yu, 2012). The sister chromatid then provides a template for error-free DNA repair. Moreover cohesion is involved in checkpoint activation (Bauerschmidt et al., 2010; Sjögren and Ström, 2010) and mediates pathway choice between HR and NHEJ (Schär et al., 2004).

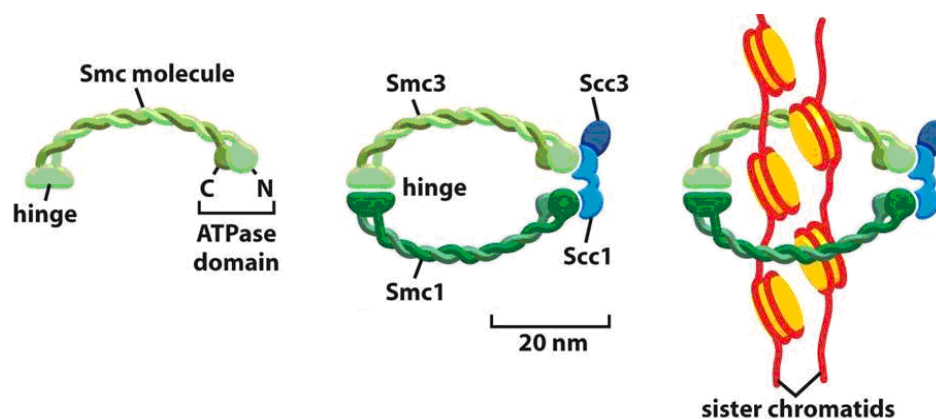


Figure 11 – The Cohesin complex in maintaining sister chromatid cohesion

Cohesin is formed by SMC1, SMC3, SCC1 and SCC3. The SMC molecules contain an ATPase domain and long coiled coil domains and are separated by a central hinge domain. An ATP driven conformational change forms a ring structure of Cohesin which can bind DNA molecules to keep them in close proximity (Alberts et al., 2008).

1.5. Nuclear matrix – Composition and cellular function

A eukaryotic cell nucleus composes of several functional compartments like the intranuclear space containing the genome, nucleoli, the nuclear matrix and the nuclear envelope which presents a boundary to the rest of the cell. The nuclear envelope consists of an inner nuclear membrane (INM) and an outer nuclear membrane (ONM), which are separated by a 40–50 nm perinuclear space (PNS). Inside the nucleus the nuclear matrix acts in nuclear stabilization and provides an anchoring place for DNA, proteins and nuclear pores, which stretch throughout the envelope for macromolecular trafficking (Burke and Stewart, 2013).

The nuclear matrix/scaffold was first described over 50 years ago (Smetana et al., 1963) and can be divided into two parts: the nuclear lamina and an internal nuclear matrix. They are composed of structural proteins like Lamins and high amounts of ribonucleoproteins (RNPs), building a network of

fibers inside the nucleus similar to the cytoskeleton. AT-rich DNA sequences called matrix attachment regions (MARs) mediate interactions between DNA, chromatin and the nuclear matrix (Barboro et al., 2012).

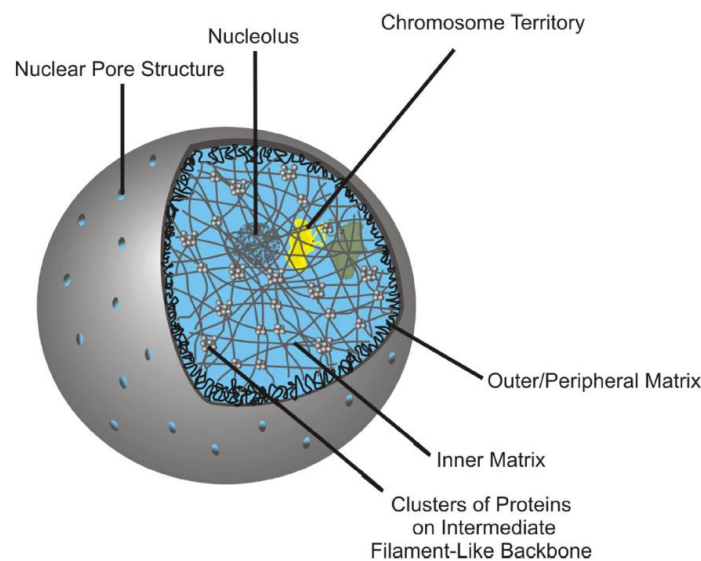


Figure 12 – Nuclear structure and components

Schematic structure of a cell nucleus. The nuclear matrix is divided into the outer matrix (nuclear lamina) and the inner matrix, both containing a filamentous protein meshwork composed of Lamin and other structural proteins. The nuclear matrix provides stabilization as well as anchoring sites for chromatin domains (Linnemann and Krawetz, 2009).

Lamin

In human cells the nuclear matrix composition depends on cell types and varies between normal and cancer cells (Lever and Sheer, 2010). However, the major components of the nuclear lamina are A-type and B-type Lamins. Encoded by a single gene (*LMNA*) A-type Lamins include Lamin A, Lamin C, Lamin C2 and Lamin A Δ 10 while B-type Lamins (Lamin B1 and B2) are encoded by two separate genes. Posttranslational splicing and modifications create cell specific subtypes. Following incorporation into the nuclear lamina Lamin A is proteolytic cleaved from progerin, the truncated form of Lamin A (Burke and Stewart, 2013). While the ONM consists of all types of Lamin, only Lamin A is found in the INM (Neri et al., 1999). Expression levels of A-type Lamins differ in many cancer types like leukemia, lymphoma or small cell lung and ovarian cancer (Gonzalez-Suarez et al., 2009a) and mutations of *LMNA* lead to several disorders like Emery Dreifuss muscular dystrophy, cardiomyopathy or the premature ageing disorder Hutchinson–Gilford progeria syndrome (HGPS) (Worman et al., 2010). Moreover A-type Lamins were found to play a role in DNA damage repair as seen by increased sensitivity to irradiation, increased genomic instability, compromised accumulation of 53BP1 to damage sites and a hindered repair of dysfunctional telomeres (Gonzalez-Suarez et al., 2009b; Liu et al., 2005; Redwood et al., 2011).

NuMA (Nuclear Mitotic Apparatus Protein)

Several hundreds of proteins are known to be associated with the nuclear matrix (Mika and Rost, 2005). NuMA was found to play a main part in the nuclear skeleton as intermediate filaments like Lamins, NuMA and hnRNPs (heterogeneous nuclear ribonucleoproteins) dominate the composition of the inner nuclear matrix.

During mitosis NuMA tethers microtubules at the spindle poles and maintains the spindle apparatus for proper chromosome alignment. The filamentous protein is distributed homogenously in the nucleus during interphase and seems to be essential for the organization of chromosome domains possibly by interactions with matrix attachment regions (MARs) (Radulescu and Cleveland, 2010). Moreover it strongly interacts with RNA as nuclear extraction with RNase causes a drastic reduction of NuMA in the nucleus while Lamins remain unaffected (Barboro et al., 2002). Its function in interphase is expected to maintain the nuclear organization through its filamentous structure. However, studies started to investigate further functions of NuMA like the link to DNA repair as it is phosphorylated by ATM and ATR and following DSB induction the nuclear distribution of NuMA is rearranged in cells with basal polarity (Matsuoka et al., 2007; Vidi et al., 2012).

2. Material and methods

2.1. Cellular and biochemical methods

2.1.1. Cell culture and cell lines

All cell lines were grown in DMEM (Dulbecco's Modified Eagle's Medium) with 10% FCS in 75 cm² culture flasks or petri dishes under standard conditions (monolayer cultures, 95% air, 5% CO₂, 37°C, 100% humid atmosphere). Passages were performed at 90% confluence by trypsin treatment for 5 min. U2OS cells stably expressing 53BP1-GFP or NBS1-GFP cells (kindly provided by Dr. Claudia Lukas Danish Cancer Society, Copenhagen, Denmark), described previously (Bekker-Jensen et al., 2005; Lukas et al., 2003, 2004), were grown in selection media with 1 µg/ml puromycin. For the U2OS-G1/S-GFP cell line G418 was added to a final concentration of 400 µg/ml and for the double mutant U2OS-G1/S-GFP NBS1-cherry 400 µg/ml G418 and 1 µg/ml puromycin were used. Stock cultures were stored in liquid nitrogen (-196°C) in culture medium enriched with 10% DMSO and 30% FCS.

In this work following cell lines were used:

AG (normal human fibroblasts)

MEF (mouse embryonic fibroblasts)

U2OS (human osteosarcoma cells)

U2OS-53BP1-GFP (human osteosarcoma cells stably expressing 53BP1-GFP)

U2OS-NBS1-GFP (human osteosarcoma cells stably expressing NBS1-GFP)

U2OS-G1/S-GFP NBS1-cherry (human osteosarcoma cell line stably expressing a GFP-tagged cell cycle marker (pCORON1002-EGFP-C1-PSLD (GE Healthcare)) double transfected with NBS1-cherry)

2.1.2. siRNA mediated knockdowns

Knockdown of proteins was performed by siRNA treatment using the INTERFERin transfection kit (PeqLab) according to the suggested protocol. Cells were seeded on round 30 mm glass coverslips 24 hours before treatment. Used proteins and according siRNA sequences are listed in Table 1. Efficiencies of protein knockdowns were determined by western blot analyses 48 hours after treatment.

Table 1 – used siRNAs for protein knockdown

Protein	siRNA sequence	End concentration	Incubation time	Reference
PARG	AAATGGGACTTTACAGCTTTG	20 pmol	48 h	(Blenn et al., 2006)
NIPBL	CAAAGAAGCAGAAGAAAA	20 pmol	48 h	MWG siRNA design
SMC1	GCAAUGCCCUUGUCUGUGA	20 pmol	48 h	MWG siRNA design
ACF1	AACACUGUGAAGCACAAGAUG	20 pmol	48 h	MWG siRNA design
MRE11	GGAGGUACGUCGUUCAGA	20 pmol	48 h	(Yuan and Chen, 2010)
NuMA	GGCGTGGCAGGAGAAGTTC	40 pmol	48 h	(Haren et al., 2009)
Lamin A/C	CUGGACUCCAGAAGAACA	40 pmol	48 h	(Elbashir et al., 2001)

2.1.3. Cell lysates and western blot analyses

For verification of knockdown efficiency, whole cell lysates of siRNA transfected cells were prepared and western blotting with specific antibodies was used to detect the expression level of desired proteins. For whole cell lysates cells were grown in Ø 3.2 cm petri dishes for two days. Lyses was carried out on ice by incubation in 70 µl 2x SDS-lysisbuffer (100 mM Tris-HCl (pH 6,8), 2 % (w/v) SDS, 20 % (v/v) Glycerol). Cells were harvested and sheared mechanically by a 25G cannula. Lysates were then incubated at 100°C for 5 min, centrifuged by 13000 G for 10 min at 4°C and the supernatant which contains the proteins was stored at -20°C until for further usage. The protein content of the supernatant was determined based on the protein assay according to Lowry (LOWRY et al., 1951) by the protein assay kit of Bio-Rad according to their protocol. Western blot analyses were performed by a standardized protocol (Fournier et al., 2004) with antibodies listed in Table 3. Quantification of western blots was performed by ImageJ analyses.

2.1.4. Protein inhibition

For inhibition of proteins specific inhibitors were diluted in cell culture medium and cells were incubated with inhibitor at least one hour before further treatment or analyses.

Caffeine (Sigma Aldrich) with an end concentration of 10 mM was used for inhibition of ATM (Sarkaria et al., 1999) but as it partly inhibits all PIK-kinases (ATM, ATR and DNA-PK), this inhibition was characterized as an unspecific inhibition. Specific inhibition of the ATM kinase activity was performed by the selective inhibitor KU55933 (Merck Millipore) (Hickson et al., 2004) with an end

concentration of 15 μM . Poly-ADP-ribosylation was prevented by inhibition of PARP with the specific inhibitor PJ34 (Sigma Aldrich) at a final concentration of 10 μM (Garcia Soriano F et al., 2001).

2.1.5. Nuclear matrix extraction

Cell extraction was performed by modifications of nuclear extraction protocols (Nickerson et al., 1997).

For PFA mediated extraction cells were incubated 10 min on ice in cytoskeleton buffer (10 mM PIPES (pH 6,8), 100 mM NaCl, 300 mM Saccharose, 3 mM MgCl_2 , 1 mM EGTA, 0,5 % (v/v) Triton X-100) and 15 min on ice in cytoskeleton buffer containing 2 % PFA. Digestion of DNA was performed by 60 min incubation at 30 °C in cytoskeleton buffer containing 500 units/ml DNase I. Two washing steps in cytoskeleton buffer and 10 min incubation in 0.5 % Triton X-100 completed the extraction.

For nuclear extraction without PFA cells were incubated 5 minutes on ice in cytoskeleton buffer and cytoskeleton stripping buffer (10 mM Tris HCl, 10 mM NaCl, 3 mM MgCl_2 , 1 % Tween, 0,5 % (w/v) Na-deoxycholate, pH 7,4) respectively, followed by 30 to 60 minutes digestion in DNaseI containing digestion buffer (10 mM Tris HCl, 10 mM NaCl, 5 mM MgCl_2 , 0.5 mM AEBSF, 100 units/ml DNaseI) at 37°C. Fixation was carried out for 30 min with modified Streck Tissue Fixative (150 mM 2-Bromo-2-nitro-1,3-propandiol, 108 mM Diazolidinylurea, 10 mM Tri-Natriumcitrat-Dihydrat, 50 mM EDTA, pH 5.7) before antibody staining (described in the following section).

2.2. Irradiation with x-rays and heavy ions

For photon irradiation an X-ray tube (Isovolt Titan 320-13) (GE Sensing & Inspection Technologies GmbH, Ahrensburg, Germany), operated at 250 kV and 16 mA was used. The X-ray beam was additionally filtered by 1 mm Cu and 1 mm Al to remove low energy photons. Doses-rates laid between 1 and 2 Gy/min.

Charged particle irradiation was performed at the accelerator facility of the GSI Helmholtzzentrum für Schwerionenforschung using different ion species with LET values as reported in Table 2. Choice of ions used in the experiments was mainly determined by the availability of beamtime at the accelerator. Cells were plated on \varnothing 30 mm glass plates in petri dishes and irradiated with a fluence of 2×10^6 particles/ cm^2 vertical or in an angle of 15° to visualize ion traversals through the cell nucleus (Jakob et al., 2003). During irradiation the cell bearing glass plates were kept without medium for a short period of 1-3 min.

Table 2 – UNILAC accelerated ions and corresponding energies and LET values

Ion	LET _{H2O} (keV/μm)	Dosis (Gy)	Energy on target (MeV/u)
Uranium (U)	15000	48	4.7
Lead (Pb)	13500	43	4.7
Gold (Au)	13000	41	4.6
Tin (Sn)	7880	25	5.1
Chromium (Cr)	2630	8.4	6.5
Titanium (Ti)	2180	6.9	7.2
Calcium (Ca)	1800	5.7	7.7
Carbon (C)	170	0.5	9.9

2.3. Microscopy and mobility analyses

2.3.1. Immunofluorescence microscopy

For Immunofluorescence staining cells were fixed at room temperature (RT) in 2% paraformaldehyde in PBS for 15 min and permeabilized for 10 min in 0.5% triton X-100 in PBS, if not mentioned otherwise. Two washing steps with PBS were carried out before storage of samples in 0.4% BSA at 4°C. Staining of MRE11 requires extraction of soluble proteins. Therefore cells were incubated with cytoskeleton and cytoskeleton stripping buffer and fixed for 30 min with modified Streck Tissue Fixative as described previously (Jakob et al., 2003). For staining of poly-ADP-ribose (PAR) cells were fixed in ice-cold 10% trichloroacetic acid (TCA) for 10 min, followed by successive washings in 70%, 90% and absolute ethanol at -20°C for 5 min each (Bürkle et al., 1993).

Antibody staining was performed in 0.4% BSA, first and second antibody both incubating one hour at RT. Washing steps in PBS were carried out between and after antibody incubation. DNA was stained for 20 min by 1 μg/ml DAPI solution and cells could be kept at 4°C in 0.4 % BSA afterwards for several days. Used primary and secondary antibodies are listed in Table 3 and Table 4.

Microscopic analysis of fixed samples was carried out on a Nikon confocal microscope (Eclipse Ti with Yokogawa CSU1-XI spinning disk unit and Andor DU iXON+ 888 EMCCD camera). Possible wavelength for excitation are 405 nm, 488 nm, 561 nm and 647 nm and an 60x oil objective (Nikon CFI PLAN APO VC 60XH) or an 100x oil objective (Nikon CFI PLAN APO VC 100XH) was used.

Table 3 – used primary antibodies

Antigen (clone)	Species	Company	Dilution
ACF1/BAZ1A (A301-318A)	Rabbit	Bethyl Laboratories	WB 1:2000
pATM (p1981)	Mouse	Rockland	IF 1:200 WB 1:1000
B-Actin (ab34731)	Rabbit	Abcam	WB 1:5000
CENPF	Rabbit	Novus	IF 1:750
Ku 80 (ab1357)	Rabbit	Chemicon	IF 1:100
Lamin A/C clone 14	Mouse	Upstate	WB 1:3000
MRE11 (ab214)	Mouse	Abcam	WB 1:750
NBS1 p95 (ab23996)	Rabbit	Abcam	IF 1:300
NIPBL (C-9) sc-374625	Mouse	Santa Cruz	WB 1:400
NuMA (ab36999)	Mouse	Abcam	WB 1:1000
PAR (Ab-1)	Mouse	Oncogene	IF 1:200
PARG (D8B10)	Mouse	Millipore	WB 1:500
PARP (46D11)	Rabbit	Cell Signaling	WB 1:1000
RPA/p34 (Ab-1) Cl. 9H8	Mouse	Thermo Scientific	IF 1:300
SMC1	Rabbit	Cell Signaling	WB 1:1000
Tubulin	Mouse	Sigma	WB 1:8000
Vinculin (ab18058)	Mouse	Abcam	WB 1:10000

Table 4 – used secondary antibodies.

Conjugate	Antigen	Species	Company	Dilution
HRP	Mouse	Sheep	GE Healthcare	WB 1:10000
HRP	Rabbit	Donkey	GE Healthcare	WB 1:10000
Alexa-488	Mouse	Goat	Molecular Probes	IF 1:400
Alexa-488	Rabbit	Goat	Molecular Probes	IF 1:400
Alexa-568	Mouse	Goat	Molecular Probes	IF 1:400
Alexa-568	Rabbit	Goat	Molecular Probes	IF 1:400
Atto 647	Mouse	Goat	Sigma Aldrich	IF 1:200
Atto 647	Rabbit	Goat	Sigma Aldrich	IF 1:200

2.3.2. Live cell microscopy

For live cell analyses of irradiation induced foci (IRIF) U2OS-53BP1-GFP cells were seeded on Ø 30 mm glass plates and irradiated by charged particle or X-ray irradiation. Cells were then transferred into a spinning disc confocal microscope (Nikon Eclipse Ti with Yokogawa CSU_X1) equipped with a temperature controlled chamber stably adjusted to 37°C and 5 % CO₂. 10 to 20 XY positions were selected. At each time-point and position a Z-stack of 5 to 15 slices at a distance of 0.3 or 0.5 µm was recorded during time intervals of 2 to 10 minutes. Excitation levels were kept below 7.5 µW in order to avoid bleaching and cellular stress.

2.3.3. Analyses of IRIF mobility

For quantitative analyses of IRIF mobility the signal to noise ratio of microscope images was increased by deconvolution. Translational movement or rotation of cells was stabilized in 3D by cross correlation method using Huygens essential software (Scientific Volume Imaging). As deformation of cells would result in enhanced movement of IRIF, cells showing higher degrees of nuclear deformation were not included in measurements of foci mobility. To analyze movements of single IRIF, representing foci were manually defined in each cell nucleus to train Huygens object tracker, which then detects the distance from track origin in 3D over all time frames by center of mass detection of each selected object. Identified tracks of foci movement can be corrected manually afterwards to minimize tracking mistakes. As representative readout the mean square displacement (msd) was used resulting from the squared distance from the track origin at a given time (eq. 7). Msd values of all cells in one experiment

were averaged and plotted against time for each experiment where n represents the number of nuclei analyzed. Several foci were scored per nucleus. As comparison some selected image series were also analyzed by tracking foci in 2D with a maximum projection map. To validate tracking analyses by Huygens essential software some experiments were analyzed by manual tracking of foci with M-TrackJ ImageJ Plugin (Meijering et al., 2012).

3. Results

Ionizing radiation induces DNA double strand breaks (DSBs) in cell nuclei, which can lead to the formation of chromosome rearrangements through error prone repair mechanisms. In mammalian cells DSB containing chromatin domains are positional stable over several hours and exhibit only diffusive mobility in a submicron scale (Jakob et al., 2009b; Soutoglou et al., 2007). However, a slight increase of mobility arises by the induction of DSBs (Krawczyk et al., 2012) and might influence the repair fidelity, pathway choice and the formation of translocations. As it is yet unknown which factors contribute to a positional stability or alter movement kinetics, this study determines the influence of different chromatin modifying proteins, known to be activated by the DNA damage response, on mobility of DSBs. Radiation induced local decondensation in the vicinity of DSBs (Müller et al., 2013) might be one factor enhancing DSB mobility. Therefore, this study induces DSBs by charged particle irradiation, known to trigger a pronounced DNA decondensation.

Parts of the results and according figures are published in (Becker et al., 2014).

3.1. Mobility of DSBs after heavy ion irradiation

Accumulations of repair proteins at DSBs are used as marker for DNA damage response and repair. The most commonly known and used marker for DSB repair is γ H2AX. Even single DSBs are marked by γ H2AX and can then be detected by immunofluorescent antibody staining. Charged particle irradiation induces multiple DSBs in a cell nucleus, detectable by repair protein accumulations along the particle tracks. The amount of induced DSBs increases with increasing linear energy transfer (LET) of the used ion species. Even though movement of DSBs is limited to a small scale Brownian movement of chromatin (Marshall et al., 1997), DSB mobility is in question to influence correct repair by NHEJ. This is remarkable as in some exceptions nuclear spreading of repair proteins over several μm was found (Figure 13) (Jakob et al., 2009a and unpublished results).

It is yet unknown what influences the dynamics or positional stability of DSBs even though several studies found hints on influences of repair proteins like Ku80 or 53BP1 and determined contributions of cell cycle or chromatin organization (Dimitrova et al., 2008; Krawczyk et al., 2012; Soutoglou et al., 2007). As an interplay between mobility of DSBs and the formation of chromosome rearrangements is considered, the dynamic behavior of DSB was analyzed in more detail during this work.

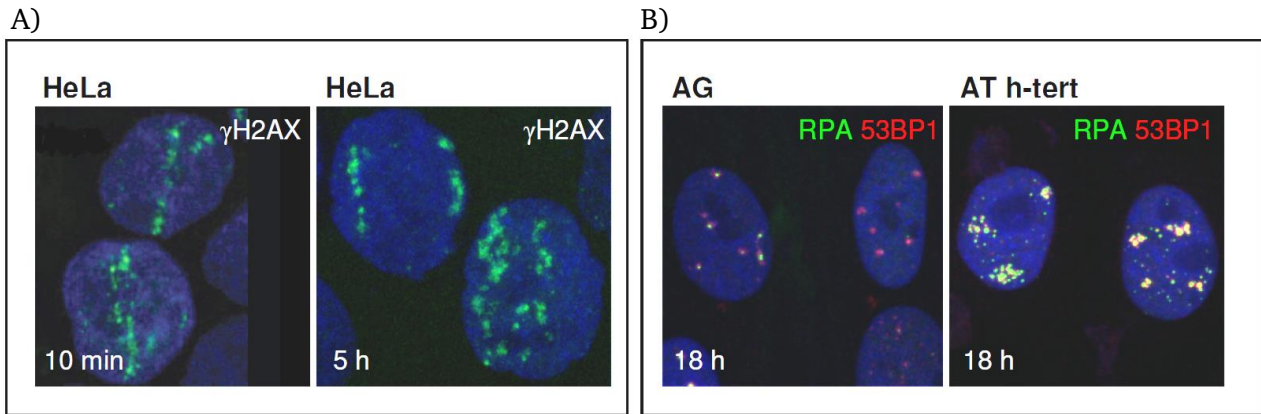


Figure 13 – Positional stability and spreading of DSBs after charged particle irradiation

A) HeLa cells 10 min and 5 hours after irradiation with U (LET: 14300 keV/ μ m) and stained for γ H2AX (Jakob et al., 2009a). In few cases a spreading of γ H2AX foci can be observed. B) AG and AT h-tert cells irradiated with U (LET: 14300 keV/ μ m) and stained for RPA and 53BP1 18 hours after irradiation. Cells of the specific AT h-tert cell line show a strong diffusion of repair foci compared to AG cells. (Images: courtesy of B. Jakob.)

Ku80 is one of the first repair proteins binding to DSBs and was shown to enhance mobility of free DNA ends (Soutoglou et al., 2007). The question remains whether Ku80 moreover influences the motion of DSB containing chromatin domains. To address this question, mouse embryonic fibroblasts (MEF) with a functional deficiency of Ku80 were used to determine changes in DSB distributions after several time points compared to non-deficient MEF cells. Tracks of ion traversals were marked by the repair proteins XRCC1 or NBS1 together with γ H2AX 15 minutes post irradiation. XRCC1 and NBS1 are early binding repair proteins, accumulating in small distinct foci, facilitating the detection of small changes in the irradiation pattern. γ H2AX however marks broader areas around DSBs. Enhanced mobility of DSBs can lead to a deformation of the linear track pattern (Jakob et al., 2009a) or a wider distribution of focal repair protein accumulations (Figure 13).

Absence of functional Ku80 was proven by fixation 5 minutes after irradiation and staining for Ku80. In deficient cells no accumulation of Ku80 at sites of DSBs could be observed while wildtype cells show an accumulation of Ku80 along the ion traversals colocalizing with γ H2AX (Figure 14). Further experiments determined that recruitment kinetics of NBS1 or XRCC1 in MEF Ku80^{-/-} and wt cells did not differ (data not shown), therefore bearing no influence on the formation of the linear track pattern of repair foci. Microscopic analyses of protein tracks did not reveal differences in foci mobility between cell lines 15 minutes after irradiation (Figure 14). It can be concluded that even though Ku80 influences mobility of free DNA ends it does not influence mobility of DSB containing chromatin domains to a larger extent of few μ m. Longer time lines of observation or a different approach might reveal further insights on the interplay of Ku80 and chromatin dynamics.

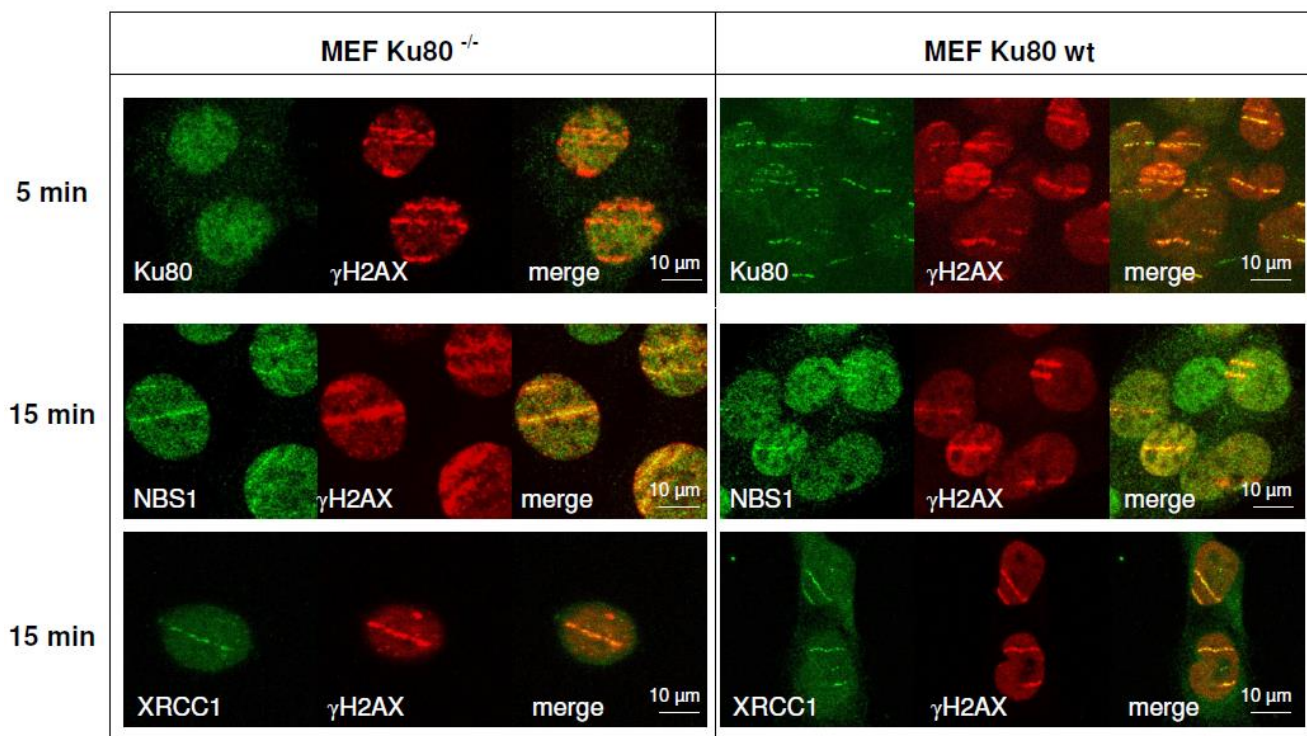


Figure 14 – Influence of Ku80 on chromatin mobility after charged particle irradiation

MEF cells lacking functional Ku80 protein are compared to wildtype MEF cells. Cells are irradiated with Sn (7880 keV/μm) under a low angle, fixed after 5 or 15 min and stained for Ku80, XRCC1, NBS1 and γH2AX. Deficiency of functional Ku80 is assured in MEF Ku80^{-/-} cells from a lack of Ku80 accumulation at damage sites. NBS1 and XRCC1 do not show differences of irradiation pattern in both cell lines.

Early repair factors like XRCC1, mostly involved in SSB or base damage repair do not persist at the break site until repair is completed. To visualize DSBs over several hours longer persisting DSB repair proteins like 53BP1, RPA or γH2AX can be used together with charged particle irradiation. Vertical ion irradiation of cells leads to distinct repair foci, marking up to hundreds of DSBs, depending on the LET. In case of an ATM deficient cell line a large spreading of repair proteins was observed after several hours (Figure 13B). ATM is one of the main players in DSB repair and signaling and loss of ATM strongly diminishes repair (Shiloh, 2003). To determine if the loss of ATM causes this enhanced mobility of DSBs, irradiation patterns of RPA and 53BP1 foci after charged particle irradiation were compared in a different ATM deficient cell line. In human fibroblasts (NFF) serving as a control RPA and 53BP1 accumulate in distinct foci at sites of ion traversals. Those foci of repair proteins were found to stay quite stable in the nucleus over 18 hours (Figure 15). However, also in the ATM deficient cell line the irradiation pattern after 3 to 18 hours did not vary from control cells (Figure 16). No long range mobility in a μm range or fusion events of IRIF and no spreading of single foci into multiple ones was observed. Therefore it could be concluded that the broad spreading of repair foci in the ATM deficient cell line used in the experiment of Figure 13B is based on different factors than loss of ATM.

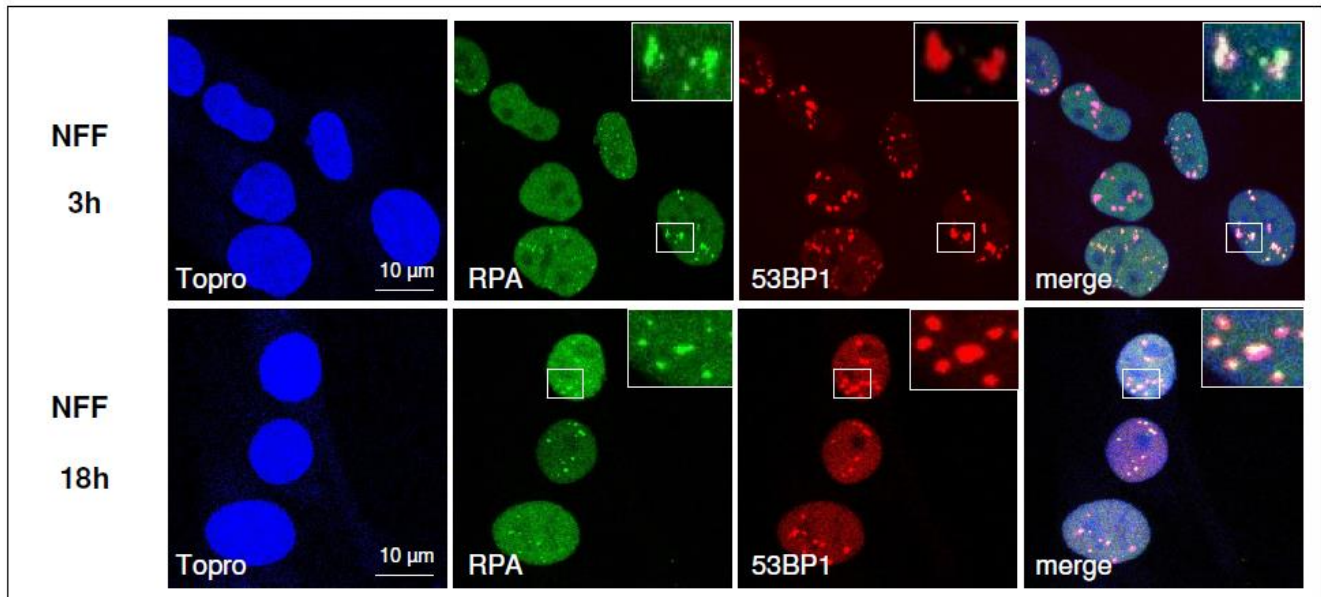


Figure 15 – Positional stability of irradiation induced repair proteins in human fibroblasts

Human fibroblasts irradiated vertical with C (170 keV/μm) fixed 3 and 18 h after irradiation. DSBs are marked by RPA (green) and 53BP1 (red), DNA is stained by Topro 3 (blue). No spreading of foci can be observed.

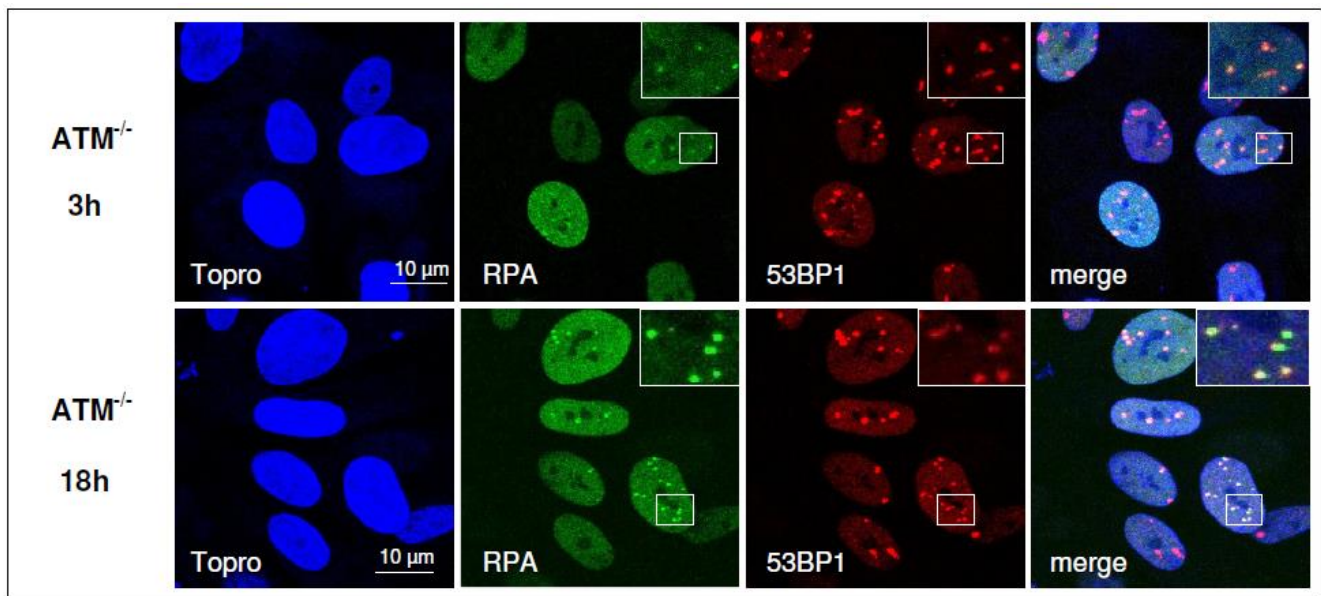


Figure 16 – ATM deficiency does not induce a spreading of IRIF

AT cells were irradiated vertical with C (170 keV/μm) and stained for RPA (green) and 53BP1 (red) after 3 and 18 hours incubation time. IRIF show a positional stability during the observed time frame. DNA is marked by Topro 3 (blue).

Despite a general positional stability of repair foci in some cells higher mobility of DSBs was observed (Aten et al., 2004; Jakob et al., 2009a). The parameters leading to enhanced mobility are still in question. Dynamics of chromatin structure might account for mobility of DSBs as well as for positional stability. However, as charged particle irradiation induces clusters of high numbers of DSBs a

connection between individual broken DNA strands can be expected, possibly leading to a stabilization of DNA breaks in the surrounding chromatin. The MRN complex is known to tether broken DNA strands by a molecular clamp structure of MRE11 and RAD50. By this complex both DNA ends of a DSB can be hold together. Moreover a longer range stabilization of separate DNA strands like sister chromatids during HR repair is possible by the complex of MRE11 and Rad50 (Figure 17).

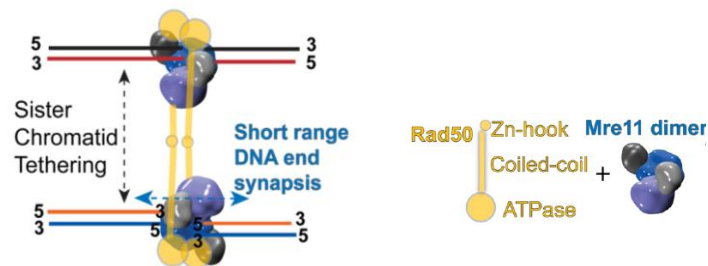


Figure 17 – Schematic view of DNA tethering by the MRN complex

MRE11 and RAD50 build a complex to tether DNA strands either in short range at individual DNA ends of a break or in a longer range between sister chromatids (Williams et al., 2008).

To determine if this tethering influences the diffusion of DSBs, irradiation patterns of $RAD50^{-/-}$ cells were analyzed. Loss of the tethering mechanism by deficiency of $RAD50^{-/-}$ was expected to diminish short range, as well as the longer range connections between broken DNA strands, leading to enhanced diffusion of DSBs. Staining with RPA or 53BP1 17 hours after irradiation did not reveal enhanced spreading of repair foci or changes in the irradiation pattern observed by vertical (Figure 18) as well as angular irradiation (data not shown).

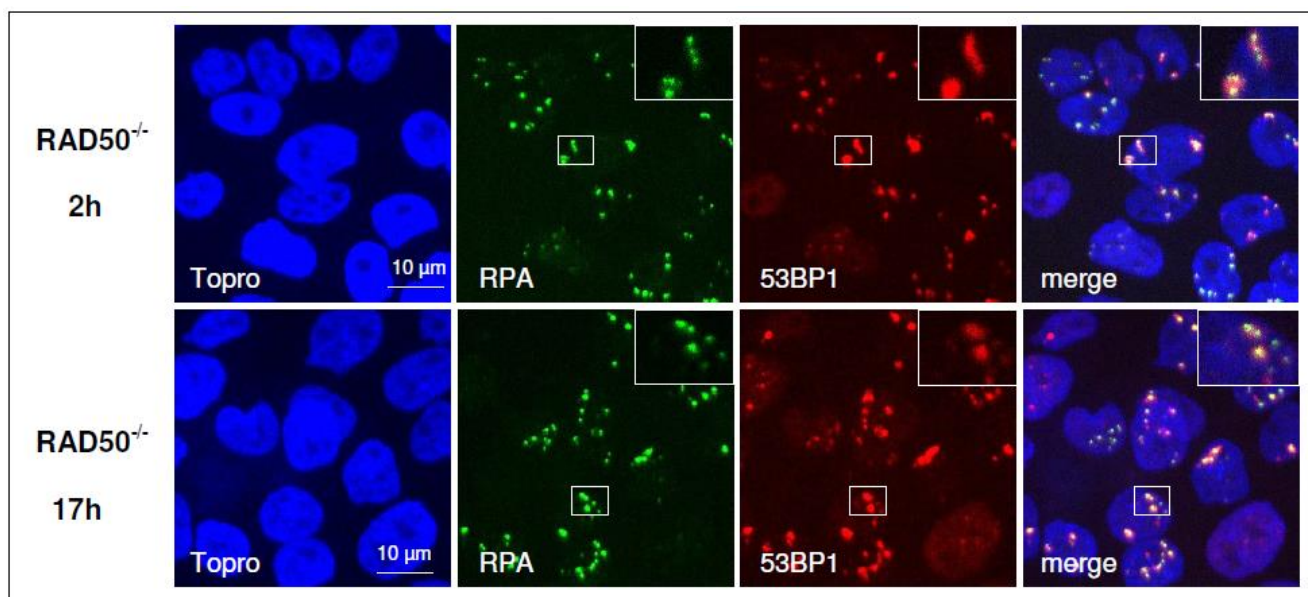


Figure 18 – Positional stability of repair proteins in $RAD50$ deficient cells

$RAD50^{-/-}$ cells were irradiated with Au (13000 keV/ μm) and stained for RPA (green) and 53BP1 (red) 2 and 17 hours post-irradiation. No focal spreading can be observed. DNA is marked by Topro 3 (blue).

Loss of RAD50 did not induce mobility of DSBs at a scale observable by foci distribution. Even though, a dependency on a smaller spatial scale can not be excluded. Further analyses using a live cell imaging approach to track movement of repair proteins elucidated influences of tethering complexes as well as repair or chromatin modifying proteins on DSB mobility in a submicron range.

3.2. Mobility characteristics of DSBs after X-ray and heavy ion irradiation

3.2.1. Experimental setup

For detailed determination of DSB mobility and its characteristics a live cell approach was used following charged particle irradiation. First the cell system as well as microscopic settings had to be established. In order to track repair foci cells need to be transfected with fluorescently marked repair proteins to detect DSBs. 53BP1 was chosen as a marker protein as it serves as a known and reliable marker of DSBs colocalizing with γ H2AX and persisting during ongoing repair (Noon and Goodarzi, 2011). Changes in the shape and size of the nucleus should be minimal during microscopy in order to follow mobility of individual foci. Moreover, long range mobility of whole cells needs to be avoided to detect single cells over a time period of several hours. In first studies it became clear that mouse embryonic fibroblasts (MEF), transiently transfected with 53BP1-GFP undergo strong nuclear deformations during live cell analysis, which hampers foci tracking. In comparison normal human fibroblasts (AG) are relatively stable but due to their limited ability to be transfected they did not provide a good cell system. U2OS cells however are easy to grow and to transfect, they keep their shape and size and provide a well-established human cell system. Transient transfections cause cellular stress which was avoided by usage of a U2OS cell line stably transfected with 53BP1-GFP.

By FACS analyses of U2OS-53BP1-GFP cells a cell cycle distribution around 50 % G1 and 20 % G2 was measured 24 hours after seeding. Similar results were observed by CENPF staining after exposure to 1 Gy X-ray irradiation and 2 hours of live cell analyses (Figure 20). CENPF serves as an immunofluorescent cell cycle marker as is expressed during late S and G2 phase, binds to kinetochores during mitosis and is degraded afterwards (Liao et al., 1995). U2OS cells can not be synchronized in

G1 by contact inhibition like AG cells. Therefore the cell cycle distribution is expected to be similar in every experiment as similar seeding times were applied.

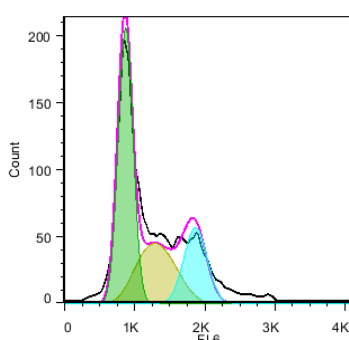


Figure 19 – Cell cycle distribution of U2OS-53BP1-GFP cells

The cell cycle distribution reveals 51% G1, 26% S and 23% G2 phase cells observed by FACS measurement carried out one day after plating of cells

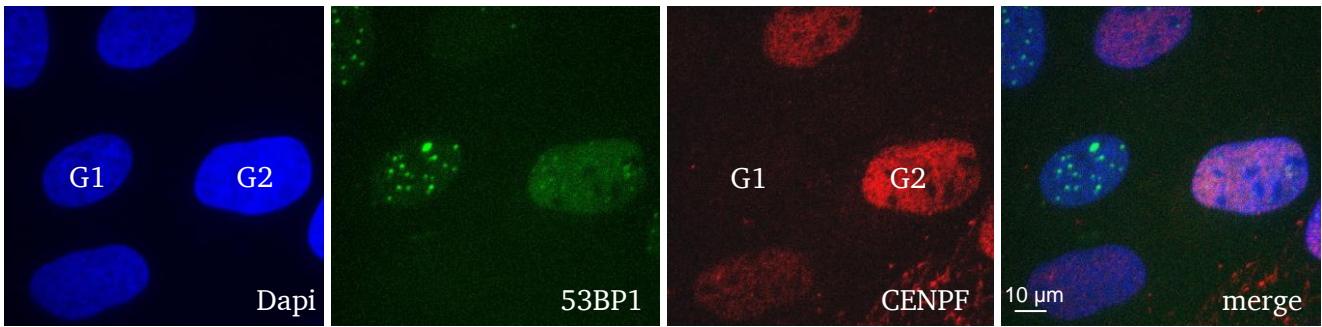


Figure 20 – CENPF marked cell cycle phases of U2OS 53BP1-GFP cells

Cells are exposure to 1 Gy X-rays, fixed after 2 hours of live cell analyses and stained for CENPF (red) and Dapi (blue). CENPF marks cell cycle phases (no signal - G1, weak signal - S and strong signal - G2) and reveals 20 % G2 phase cells.

By 24 hours of live cell imaging it was confirmed that cells behave and divide normally and no enhanced apoptosis or other form of cell death occurred. To reduce stress induction during live cell microscopy, laser intensity, exposure time, Z-stack dimensions and frame rate were kept as low as possible. Laser intensity was kept below $7,5 \mu\text{W}$ with an exposure time of maximum 200 ms to avoid photobleaching and 5 to 15 slices at a distance of 0.3 or 0.5 μm were recorded in a frame rate between 2 and 5 minutes, depending on overall observation time.

DSBs were induced either by X-ray or charged particle irradiation and accumulating 53BP1 foci were tracked over 2 hours in average. Irradiation patterns of 1 Gy X-rays and high LET irradiation compared to untreated cells are shown in Figure 21. Untreated cells contain several nuclear 53BP1 bodies marking replication-stress-induced DNA lesions (Lukas et al., 2011a). X-ray irradiation induces separated DSBs while linear tracks of clustered DSBs result from charged particle irradiation.

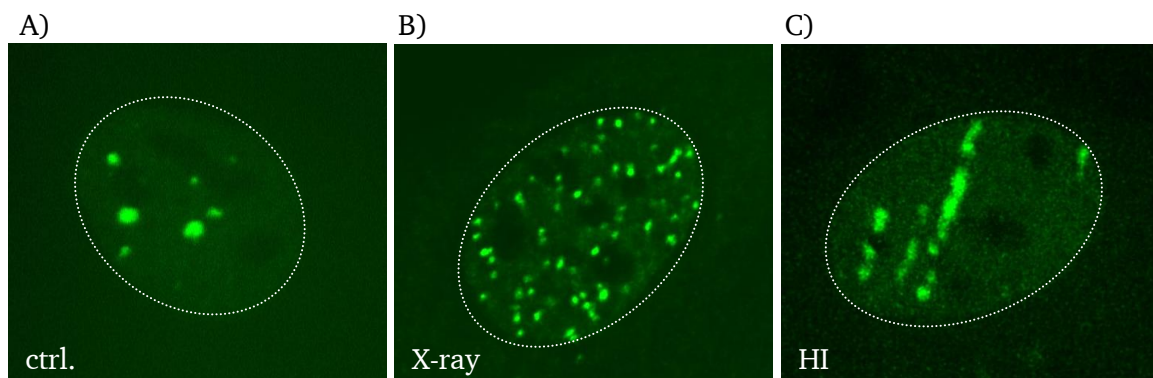


Figure 21 – Irradiation pattern in U2OS-53BP1-GFP cells

A) Control cell during normal cell conditions. B) Cell 20 minutes after irradiation with 1 Gy X-rays. C) Cell 20 minutes after low angle irradiation with Pb ($13500 \text{ keV}/\mu\text{m}$).

For X-ray induced DNA damage a high percentage of DSBs are repaired during the first hours after induction (Löbrich et al., 2010) which limits the possible observation time. Charged particle irradiation has several advantages for analyses of foci mobility. Due to a defined linear irradiation pattern which results from low angle irradiation, irradiation induced foci (IRIF) can be distinguished from pre-irradiated accumulations of repair proteins which might exhibit different dynamics. Moreover, repair of DSBs is slower due to the high complexity of breaks why breaks can be observed over several hours. However, many DSBs are repaired by a fast component during the first hours as well (Tommasino et al., 2013) and translocations can be expected to occur. An observation time of few hours revealed to be sufficient to determine changes in chromatin dynamics after various treatments.

A local chromatin decondensation was observed at the break site after the induction of DSB by charged particles or X-rays (Falk et al., 2007; Jakob et al., 2011; Müller et al., 2013). This relaxation is suggested to affect IRIF mobility. The pronounced decondensation seen after charged particle irradiation thus might be helpful to elucidate contributions of chromatin modifying proteins on DSB mobility.

For tracking of radiation induced foci translational as well as rotational mobility in xy plane can be compensated using stabilization software. Deformation as well as rotational movement in z dimension can not easily be corrected by rigid body transformation, thus cells showing those effects were excluded from analyses. Huygens essential software was used for deconvolution of images and cell stabilization. Huygens essential particle tracker was used for motion detection of IRIF. The tracking algorithm uses manual parameter selection followed by automatic processing of tracks in 2D or 3D. To ensure correct tracking of foci the system was compared to manual detection of foci mobility by “ImageJ – M-TrackJ” (Meijering et al., 2012). In both systems, from the intensity weighted center of each focus over time, the mean square displacement (msd) (described in more detail in the next chapter) is calculated and plotted against time. Tracks estimated by Huygens essential particle tracker were checked for inconsistencies by visual inspection. Only correctly identified tracks were used for the analysis.

Comparison of both systems revealed similar results. An example of foci tracking by Huygens software is shown in Figure 22 and results of both systems are compared in (Figure 23). As manual tracking by ImageJ M-TrackJ is only possible in two dimensions and more time consuming analyses of further experiments were all carried out by Huygens essential particle tracker.

By tracking of IRIF in samples fixed prior to microscopic analyses the error was determined which can result from live cell observations and tracking. U2OS-53BP1-GFP cells were irradiated with chromium ions and foci were tracked prior to fixation and in fixed cells of the same sample afterwards. While in living cells a msd of DSB mobility around 1 μm was found after 100 min, fixed cells show a msd below 0.1 μm in the same time frame (Figure 24), marking the expected error for these kind of experiments.

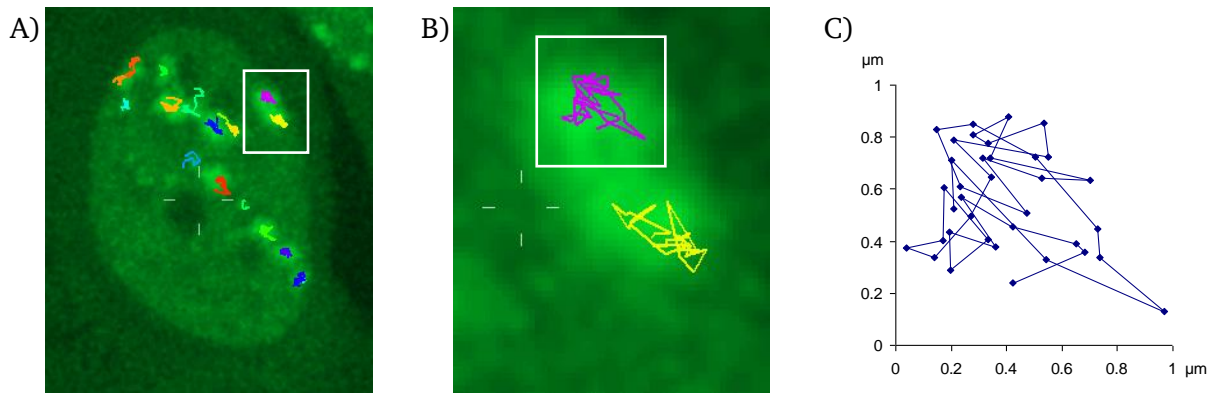


Figure 22 – Mobility measurement of 53BP1 IRIF in U2OS-cells.

A) 2D maximum projection of a U2OS cell nucleus after irradiation with Cr ions (LET: 2360 keV/ μm) showing 53BP1-GFP accumulation along the ion trajectory at sites of DSBs. Colored tracks of 53BP1 foci demonstrate foci mobility within three hours of observation. B) Magnification of two exemplary tracks of 53BP1 mobility. C) Mobility of 53BP1 foci (selected in B) over three hours showing a random walk behavior in a spatial scale below 1 μm .

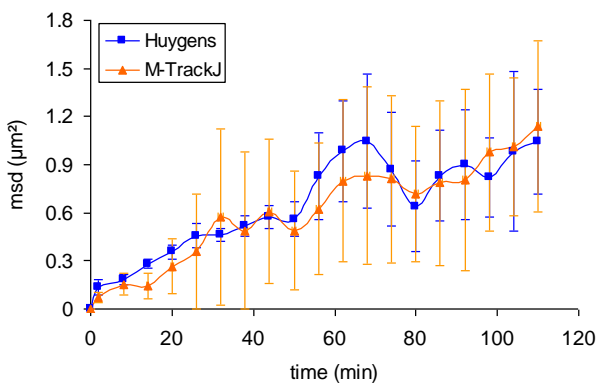


Figure 23 – Comparison of two particle tracking programs.

Foci of a 2D maximum projection of U2OS NBS1-GFP cells, irradiated with Au ions (LET: 13000 keV/ μm) were tracked over 2 hours with either Huygens essential software (blue line $n = 6$) or ImageJ M-TrackJ (orange line $n = 6$) and the msd is plotted over time. Results reveal comparable mobility and standard deviation.

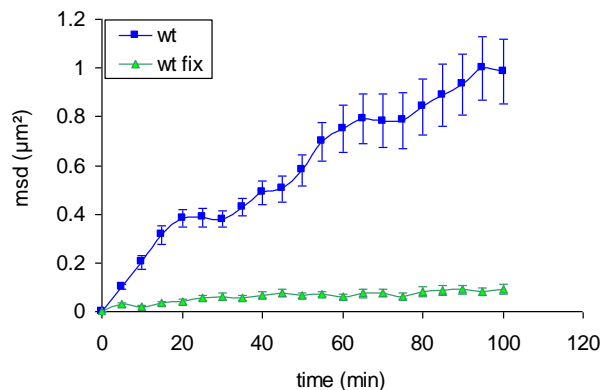


Figure 24 – Tracking of DSB in fixed samples

Msd plots of U2OS-53BP1-GFP cells after irradiation with Cr (LET: 2630 keV/ μm). Living cells (blue) ($n = 11$) show a msd around 1 μm after an observation time of 100 min while fixed cells from the same sample (green) ($n = 7$) show a msd around 0.1 μm in the same time frame. Errors represent SEM.

3.2.2. Mobility of 53BP1 and NBS1 foci after X-ray irradiation

U2OS 53BP1-GFP cells were chosen for analyses of DSB mobility. However, to determine the influence of repair and chromatin related proteins on mobility of chromatin domains a dependency of 53BP1 as DSB marker needed to be excluded. 53BP1 was shown to influence mobility of uncapped telomeres as deficiency of 53BP1 led to a decreased mobility (Dimitrova et al., 2008). Expression of GFP tagged 53BP1 in a wildtype cell causes overexpression of 53BP1. By comparison of IRIF mobility in U2OS cells

stably expressing 53BP1-GFP and NBS1-GFP it was determined if 53BP1 overexpression influences kinetics and range of foci mobility. Irradiation was performed by 1 Gy X-rays and foci were tracked over one hour. NBS1 cells have the disadvantage to create smaller foci and show a high background level of NBS1 accumulation making it a difficult task to distinguish between preirradiated and irradiation induced foci. However, besides differences in foci size, the diffusion kinetics and msd were found to be in the same range. Therefore an influence of 53BP1 overexpression on irradiation induced DSB mobility could be excluded.

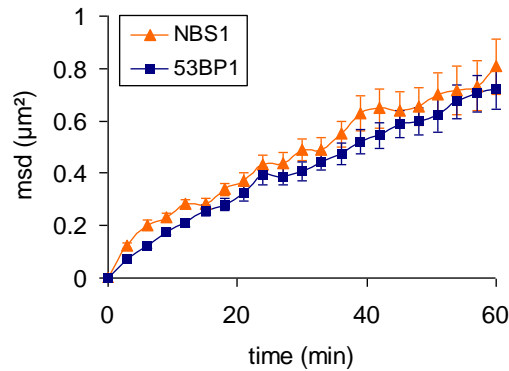


Figure 25 – 53BP1 and NBS1 foci exhibit similar mobility characteristics.

Msd plots of U2OS cells expressing either 53BP1-GFP (blue) (n = 7) or NBS1-GFP (orange) (n = 9) irradiated with 1 Gy X-ray show no significant variation between IRIF mobility of both cell lines. Errors represent SEM.

3.2.3. Dynamic behavior of IRIF

Irradiation induced foci (IRIF) dynamics measured over two hours display mobility that is indicating a random walk in a submicron range (Figure 23). Few exceptions are found where single foci extend mobility over longer distances (few μm) in the cell nucleus or undergo fusion with other foci.

Random walks and diffusion of particles can be described by the mean square displacement (msd) which represents the average of the squared distance (Δr^2) a particle is displaced from its origin in a given time frame (t). With N being the number of particles and $r_i(t) - r_i(0)$ the vector distance of the given time interval.

$$\text{msd}(\Delta t) = \langle r^2(t) \rangle = \left\langle \frac{1}{N} \sum_{i=0}^N (r_i(t) - r_i(0))^2 \right\rangle \quad (\text{eq. 7})$$

For normal diffusion the msd has a linear dependency on time and yields a constant diffusion coefficient (D) corresponding to the Einstein-Stokes equation with the spatial dimension (d).

$$msd(\Delta t) = \langle r^2(t) \rangle = 2dD\Delta t \quad (\text{eq. 8})$$

For a 3 dimensional system this results in

$$D = \frac{msd(\Delta t)}{2d\Delta t} = \frac{msd(\Delta t)}{6\Delta t} \quad (\text{eq. 9})$$

To distinguish between different dynamic behaviors like normal or confined diffusion the curvature of a msd plot can be used. If the diffusion coefficient varies over time, a bending of the slope arises. A bending downward is seen in cases of confined mobility whereas an upwards curvature indicates directed motion (Dion and Gasser, 2013).

If the mobility is constrained to a certain radius (r_c) the msd changes to

$$\lim_{\Delta t \rightarrow \infty} msd(\Delta t) = r_c^2 \quad (\text{eq. 10})$$

and confined mobility can be described by (eq. 11) (Jegou et al., 2009).

$$msd(\Delta t) = \langle r_c^2 \rangle * \left[1 - \exp\left(-\frac{2dD_c\Delta t}{\langle r_c^2 \rangle}\right) \right] \quad (\text{eq. 11})$$

This equation takes into account the diffusion coefficient D_c and the confinement radius r_c . Confined mobility results from restriction of mobility to a defined volume, trapping in a certain domain or by tethering to a nuclear structure (Platani et al., 2002). In contrast, subdiffusion which exhibits a similar bending of the msd, is caused by viscoelasticity of the surrounding medium, obstruction by immobile obstacles and binding events (Guigas et al., 2007; Lukacs et al., 2000). It occurs in various biological systems and recently also the mobility of IRIF was shown to follow anomalous subdiffusion (Girst et al., 2013), commonly defined via a power-law dependent increase of the mean square displacement

$$msd(\Delta t) = \Gamma \Delta t^\alpha \quad (\text{eq. 12})$$

with $\alpha < 1$; where α represents the anomaly parameter and Γ the transport coefficient.

By analyzing the msd plots of 53BP1 foci in irradiated U2OS cells dynamics were found which can be described as both, either subdiffusional movement or confined diffusion (Figure 26B). However, independent experiments revealed variations in the extent of mobility (Figure 26A). These variations occur in heavy ion as well as in photon irradiated samples and might be attributed to influences of the cell lot and cultivation time used, as the experiments were executed over a longer time period. To keep the impact of this variability on the obtained results as low as possible repeated measurements in independent experiments were carried out for each condition and only results of contiguous experiments were directly compared.

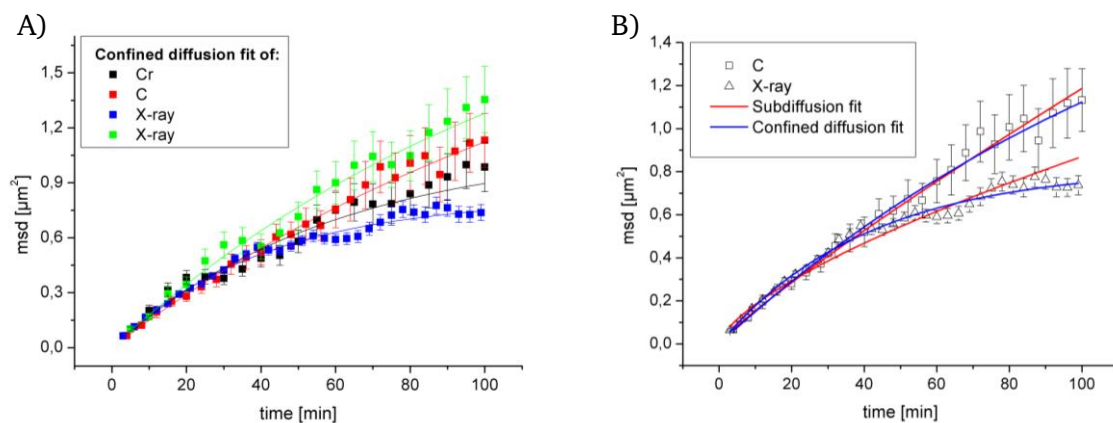


Figure 26 – Mobility of DSBs can be described by the model of confined diffusion or subdiffusion.

Plots show the msd of four individual experiments of U2OS 53BP1-GFP cells measured over 100 minutes. Errors represent SEM. A) Two independent experiments using 1 Gy X-ray irradiation (blue and green) are compared to experiments where carbon (170 keV/ μm) (red) or chromium ions (2630 keV/ μm) (black) were used for irradiation. In A) data is fitted for confined diffusion. B) Msd plots after C ion and X-ray irradiation fitted for subdiffusion (red line) and confined diffusion (blue line) show equally good fits.

Generally, good correlations of both types of fits ($R^2 < 0.97$) were obtained for 53BP1 mobility of U2OS cells. Exemplary one carbon irradiated and one X-ray irradiated wildtype are fitted to subdiffusion and confined diffusion (Figure 26B). For the X-ray irradiated wildtype of Figure 26B both fits describe the curve similarly well ($R^2 = 0.99$ for subdiffusion vs. 0.97 for confined mobility). The carbon irradiated U2OS cells of Figure 26 also acts as a reference in analyses of poly-ADP-ribosylation (chapter 3.2) and displays mobility kinetics similar to the average of all measured wildtype cells (data not shown). Therefore its kinetics are described in more detail, exemplary representing mobility of U2OS cells after irradiation.

By taking a subdiffusive mobility into account a fit correlation of 0.996 for R^2 was observed and an α value of 0.89 ± 0.01 calculated. The α parameter close to one points to a mobility similar to normal diffusion. Fitting to confined diffusion reveals a R^2 value of 0.995 as well. The diffusion coefficient lay at $4.32 \pm 0.09 \times 10^{-5} \mu\text{m}^2/\text{s}$ and the confinement radius, revealing the restriction of mobility was

$1.5 \pm 0.08 \mu\text{m}$. These data provide insight into the dynamics of IRIF, locally diffusing in a restricted environment.

Different ion species with different LET values ranging from C (170 keV/ μm) to U (15000 keV/ μm) were used for analyses of mobility as well as X-ray induced DNA damage. No indication for a direct LET effect on mobility was found during those experiments. This is consistent with the previously described msd values for nickel ions (LET: 3430 keV/ μm) and low LET photons (X-rays) which are in the same range (Jakob et al., 2009b).

3.2.4. Depletion of ATP

The main source of energy in every cell is adenosine triphosphate (ATP), a nucleotide containing three phosphate groups. From adenosine monophosphate (AMP) or adenosine diphosphate (ADP) it is produced by redox reactions during cellular respiration like glycolysis or the citric acid cycle. By hydrolysis to ADP energy can be transferred to enzymes utilized in cell metabolism, motility or signal transduction. Moreover ATP is incorporated in nucleic acids. Enzymes like kinases or chromatin remodelers depend on the availability of ATP and depletion of ATP causes a reduction of cellular functions up to occurring cell death.

Energy starvation in early stages of ATP depletion influences both, the movement of undamaged chromatin (Clapier and Cairns, 2009) as well as mobility of IRIF. Mobility of IRIF is diminished (Krawczyk et al., 2012) and chromatin was shown to be more condensed after ATP depletion (Görisch et al., 2004). This system provides an excellent tool to explore the extent in which cellular processes can influence mobility of 53BP1 foci.

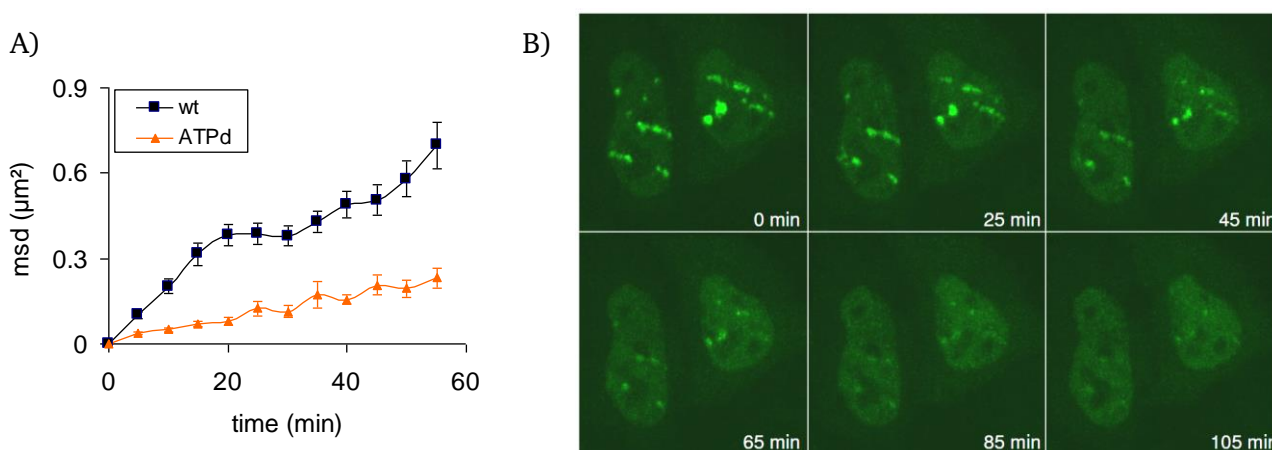


Figure 27 – ATP depletion causes drastic reduction of foci mobility

A) Msd plot of IRIF in control cells (blue) ($n = 16$) and cells which were depleted for ATP 30 min prior to Cr irradiation (LET: 2360 keV/ μm) (orange) ($n = 7$). Errors represent SEM. B) Live cell observations of U2OS-53BP1-GFP cells depleted for ATP 30 min prior to Cr irradiation (LET: 2360 keV/ μm). 2D maximum projection reveals foci formation and degradation during 105 min of live cell microscopy.

For wildtype U2OS 53BP1-GFP cells a msd of $0.7 \mu\text{m}^2/\text{h}$ for the first 55 min was measured (Figure 27A). Depletion of ATP was performed by incubation in cell culture medium containing 10 mM sodium azid and 50 mM 2-deoxyglucose. Starting depletion 30 minute prior to irradiation with chrome ions ensured a low remaining level of ATP in the cell to ensure the formation of repair foci. However, by further incubation in ATP depletion medium, those foci were losing intensity and vanished between 30 to 90 minutes after irradiation as observed by live cell microscopy (Figure 27B). The inability of repair proteins to accumulate at DSBs indicates a proceeding in energy starvation as observed before (Kruhlak et al., 2006). Tracking of irradiation induced 53BP1 foci demonstrated a drastic reduction of mobility around $\sim 66\%$ after one hour compared to the msd of untreated cells (Figure 27). The diffusion coefficient D was strongly reduced from $6.5 \pm 0.6 \times 10^{-5} \mu\text{m}^2/\text{s}$ to $1.5 \pm 0.1 \times 10^{-5} \mu\text{m}^2/\text{s}$. The obtained results confirm that metabolic perturbation can lead to pronounced differences in IRIF mobility which can be detected by the experimental approach and validate the experimental composition.

3.3. Poly-ADP-ribosylation and the chromatin remodeler ACF1

3.3.1. ACF1 does not influence chromatin mobility

Chromatin remodelers maintain cell integrity and regulate many cellular processes by rearranging, moving or ejecting nucleosomes in an ATP-dependent manner. These alterations influence chromatin structure and thus possibly mobility of DSB containing chromatin domains. To determine if the dramatic reduction of IRIF mobility observed after ATP depletion can be attributed to the absence of radiation-induced local remodeling, ACF1 was downregulated. ACF1 is a chromatin remodeler of the ISWI family known to participate in DSB repair and the relaxation of chromatin structure (Collins et al., 2002; Lan et al., 2010). By siRNA treatment ACF1 expression was reduced around 80 % (Figure 28B). No differences in recruitment of 53BP1 could be observed after knockdown of ACF1 and tracking of IRIF revealed a msd in the same range like wildtype cells. Even though it might be slightly reduced, it was found not to be statistically significant by 5 % level of students t-test (Figure 28). In conclusion, knockdown of ACF1 does not influence mobility of IRIF on a scale observed by the used system.

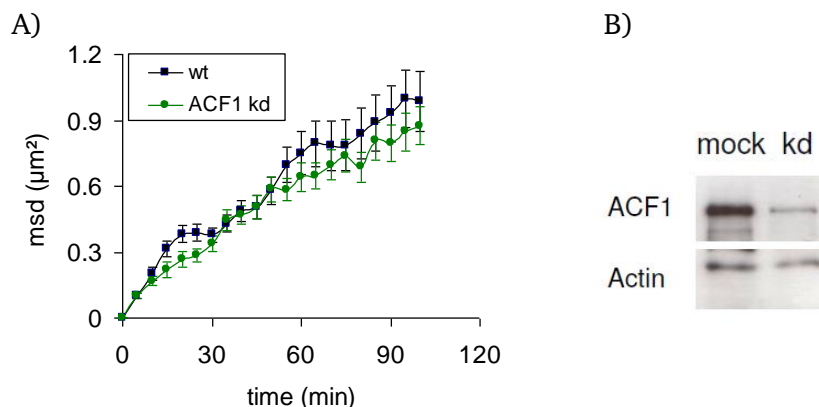


Figure 28 – Knockdown of ACF1 does not change mobility of IRIF

A) Msd plots of control (blue) (n = 23) and ACF1 downregulated (green) (n = 11) U2OS-53BP1-GFP cells irradiated with with Cr (LET: 2360 keV/μm). Errors represent SEM. Tracking of 53BP1 foci reveals no difference in movement kinetics. B) Western blot indicates 80 % reduction of ACF1 expression 48h after siRNA treatment. Actin is used as loading control.

3.3.2. Chromatin mobility is not altered by poly-ADP-ribosylation

To investigate if a mediator protein involved in a wider spectrum of repair processes upstream of chromatin remodeling complexes has a more pronounced impact on DSB mobility the effect of the radiation-induced poly-ADP-ribosylation was analyzed.

Poly-ADP-ribose polymerase 1 (PARP1) synthesizes long branched chains of poly-ADP-ribose (PAR), covalently attached to proteins and histones as response to DNA damage (D'Amours et al., 1999; Haince et al., 2008). These chains, acting as a signal cascade, are afterwards degraded by poly-ADP-ribose glycohydrolase (PARG) and the dynamic turnover of PAR is essential for the maintenance of genomic integrity (Gagné et al., 2008). Poly-ADP-ribosylation plays a role in several repair pathways and influences chromatin organization through multiple pathways. Because of this versatile role, its influence on mobility of DSB containing chromatin domains was determined.

Inhibition of PARP1 is used for sensitization in cancer treatment and specific inhibitors are commercially available. Efficiency of the applied inhibitor PJ34 was confirmed by treatment of cells with H₂O₂. By incubation with H₂O₂ single strand breaks are produced where PARP1 binds. PAR is synthesized and can be detected by immunofluorescence staining. Inhibition of PARP prevents the formation of PAR as shown in Figure 29. To prevent the degradation of PAR, in a separate experiment PARG was downregulated by usage of siRNA. Only a low amount of around 10 % of the original endogenous protein level remained after knockdown. This reduction is sufficient to prevent degradation of PAR after treatment with H₂O₂ as seen by immunofluorescent staining of PAR (Figure 29).

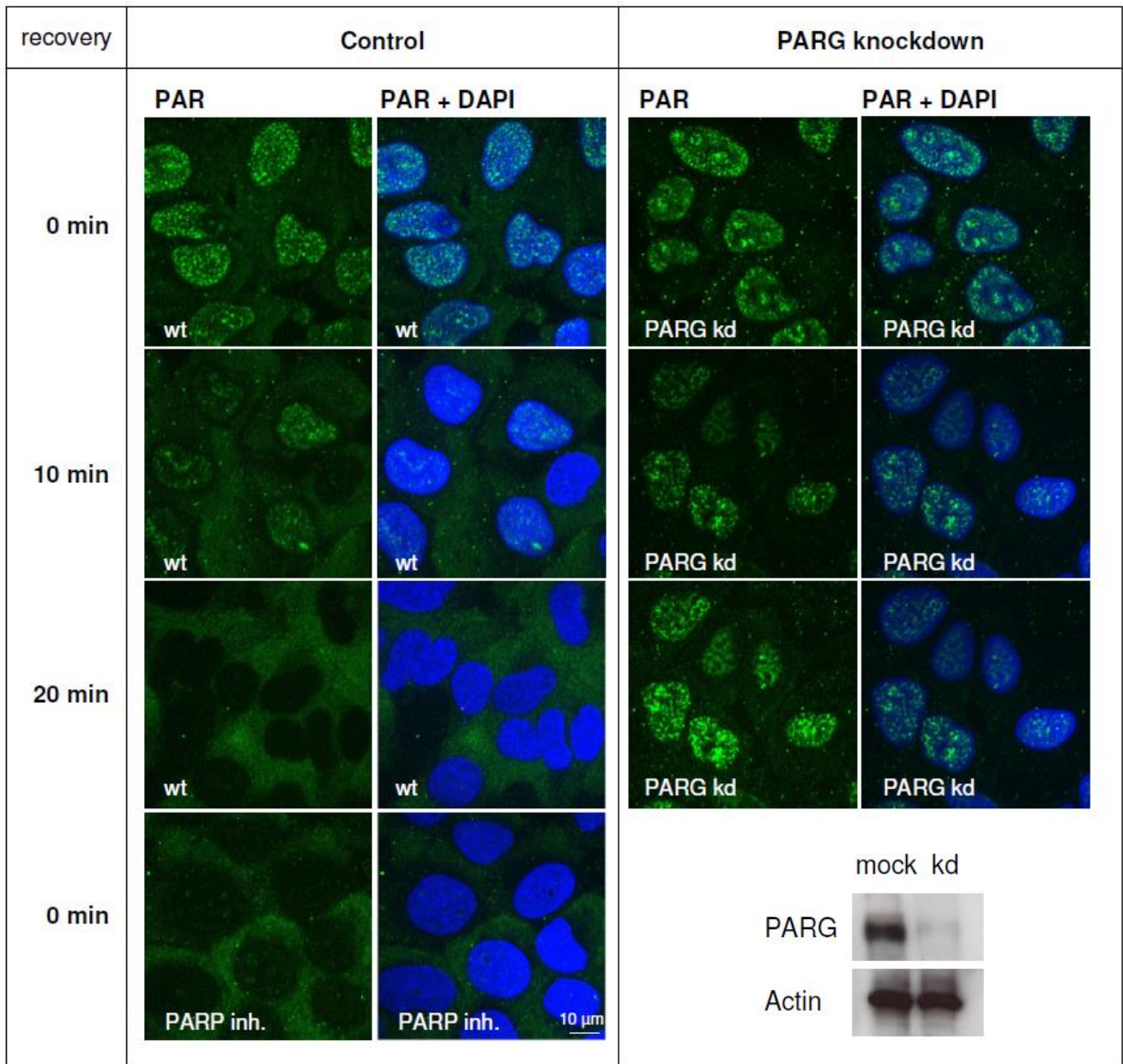


Figure 29 – Functional assay of inhibition of PARP and knockdown of PARG after H₂O₂ treatment

U2OS cells were treated with 1 μ M H₂O₂ for 5 min. After indicated recovery times cells were fixed and stained for PAR (green) and DNA (blue). PAR is not produced after inhibition of PARP (10 μ M PJ34) (left bottom). Compared to wildtype cells PAR is not degraded in cells knocked down of PARG. B) Western blot showing 90 % knockdown efficiency of PARG. Actin serves as loading control.

Tracking 53BP1 foci after irradiation with carbon or chrome ions revealed that the extent of DSB mobility is not influenced by changes in poly-ADP-ribosylation. Neither inhibition of PARP nor knockdown of the antagonist PARG induced significant alterations in chromatin mobility (Figure 30). It can be concluded that even though poly-ADP-ribosylation is known to effect chromatin structure, those alterations are not sufficient to vary mobility of DSB containing chromatin in the observed spatial scale.

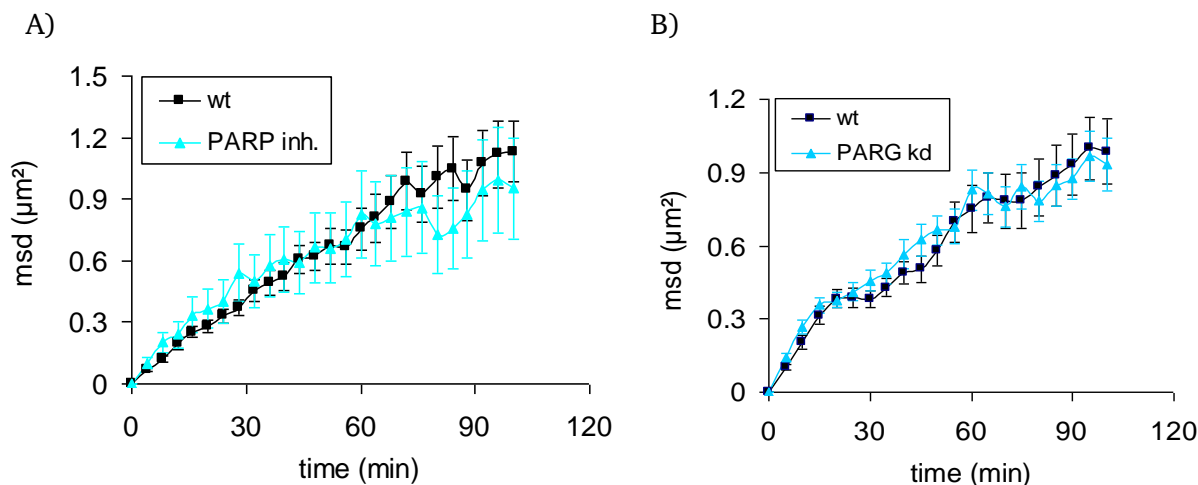


Figure 30 – Influence of poly-ADP-ribosylation on DSB mobility

A) Comparison of the msd of IRIF in cells after inhibition of PARP (blue) ($n = 15$) and controls (black) ($n = 17$). Cells were irradiated with C (LET: $170 \text{ keV}/\mu\text{m}$). B) Msd of IRIF in cells after knockdown of PARG (blue) ($n = 15$) and non-treated controls (black) ($n = 11$). Cells were irradiated with Cr (LET: $2360 \text{ keV}/\mu\text{m}$). Both plots show an independence of poly-ADP-ribosylation on DSB mobility. Errors represent SEM.

3.4. Inhibition of ATM confines mobility of broken chromatin sites

3.4.1. ATM alters mobility of high LET irradiation induced DSBs

Induction of DSBs activates several signal cascades to promote DNA repair. Initiated by binding of the MRN complex, ataxia-telangiectasia mutated (ATM) kinase is recruited and acts as a main player in DNA damage signaling. Phosphorylation by ATM regulates recruitment of repair proteins, cell cycle arrest, apoptosis and changes in chromatin structure. Therefore the influence of ATM on DSB mobility was determined. In order to address this question specific ATM inhibition as well as a more general inhibition of PIKK kinases was applied. Caffeine inhibits PIKK family proteins dependent on its concentration. PIKK family proteins include ATM, ATR and DNA-PKcs, all acting in DNA damage signaling (Shiloh, 2003). The used concentration of 10 mM caffeine inhibits mainly ATM and to a lesser extent ATR. DNA-PKcs has a higher IC_{50} value for caffeine and should be only slightly affected by this treatment (Sarkaria et al., 1999). Tracking of IRIF revealed a strong bending of the msd curve, starting about 30 min after irradiation due to treatment with caffeine (Figure 31).

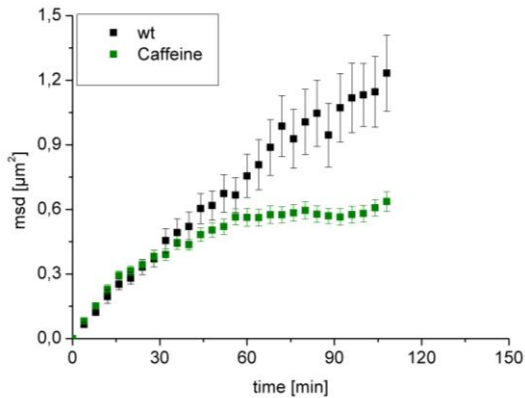


Figure 31 – Caffeine confines mobility of IRIF

Msd plots of 53BP1 foci after irradiation with C (170 keV/μm) for wildtype (black) (n = 15) and cells treated with 10 mM caffeine (green) (n = 48). Errors represent SEM.

To determine if the kinase function of ATM accounts for this effect specific inhibition of ATM by 15 μM Ku55933 was applied. Efficiency of inhibition was tested by irradiation of U2OS-53BP1-GFP cells with 1 Gy X-rays and subsequent immunostaining for auto-phosphorylation of ATM at serine 1981 (pATM). Control cells exhibit a strong pATM signal, colocalizing with 53BP1 and marking sites of induced DSBs. Inhibition of ATM hampers phosphorylation and the recruitment of phosphorylated ATM to DSBs (Figure 32).

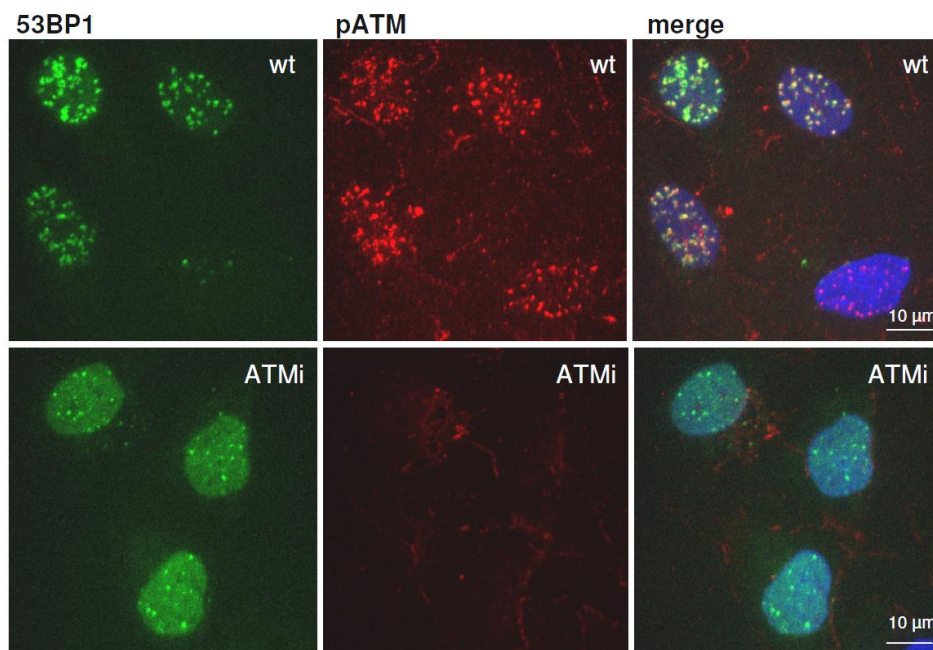


Figure 32 – ATM inhibition observed by immunofluorescent staining of U2OS-53BP1-GFP cells

U2OS-53BP1-GFP cells irradiated with 1 Gy X-rays, fixed after 30 min and stained for pATM (red) and DNA (blue). Efficiency of ATM kinase inhibition (ATMi) was show by loss of pATM signal compared to wildtype cells (wt).

Even though ATM is a central player in the DNA damage response and affecting γ H2AX formation as well as MDC1 recruitment, 53BP1 foci still form after inhibition of ATM activity. However, a delay in the recruitment of 53BP1 was observed after charged particle as well as after photon irradiation (data

not shown). Live cell microscopy started in average 30 minutes post irradiation, a time when all 53BP1 foci already accumulated and measurements were not influenced from this delay.

Tracking of individual 53BP1 foci after irradiation with Cr (LET: 2630 keV/ μm) displays a drastic reduction in the msd from 1.0 μm^2 in control to 0.53 μm^2 in ATM inhibited cells at the end of an observation period of 100 minutes (Figure 33). Compared to the reduced movement after treatment with caffeine the effect is even more pronounced after specific inhibition of ATM and a bending of the msd curve can be observed from the beginning on.

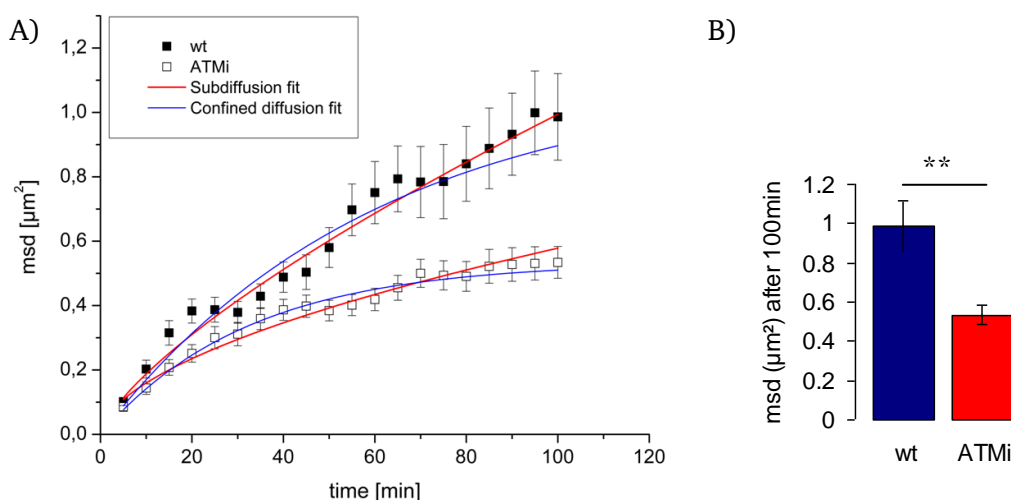


Figure 33 – Influence of ATM on DSB mobility after charged particle irradiation

A) Msd plots of control (solid squares) ($n = 11$) and ATM inhibited cells (open squares) ($n = 31$) after irradiation with Cr (LET: 2630 keV/ μm). Fits for subdiffusion (eq. 12) (red lines) and confined diffusion (eq. 11) (blue lines) were applied. B) Bar graphs show a highly significant reduction of the average msd after 100 min observation time for ATM inhibited cells compared to controls after irradiation with Cr. Errors represent SEM in both figures.

By applying a fit for subdiffusion a drop of the α value from 0.72 ± 0.03 in wildtype to 0.56 ± 0.02 in ATM inhibited cells was obtained. Inhibition of ATM seems to provoke a strong hindrance to the subdiffusional behavior of foci as seen by the reduced α value and the change of the diffusion coefficient D_c from $5.1 \times 10^{-5} \mu\text{m}^2/\text{s}$ for wildtype cells to $4.6 \times 10^{-5} \mu\text{m}^2/\text{s}$. Fits for subdiffusion as well as for confined diffusion both match the experimental data with a similar R^2 ($R^2 = 0.98$ for subdiffusion vs. 0.99 for confined mobility in ATM inhibited samples and $R^2 = 0.98$ for subdiffusion vs. 0.96 for confined mobility in wildtype cells).

Using the model of confined motion, the predicted confinement radius for DSB mobility in wildtype cells was $1.05 \pm 0.07 \mu\text{m}$ while ATM inhibition resulted in a confinement to a much smaller radius of $0.73 \pm 0.01 \mu\text{m}$ in the corresponding experiment (for comparison see Figure 49). This reduction of the confinement radius leads to a reduction of the sampled volume within the cell nucleus by a factor of three ($4.85 \mu\text{m}^3$ vs. $1.63 \mu\text{m}^3$).

3.4.2. Effect of ATM inhibition after X-ray irradiation

Heavy ion irradiation induces high numbers of DSBs in close proximity which was shown to lead to a hyperactivation of ATM (Meyer et al., 2013). To examine if the reduction of mobility in ATM inhibited cells is dependent on radiation quality comparative studies were performed by the induction of isolated DSBs with 1 Gy of photon irradiation (X-rays).

Individual 53BP1 foci after irradiation with 1 Gy X-rays were tracked and analyses of msd plots confirmed a confinement in mobility due to inhibition of ATM also in the case of low LET irradiation (Figure 34).

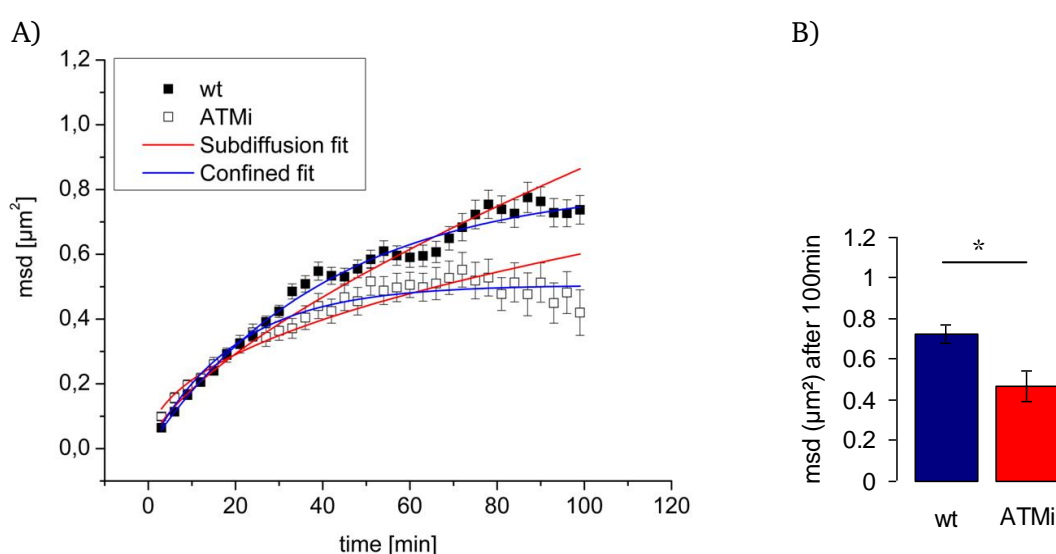


Figure 34 – Mobility of X-ray induced damage is reduced after inhibition of ATM

A) Msd plots of control (solid squares, $n = 21$) and ATM inhibited cells (open squares, $n = 11$) irradiated with 1 Gy X-rays. Fits for subdiffusion (eq. 12) (red lines) and confined diffusion (eq. 11) (blue lines) are applied. B) Bar graphs of the msd after 100 min observation time show a significant decrease in the msd of ATM inhibited cells. Errors represent SEM in both figures.

In this experiment mobility of wildtype cells was found to be lower than in most other experiments and slightly better described by a confined diffusion than by subdiffusion ($R^2 = 0.99$) vs. ($R^2 = 0.97$). ATM inhibition leads to a more pronounced confinement of DSB mobility and a change in the resulting diffusion coefficient from $7.1 \pm 0.3 \times 10^{-5} \mu\text{m}^2/\text{s}$ in wildtype to $5.6 \pm 0.1 \times 10^{-5} \mu\text{m}^2/\text{s}$ in ATM inhibited cells indicating a stronger confinement over time as observed after irradiation with chromosome ions (Figure 33). Resulting confinement radii were found to be in the same range in both experiments after inhibition of ATM yielding $0.71 \pm 0.01 \mu\text{m}$ after irradiation with X-rays and $0.73 \pm 0.01 \mu\text{m}$ after charged particle irradiation. Meanwhile the confinement radius in wildtype cells after X-ray irradiation was $0.90 \pm 0.01 \mu\text{m}$ proving a reduction in the sampled volume from $3.05 \mu\text{m}^3$ to $1.5 \mu\text{m}^3$.

Taken together the experiments show a significant decrease in mobility of DSB containing chromatin domains due to inhibition of ATM, independent on the used irradiation quality. The msd after photon irradiation was reduced in case of control as well as for ATM inhibited cells. As described in chapter 3.2.3. variations in the extent of mobility between individual experiments might be attributed to influences of culturing conditions. The fact that ATM strongly reduces mobility independent on irradiation quality proves the importance of this finding and opens new questions determining the mechanism of action, which might be attributed to changes in chromatin structure.

3.5. Tethering of DNA strands by Cohesin or the MRN complex

Not only accumulation of repair proteins or a change in the chromatin density surrounding the DSB, but also a direct interaction of DNA strands could account for differences in mobility kinetics. Tethering of DNA strands is a known mechanism in processes like mitosis, transcription or gene regulation. By binding of protein complexes DNA strands like sister chromatids are kept in close proximity, a function which can be expected to influence mobility of DSBs. Two mayor complexes act in tethering of DNA strands and play a role in DNA damage repair (Dorsett and Ström, 2012; Thompson, 2012): the Cohesin complex, which maintains sister chromatid cohesion and helps strand invasion in HR repair (Wu and Yu, 2012) and the MRN complex that is known to tether broken DNA strands (Lammens et al., 2011).

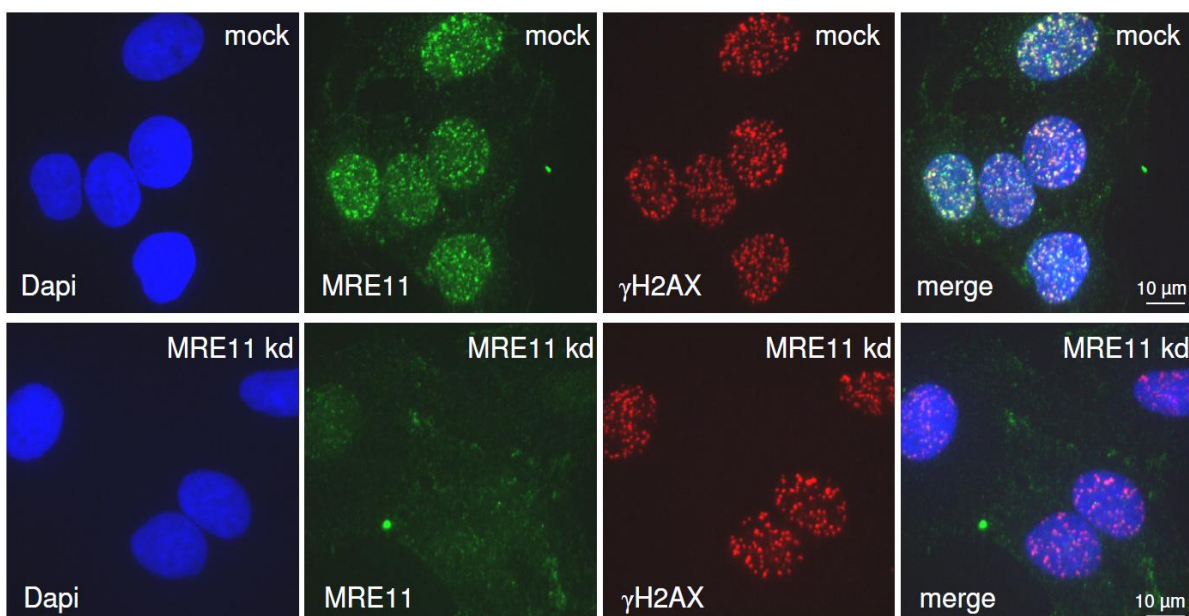


Figure 35 – Knockdown of MRE11 hampers recruitment of MRE11 to DSBs

Efficiency of siRNA mediated knockdown of MRE11 is proven by immunofluorescent staining of MRE11 in U2OS cells treated with 2 Gy X-rays and fixed after 15 minutes incubation. While γ H2AX foci (red) still form MRE11 (green) recruitment is strongly reduced. Nuclei are stained by Dapi (blue).

Loss of one of those tethering complexes was expected to locally decrease chromatin stability, especially in the surrounding of multiple DSBs as induced by heavy ion irradiation. To test this hypothesis MRE11, a key component of the MRN complex and SMC1, part of the backbone of the Cohesin complex were knocked down in independent experiments. By siRNA treatment a 5 fold reduction of the respective protein levels was reached as shown by western blot analyses (Figure 36). Knockdown efficiency of MRE11 was moreover proven by immunofluorescence staining (Figure 35). Photon irradiation causes the recruitment and accumulation of MRE11 at DSBs. Recruitment of MRE11 prevented the accumulation of MRE11 to the break site in 75 % of cells and remaining cells showed strongly reduced accumulation of MRE11. Accumulation of the repair protein γ H2AX was not impaired.

53BP1 accumulates in distinct foci and no differences of this accumulation could be observed in cells depleted of MRE11 or SMC1 (data not shown). Tracking of 53BP1 foci after irradiation with lead (LET: 13500 keV/ μ m) revealed no significant differences in mobility of wildtype compared to knockdown cells (Figure 36).

Likewise, knockdown of the human SCC2 analogue loading factor NIPBL to prevent loading of the functional Cohesin complex onto DNA, showed no increased movement compared to wildtype or SMC1 depleted cells (Figure 37).

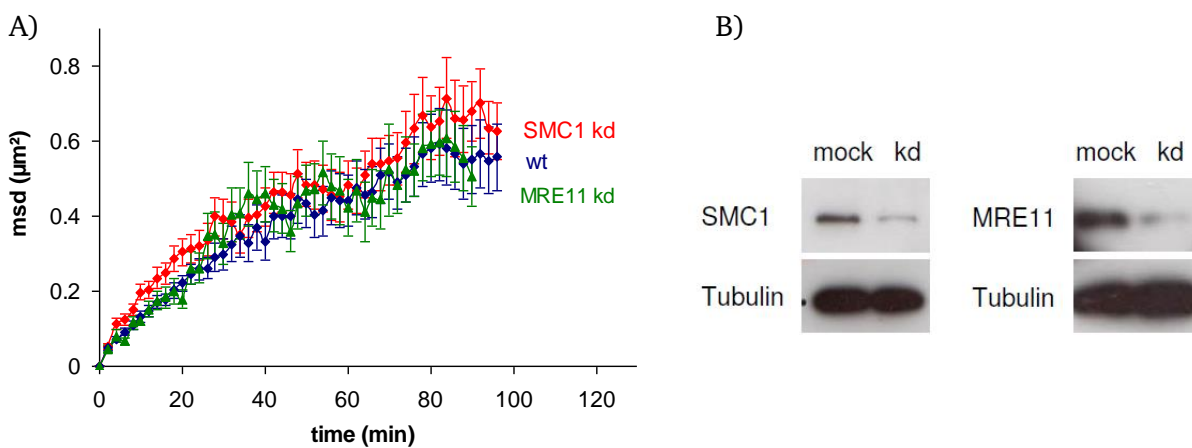


Figure 36 – Tethering of DNA strands does not influence DSB mobility

A) Mean square displacement (msd) of 53BP1 foci after irradiation with Pb (LET: 13500 keV/ μ m) is plotted against time for control (blue) (n = 11), SMC1 knockdown (red) (n = 11) and MRE11 knockdown cells (green) (n = 10). Errors represent SEM. B) Western blots of U2OS cells 48h after knockdown of SMC1 and MRE11 with Tubulin as loading control. No difference in mobility of DSBs occurs due to knockdown of SMC1 or MRE11.

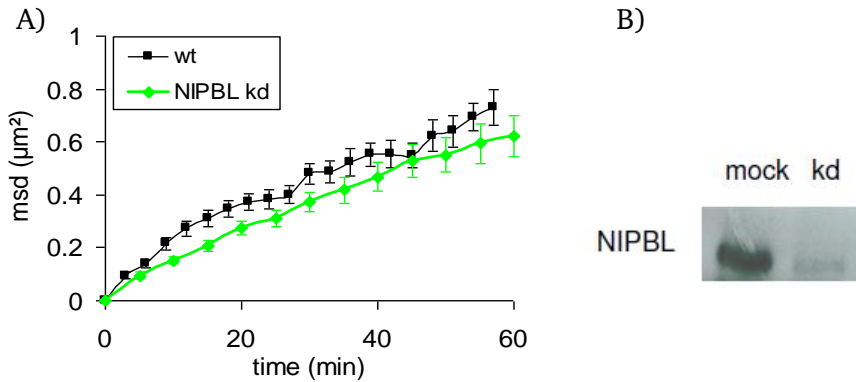


Figure 37 – Knockdown of NIPBL does not increase the msd of radiation induced 53BP1 foci

Msd plots of 53BP1 foci after irradiation with U (15000 keV/μm) is plotted against time for wildtype (blue) (n = 25) and NIPBL knockdown cells (green) (n = 18). Errors represent SEM. B) Western blot of U2OS cells knocked down of NIPBL, 48h after siRNA treatment.

3.5.1. Cell cycle analyses

The Cohesin complex is known to act cell cycle dependent (Dorsett and Ström, 2012). As cohesion of sister chromatids during HR takes place only in S/G2 phase, knockdown of SMC1 is expected to cause a stronger effect on DSB mobility during these stages of the cell cycle. MRE11 can tether proximal ends of DSBs as well as DNA strands. Likewise, an increased importance of MRE11 is expected during cell cycle phases in which sister chromatids are available. During HR repair sister chromatids can be tethered to the unrepaired break either by MRE11 or Cohesin.

To determine the cell cycle phase during live cell microscopy, advantage was taken from a double transfected cell line. These U2OS cells were stably expressing a GFP-tagged cell cycle marker together with the tagged repair protein NBS1-cherry. NBS1 was proven to exhibit mobility in the same range as 53BP1 (chapter 3.1.3) thus acting as a comparable cell system for mobility studies. The cell cycle marker in the used U2OS-G1/S-GFP NBS1-cherry cells consists of a GFP-tagged version of the localization domain (PSLD) of helicase B. By phosphorylation of this domain a transport between the nucleus and cytoplasm is mediated. During G1 phase the GFP-tagged domain is found inside the cell nucleus while in late G1/early S Phase a translocation to the cytoplasm starts which is completed in G2 phase (Figure 38) (Gu et al., 2004). Together with the fluorescently tagged repair protein NBS1 this system allows a cell cycle dependent observation of DNA damage.

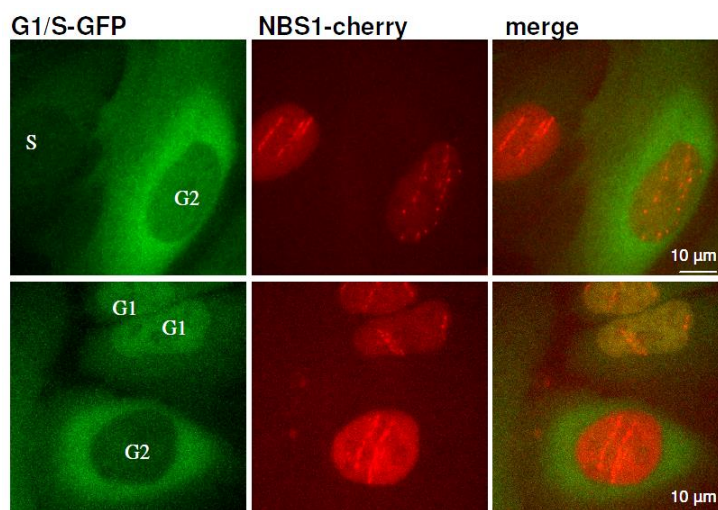


Figure 38 – Simultaneous determination of cell cycle phase and DSB sites

Immunofluorescent images (maximum projection) of U2OS-G1/S-GFP NBS1-cherry cells after irradiation with U (15000 keV/ μm). Cell cycle phases can be revealed by PSLD-GFP distribution in the cell nucleus (green) as well as the accumulation of NBS1 along the ion traversals (red).

To first test the new cell system independent on cell cycle phase, knockdowns of MRE11 as well as double knockdown of SMC1 and NIPBLE to prevent formation, as well as loading of the Cohesin complex were performed in U2OS-G1/S-GFP NBS1-cherry cells. After irradiation with uran ions mobility of occurring NBS1 foci was determined (Figure 39). Tracking NBS1 foci in these cells, independent of cell cycle phase, confirmed an independency of DSB mobility on tethering of DNA strands. In the new cell system of U2OS-G1/S-GFP NBS1-cherry cells foci mobility was higher compared to U2OS-53BP1-GFP cells. Double transfection causes cellular stress why this cell line responds more sensitive to radiation or light emission during microscopy, exhibiting enhanced mobility and deformation effects.

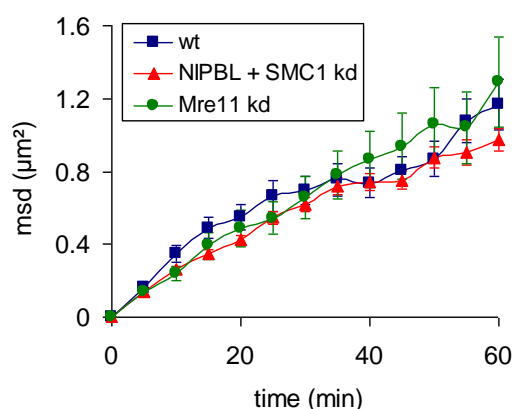


Figure 39 – DSB mobility in U2OS G1/S-GFP NBS1-cherry cells

A) Msd plot revealing mobility of U2OS-G1/S-GFP NBS1-cherry cells irradiated with U (15000 keV/ μm) independent on cell cycle phase. Plots show mobility of cells after knockdown of MRE11 (n = 6) (green), double knockdown of NIPBL and SMC1 (n = 12) (red) or control cells (blue) (n = 13). Error bars represent SEM.

U2OS-G1/S-GFP NBS1-cherry cells analyzed for DSB mobility in Figure 39 were plotted separately regarding their cell cycle to investigate a possible influence of the cell cycle phase on chromatin mobility. Only cells, which could be clearly assigned to a cell cycle phase, were used. Wildtype cells were divided into a group containing G1 and S phase cells and one group containing G2 phase cells. Cells knocked down in NIPBL and SMC1 were divided into a group of G1 and a group of G2 phase cells. As foci mobility already varies between individual cells for each cell the median mobility of all foci was plotted (Figure 40). Due to a low number of cells which could be clearly assigned to one cell cycle phase no plot of cells knocked down in MRE11 is shown.

In wildtype cells a tendency of G2 cells to exhibit higher mobility than S/G1 cells can be observed (Figure 40A). A comparison between G1 and G2 phase in NIPBL and SMC1 knockdown cells showed relatively high variations between individual cells and no clear cell cycle phase dependency (Figure 40B). To obtain reliable statistics for individual cell cycle phases higher numbers of cells and experiments are needed and cell cycle dependent results can only serve as preliminary data so far. However, by the introduction of this cell cycle revealing cell system further studies can contribute to the observed characteristics of DSB dynamics regarding influences of the cell cycle.

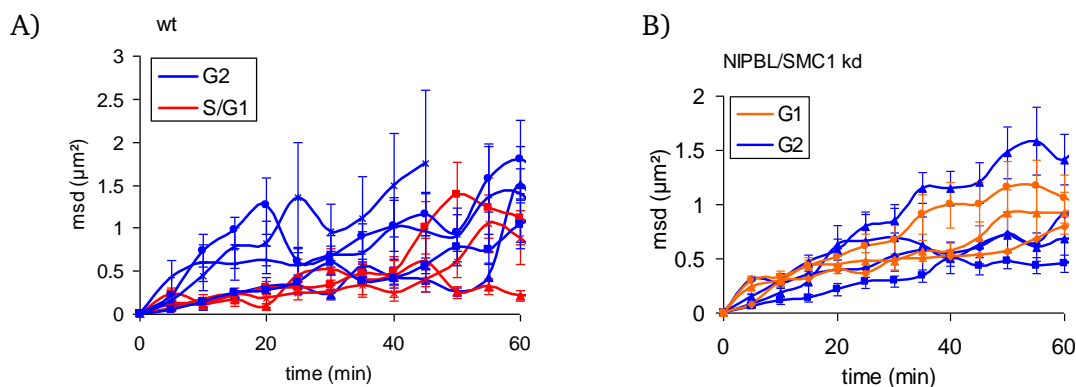


Figure 40 – Cell cycle specific determination of foci mobility

Msd plots of U2OS-G1/S-GFP NBS1-cherry cells irradiated with U (15000 keV/μm) tracked for NBS1 depending on cell cycle phase. Error bars represent SEM. A) DSB mobility of wildtype cells in G2 phase (blue) (n = 5) and during S/G1 phase (red) (n = 3). B) DSB mobility of cells after double knockdown of NIPBL and SMC1 during G1 phase (orange) (n = 3) compared to G2 phase (blue) (n = 3).

3.6. Interplay between nuclear matrix proteins and IRIF mobility

The nuclear matrix or skeleton is a filamentous structure inside the nucleus similar to the cytoskeleton. It accounts for nuclear stability and some of its structural elements are moreover related to DNA repair. The main part of the outer nuclear matrix is composed of Lamin A/C, which also occupies the inner nuclear matrix in reduced levels together with NuMA, other nuclear matrix proteins and ribonuclear proteins. By eliminating parts of the nuclear matrix it was intended to diminish stability

and function of the nuclear skeleton to investigate its influence on chromatin dynamics. Knockdown of Lamin A/C led to 9 % remaining protein level as observed by western blotting (Figure 41). By this treatment mainly stability of the outer nuclear lamina should be affected. Knockdown of NuMA was found to reduce the proteins level around 76 % (Figure 41) and is expected to diminish stability of the inner nuclear matrix.

Knockdown of Lamin strongly affects cell viability and cells tended to deform and detach from the surface after loss of Lamin A/C (data not shown). However, 53BP1 still accumulated at sites of DNA breaks after X-ray irradiation. While knockdown of NuMA revealed only a slight enhancement (31 %) of DSB mobility treatment with siRNA against Lamin A/C provokes a significant increase in mobility (72 % after 130 minutes) (Figure 41). Knockdown of NuMA resulted in an enhanced α value from 0.61 ± 0.01 in control to 0.72 ± 0.02 and the slope is better described by subdiffusion ($R^2 = 0.98$) than confined diffusion ($R^2 = 0.93$). In contrast, cells knocked down of Lamin A/C exhibit the same α value as non-treated cells (0.60 ± 0.01). However, the diffusion coefficient is raised from $4.5 \pm 0.2 \times 10^{-5} \mu\text{m}^2/\text{s}$ in wt cells to $8.1 \pm 0.2 \times 10^{-5} \mu\text{m}^2/\text{s}$ after knockdown of Lamin A/C while the diffusion coefficient is only slightly affected by knockdown of NuMA ($3.6 \pm 0.2 \times 10^{-5} \mu\text{m}^2/\text{s}$). Even though the diffusion coefficients differ, cells are displaying a similar confinement radius after knockdown of NuMA ($1.01 \pm 0.06 \mu\text{m}$) or Lamin A/C ($1.04 \pm 0.02 \mu\text{m}$). In both cases the radius is enhanced around 25 % compared to the wildtype cells ($r_c = 0.80 \pm 0.02 \mu\text{m}$) leading to an increase in the sampled volume by the factor of 2 ($2.1 \mu\text{m}^3$ in wt vs. $\sim 4.5 \mu\text{m}^3$ after knockdown of NuMA or Lamin A/C). However, those experiments remain preliminary results and need to be repeated. Further investigations should reveal more details on the interplay between nuclear matrix and DSB repair.

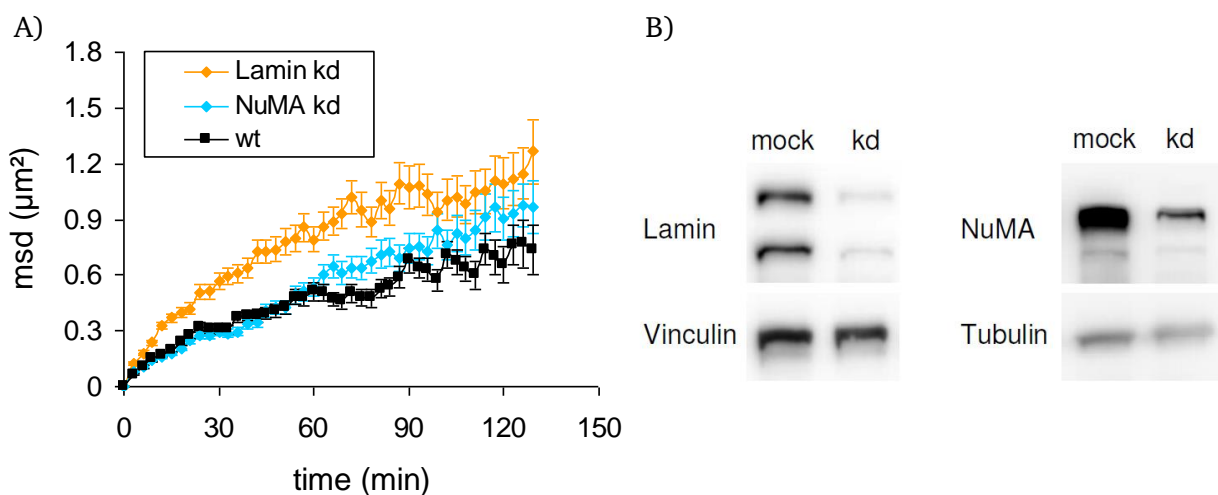


Figure 41 – Influence of nuclear matrix proteins on DSB mobility

A) Msd plot of tracked 53BP1 foci after irradiation with 1 Gy X-rays in wildtype cells (black) ($n = 8$) compared to cells knocked down in NuMA (blue) ($n = 8$) or Lamin A/C ($n = 5$) (orange). A significant difference between wildtype and Lamin A/C depleted cells was observed. Error bars represent SEM B) Western blot reveals knockdown efficiency of Lamin A/C (91 % reduction) and NuMA (76 % reduction).

3.7. Nuclear matrix interactions with repair proteins

A contribution of the nuclear matrix to repair of DSBs was investigated by an approach independent on mobility analyses. Nuclear extractions were performed using DNA digestion and extraction of unbound proteins from the cell nucleus. Following such a procedure electron microscopic studies revealed a network of highly structured branched fibers, connected to the nuclear lamina – the nuclear matrix (Nickerson et al., 1997). By immunofluorescent microscopy removal of DNA as shown by the absence of DAPI staining can be visualized. RNA is not extracted by this approach and remaining RNA can be observed by propidium iodide (PI) staining, marking RNA containing nucleoli after extraction procedures. This staining pattern was used as a positive control for complete digestion of DNA during extraction studies.

By applying a nuclear extraction protocol with PFA mediated fixation prior to DNase I digestion (chapter 2.1), matrix-binding nuclear proteins could be visualized by immunofluorescence staining (Figure 42). In first experiments the extraction of histones was elucidated after complete extraction of DNA, proven by the absence of Dapi and PI staining. Histone 3 (H3) staining together with staining of the phosphorylated form of ATM following nuclear extraction in U2OS cells is shown in Figure 42. As expected histone H3 was found in the whole cell nucleus in control cells without DNase I digestion. After removal of DNA a low level of homogenous distributed H3 remained in the nucleus. However, in the same experiment distinct foci of pATM mark sites of naturally occurring DSBs in control cells, which could not be observed after digestion with DNase I. Only a low background level of pATM was not extracted from the nucleus after digestion of DNA and remained visible (Figure 42).

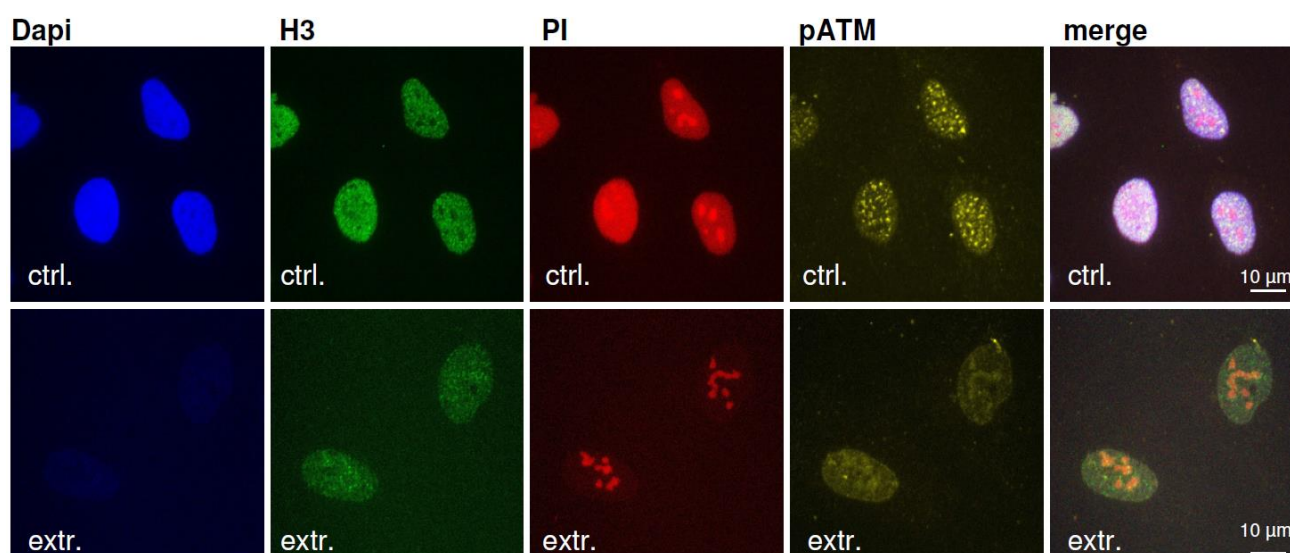


Figure 42 – Nuclear extraction of U2OS cells

Unirradiated U2OS cells were fixed with PFA and a nuclear extraction was performed with (extr.) and without (ctrl.) DNase I digestion. Cells are stained for Dapi (blue), histone 3 (green), PI (red) and pATM (yellow). Extracted cells show the absence of DNA but a background of H3 and pATM remain visible.

During this experiment many unirradiated U2OS cells already showed high DNA damage levels as seen by accumulations of repair proteins like pATM, 53BP1 or MRE11. DNase I digestion and extraction removed focal accumulations of pATM but focal accumulations of 53BP1 and MRE11 as well as a sprinkled nuclear background of both proteins remained visible (Figure S 1 and Figure S 2). In contrast, MDC1 is found in the whole cell nucleus in control cells and is extracted completely after digestion of DNA (Figure S 2).

PFA cross-links proteins mostly by a $-CH_2-$ linkage between primary amino groups and nitrogen atoms in proteins or DNA. This cross-linking prior to DNA digestion can influence the extraction of proteins from the cell nucleus. Proteins might be cross-linked to proteins of the nuclear matrix if they are in close proximity even though no natural interaction occurs. To avoid a misinterpretation of interactions between repair proteins and the nuclear skeleton the extraction protocol was modified to complete DNase I containing extraction of proteins prior to fixation of cells. Moreover, irradiation was applied to visualize accumulations of repair proteins at DSBs. In U2OS cells soluble proteins were extracted by applying two extraction buffers (Streck 1 and 2, see methods for details). Irradiation with 2 Gy X-rays leads to the accumulation of repair proteins like 53BP1 or pATM, clearly visible in distinct foci after protein extraction without digestion of DNA (Figure 43). However, combining extraction and DNA digestion led to almost complete loss of both proteins in the cell nucleus (Figure 43).

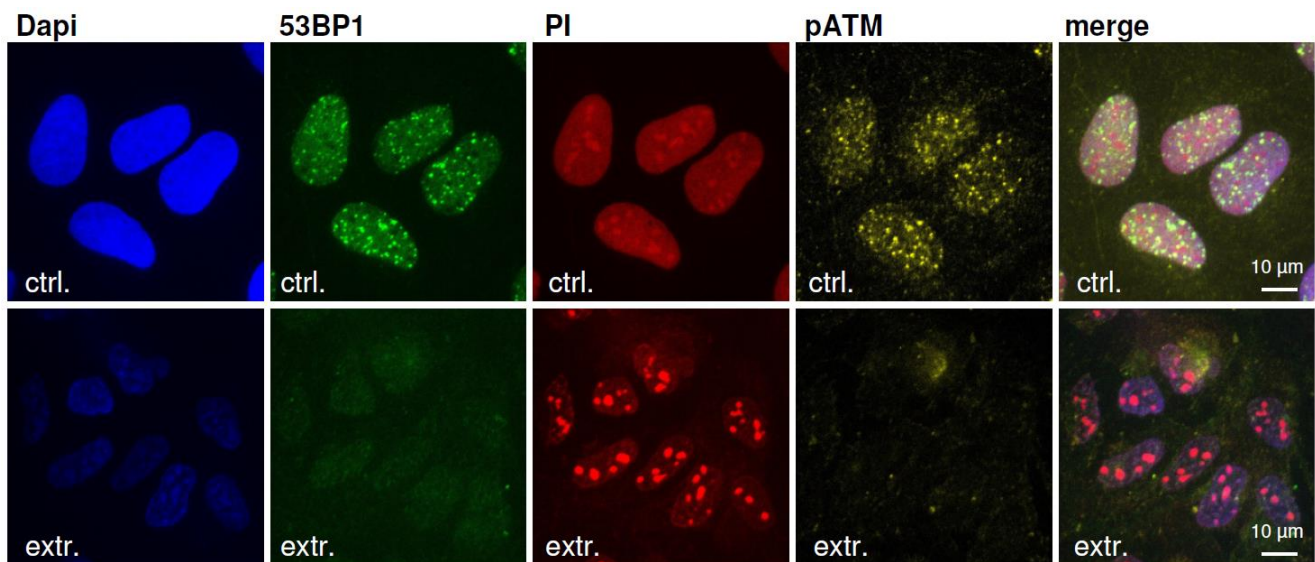


Figure 43 – Labeling of 53BP1 and pATM after nuclear extraction.

U2OS cells were irradiated with 2 Gy X-rays and incubated for 20 minutes. Nuclear extraction was applied (extr.), removing repair proteins 53BP1 (green) and pATM (yellow). Upper row (ctrl.) served as a control without DNase I digestion. Absence of DNA staining by Dapi (blue) and DNA/RNA staining by PI (red) reveal completeness of DNA digestion.

To further investigate contributions of the nuclear matrix to the recruitment and accumulation of repair proteins, other proteins known to accumulate at sites of broken DNA were analyzed.

Accumulation of MRE11 and formation of γ H2AX at DSBs was clearly visible after irradiation with 2 Gy X-rays (Figure 44). By nuclear extraction and digestion of DNA, histones are removed together with DNA, visualized by the absence of γ H2AX inside the nucleus. However, it was observed that focal accumulations of MRE11 remained inside the nucleus after extraction and removal of DNA (Figure 44). MRE11 foci were reduced in number but a subset remained visible.

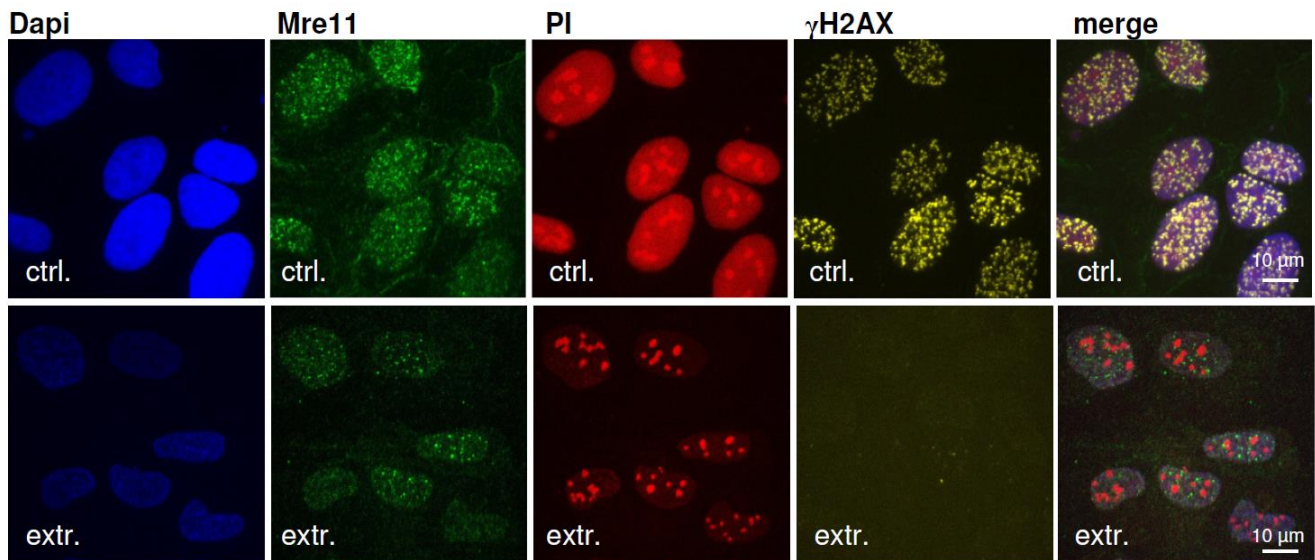


Figure 44 – Immunofluorescent labeling of repair proteins after nuclear extraction.

U2OS cells 20 min post irradiation with 2 Gy X-rays. Nuclear extractions were applied (extr.) compared to controls (ctrl.) without digestion of DNA. A subset of MRE11 foci (green) remains after extraction while γ H2AX (yellow) is completely removed. Absence of DNA (blue) and DNA/RNA staining by PI (red) reveal completeness of extraction.

PFA mediated fixation prior to DNA digestion leads to a low remaining level of 53BP1, pATM and histone 3 in the nucleus while almost complete removal of all these proteins can be seen by digestion without prior PFA fixation. It can be suggested that cross-linking of proteins by PFA impairs the efficient proteins extraction. To prevent this influence following studies were all carried out by DNA digestion prior to fixation. However, nuclear extractions of U2OS cells also revealed some cases where 53BP1 is not extracted completely but remains inhomogenously scattered throughout the nucleus (Figure S 3). The nuclear matrix consists of several filamentous proteins like Lamins or NuMA. By immunofluorescent staining of NuMA parts of the nuclear matrix were visualized serving as a control of the remaining nuclear matrix following extraction. Without extraction a homogenous nuclear distribution of NuMA was found during interphase of U2OS cells. Extraction of DNA and proteins leads to a strongly reduced immunofluorescence signal of NuMA (Figure 45) most probably revealing protein levels contributing to the filamentous network of the nuclear matrix.

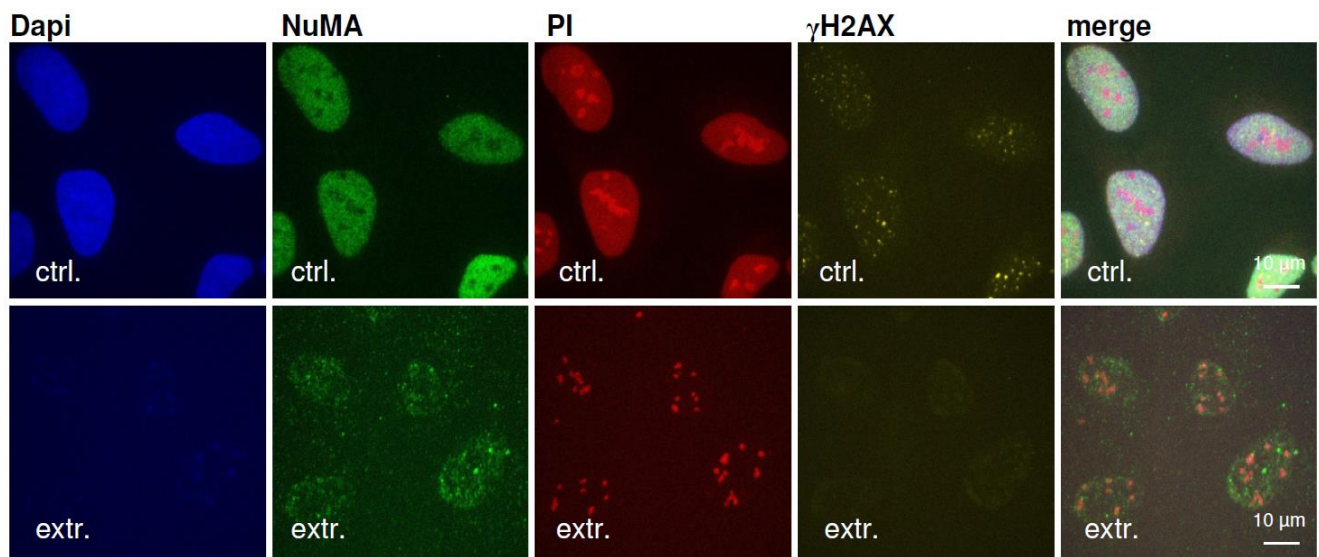


Figure 45 – NuMA signal is reduced after nuclear extraction of U2OS cells

U2OS cells after nuclear extraction (extr.) and controls without DNase I digestion (ctrl.). Cells are stained for Dapi (blue), NuMA (green), PI (red) and γ H2AX (yellow). Extraction is complete as shown by removal of DNA and histone γ H2AX. NuMA levels are reduced after extraction.

Nuclear extraction and digestion of DNA prior to fixation of cells causes cellular stress and cells detach from the surface with increasing extraction time. Therefore the extraction time, DNase I concentration and buffer conditions needed to be optimized ensuring complete digestion and extraction of DNA without the induction of cell death and detachment from the surface. To determine if human fibroblasts (AG) show less detachment from the surface by extraction, experiments were carried out under the same conditions in AG cells. No differences were found in AG cells compared to U2OS cells following the extraction treatment and a similar retention of radiation induced MRE11 foci could be observed (Figure S 4). However, by staining of NuMA differences in the protein localization pattern were observed without extraction. An inhomogenous distribution of NuMA throughout the cell population was found. Cells were exhibiting either a strong and homogenous staining as seen in U2OS cells, a weak homogenous signal or in few cases a distribution of NuMA in distinct foci (Figure 46). The appearance of each pattern could not be related to size or DNA content of the nucleus and is not induced by DSBs as cells were not exposed to irradiation. By DNase I mediated nuclear extraction the signal was reduced compared to the strong homogenous pattern but remained and focal accumulations of NuMA could only be detected in few cases (Figure S 5).

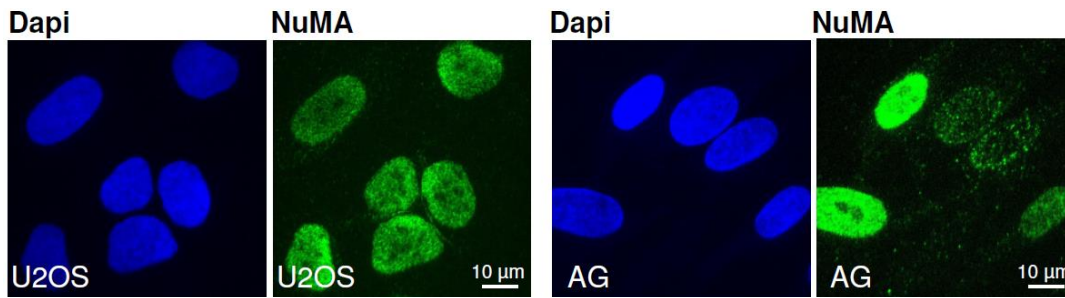


Figure 46 – Distribution of NuMA in U2OS compared to AG cells

U2OS and AG cells were extracted without DNase I digestion and fixed afterwards. Staining of DNA (blue) and NuMA (green) reveals a different distribution pattern of NuMA in both cell lines. While U2OS have a homogenous distribution of NuMA, AG cells show moreover focal distribution and differences in staining intensity.

As knockdown of NuMA and Lamin A/C resulted in an enhanced mobility of IRIF (Figure 41) the effect of those nuclear matrix proteins on binding and recruitment of repair proteins was determined. NuMA and Lamin A/C were knocked down by siRNA treatment in different experiments. In some cells knockdown of Lamin A/C resulted in strong nuclear deformations (Figure 47). Cells were irradiated with 2 Gy X-rays and nuclear extractions were performed. A reduced recruitment of 53BP1 to DSBs in cells deficient for Lamin A/C was described in the literature (Gonzalez-Suarez et al., 2009b). However, only a slight reduction in 53BP1 foci could be observed in cells knocked down in Lamin (Figure 47) compared to untreated cells (Figure 43). 53BP1 recruitment seems to be independent on NuMA as no differences in the recruitment could be observed after knockdown of NuMA (Figure S 6).

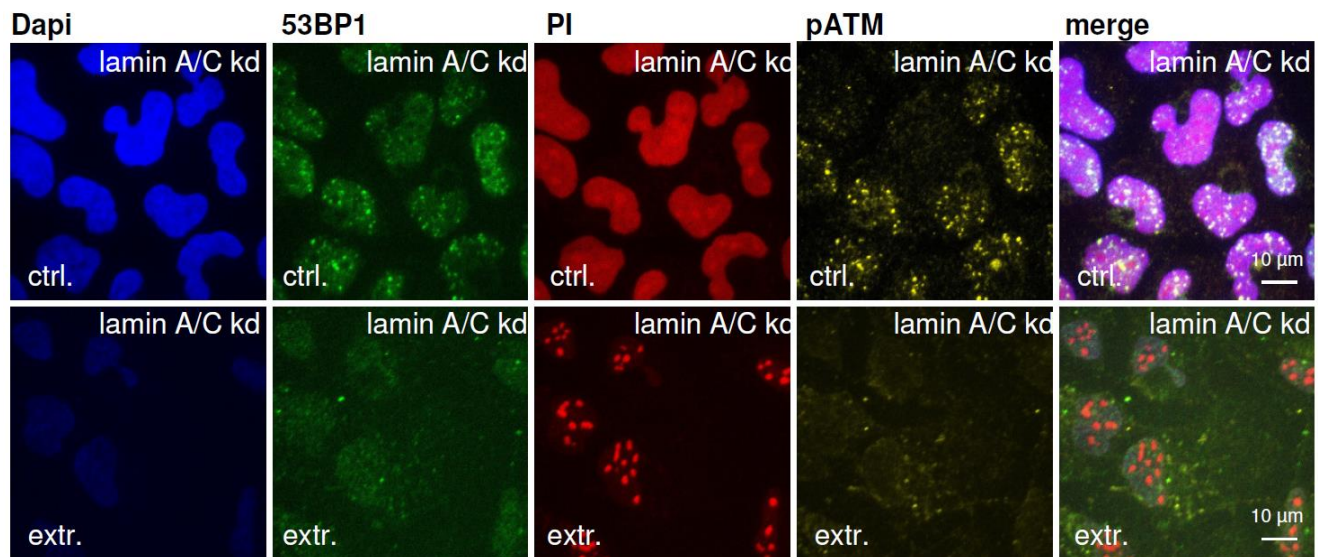


Figure 47 – Extraction of U2OS cells following knockdown of Lamin A/C

U2OS cells 48 hours after knocked down of Lamin A/C were irradiated with 2 Gy X-rays and incubated for 20 minutes. Cells were treated with extraction buffer (ctrl.) and DNase I digestion (extr.) before fixation and stained with Dapi (blue), PI (red), 53BP1 (green) and pATM (yellow).

Foci formation of pATM was not impaired, neither by knockdown of NuMA nor of Lamin (Figure S 6 and Figure 47) and extraction of proteins and DNA revealed no differences in remaining levels of 53BP1 and pATM as both vanished to a large part similar to the observation in wildtype cells (Figure 43). The influence of downregulated nuclear matrix proteins on the retention of MRE11 following nuclear extractions needs to be determined in future experiments.

The results prove that the approach of nuclear extraction combined with immunofluorescent labeling of repair proteins provides a helpful tool to investigate interactions between repair-related proteins and the nuclear matrix. The interaction of MRE11 with insoluble structures of the nuclear matrix gives first insights into dependencies of repair proteins on the nuclear matrix and further studies can provide more insight into these interactions.

4. Discussion

In eukaryotes DNA is highly organized and packed in the nucleus by the formation of chromatin, a highly structured nucleoprotein complex. Different condensation states of chromatin regulate essential cellular processes like cell division, gene regulation or DNA repair (Woodcock and Ghosh, 2010). In the context of DNA repair chromatin structure is known to strongly influence repair kinetics, pathways and repair efficiency (Goodarzi et al., 2008; Shi and Oberdoerffer, 2012). An interplay between chromatin structure and DSB repair was moreover demonstrated by the fact that densely packed chromatin areas relax upon DSB induction, which is expected to facilitate the accumulation of repair proteins at sites of broken DNA (Gontijo et al., 2003; Goodarzi et al., 2010). The DSB induced relaxation or decondensation of chromatin is mediated by various proteins like chromatin remodelers and comes along with the relocation of heterochromatic DSBs to euchromatic areas (Falk et al., 2007; Jakob et al., 2011; Price and D'Andrea, 2013).

Chromosome aberrations like rearrangements favor the development of cancer and can arise by error prone repair of DSBs. It is not yet clear what contributes to their formation. Besides the repair mechanism, current studies consider that movement of chromatin, proximity of induced DSBs and the overall chromatin organization all contribute to the formation of chromosome rearrangements (Dion and Gasser, 2013; Ježková et al., 2014; Roukos et al., 2013). Already a higher probability for chromosomal translocations between proximal chromosome territories could be demonstrated in interphase (Meaburn et al., 2007; Parada and Misteli, 2002). In this context the roaming volume of DSBs is expected to determine interactions between individual DNA ends, leading to the formation of translocations (Parada and Misteli, 2002).

Dynamics of DSBs but also of undamaged chromatin were observed in yeast as well as in mammalian cells. An enhanced chromatin mobility was found by the induction of DSBs which might be related to a local decondensation of chromatin (Krawczyk et al., 2012). DSBs are embedded in the context of chromatin and thus the motion characteristics of DSBs come along with the general mobility of chromatin. In budding yeast a high mobility of DSBs is seen as DSBs form repair centers at the nuclear periphery (Lisby et al., 2003; Nagai et al., 2008; Oza et al., 2009). Recent studies in budding yeast moreover relate enhanced chromosome mobility following DSB induction to a facilitated homology search for HR repair, which is the predominant repair pathway in yeast (Dion et al., 2012; Miné-Hattab and Rothstein, 2012). In mammalian cells several studies described a Brownian movement of chromatin (Marshall et al., 1997) which is slightly enhanced by the induction of DSBs (Krawczyk et al., 2012). However, a general positional stability of DSBs over several hours is shown (Jakob et al., 2009a; Soutoglou et al., 2007), besides few exceptions where enhanced mobility was found (Aten et al., 2004).

4.1. Characteristics of DSB mobility

It is still largely unknown which factors influence chromatin mobility. Therefore this study addressed contributions of DNA repair and chromatin modifying proteins on DSB mobility in mammalian cells. A spreading of repair proteins observed in fixed samples of charged particle irradiated cells gave indications of an enhanced chromatin mobility in specific cell lines (Figure 13) (Jakob et al., 2009a and unpublished results of B. Jakob). While in most cells 18 hours after irradiation remaining tracks of ion traversals were still visible showing a positional stability of DSBs, in some cells a spreading of DSBs over few μm was visible.

To determine a possible influence of repair proteins and chromatin modifying proteins on the dynamic behavior of DSBs, knockdown, inhibition or deficiency of selected repair proteins was used and the mobility of DSBs analyzed. Charged particle irradiation under a low angle as well as X-ray irradiation was used to induce DSBs. In analyses of fixed samples the broadening of the linear irradiation track of repair proteins was used to measure mobility of DSBs at different time points. To determine more detailed mobility kinetics in a submicron range live cell microscopy of GFP-tagged repair proteins was used similar to previous studies (Jakob et al., 2009b; Krawczyk et al., 2012).

The used the mean square displacement (msd) (eq. 7) is well established to measure mobility of particles or IRIF (Dion and Gasser, 2013). As described in chapter 3.2, U2OS cells, stably expressing 53BP1-GFP were used for detection of DSB mobility in living cells. They provide a reliable cell system with relatively stable nuclear shape, where siRNA mediated knockdown of proteins is easily possible. The fluorescent-tagged repair protein 53BP1 serves as a well known DSB marker for tracking mobility of DSB containing chromatin domains. As the absence of the repair mediator protein 53BP1 was shown to reduce mobility of uncapped telomeres (Dimitrova et al., 2008) comparison of DSB mobility with NBS1-GFP ensured that mobility of IRIF was not influenced by the overexpression of 53BP1 (Figure 25) which is in line with previously described results (Krawczyk et al., 2012).

During this thesis, IRIF were found to undergo a diffusive mobility, which can be described by either subdiffusion or confined diffusion similarly well (Figure 26). This result is in line with observations of a subdiffusive type of DSB mobility found by other groups (Girst et al., 2013). Subdiffusion occurs in most biological systems due to viscoelasticity of the surrounding medium, obstruction by cell organelles or other cellular obstacles and binding events (Guigas et al., 2007; Lukacs et al., 2000). Mathematically it belongs to the anomalous diffusion, defined by the power law term α (eq.12) which is <1 for subdiffusion, 1 in normal diffusion and >1 in super-diffusion. Measured wildtype U2OS cells showed α terms between 0.54 and 0.89 with an average of 0.64. These results are in accordance with other findings of subdiffusive DSB mobility and were suggested to support the rejoining of DSB ends compared to a normal diffusion as ends diffuse in a more restricted volume (Girst et al., 2013).

DSB mobility could also be described by the confined mobility model. Especially inhibition of ATM led to a strong confinement and mobility kinetics are better described by confined mobility after inhibition of ATM (Figure 34). Confined mobility is characterized by a defined restrictive space or domain where particles are trapped but can also result from tethering of particles to immobile structures (Platani et al., 2002). For mobility of DSBs a maximal confinement is given by the size of the cell nucleus but restrictions can also be mediated on a smaller scale through chromatin structure and nuclear protein interactions. By matrix attachment sites (MARs) chromatin is tethered to the nuclear lamina (Parada and Misteli, 2002) which can induce a confinement of chromatin mobility.

By fitting observed mobility kinetics to the model of confined mobility the diffusion coefficient D and confinement radius r_c (eq.11) were determined. The diffusion coefficient of a particle moving in a random Brownian walk is directly proportional to the initial slope of the msd graph (Dion and Gasser, 2013). In the displayed experiments in U2OS cells it ranged between $7 \times 10^{-5} \mu\text{m}^2/\text{s}$ and $2 \times 10^{-4} \mu\text{m}^2/\text{s}$ for wildtype cells. Together with the diffusion coefficient a confinement radius around $1 \mu\text{m}$ in average was determined, predicting the maximum radius the DSB will travel. The average distance and diffusion coefficients were in a range similar to observations of other studies in mammalian cells (Krawczyk et al., 2012; Kruhlak et al., 2006; Roukos et al., 2013). However, absolute values might depend on the time-regime and methods of evaluation.

Compared to yeast, mammalian diffusion coefficients are generally lower (Miné-Hattab and Rothstein, 2013). In budding yeast cells diffusion coefficients from $5 \times 10^{-4} \mu\text{m}^2/\text{s}$ to $10^{-3} \mu\text{m}^2/\text{s}$ were found (Miné-Hattab and Rothstein, 2013). Their nuclei have a far smaller volume than mammalian nuclei. Therefore, in human cells DSB can explore a much smaller percentage of the nuclear volume compared to yeast cells (Chubb and Bickmore, 2003; Miné-Hattab and Rothstein, 2013). DSB mobility was attributed to a facilitated homology search in budding yeast as they use HR repair as the major pathway (Miné-Hattab and Rothstein, 2012). The lower mobility of DSBs in mammals could probably be attributed to the predominant use of NHEJ repair, independent of the cell cycle (Lieber, 2010; Thompson, 2012). However, further factors were expected to be involved in the regulation of chromatin and DSB mobility in both systems. This expectation was confirmed for mammalian cells during this work, showing an influence of repair proteins and nuclear matrix proteins on DSB mobility.

During this study different ion species as well as photon irradiation were used for the induction of DSBs. For example low angle irradiation with chromium ions with a LET of $2630 \text{ keV}/\mu\text{m}$ and a fluence of $2 \times 10^6 \text{ particles}/\text{cm}^2$ corresponds to an absorbed dose of 8.4 Gy . As ion traversals are randomly distributed, the majority of cells will receive two to three traversals but the actual dose of a single cell can vary as it depends on the number and length of tracks. By using X-ray irradiation a homogeneous dose distribution is applied and induced DSBs are not expected to be clustered but separated from each other. 1 Gy photon irradiation induces around 20 DSBs (Löbrich et al., 2010). In

contrast by charged particle irradiation several DSBs per μm can be induced along the trajectory by carbon irradiation with a LET of $170 \text{ keV}/\mu\text{m}$ and hundreds of DSBs per μm by the heavier ions used in this study (Jakob et al., 2003, 2009b; Kase et al., 2008). No systematic dependence of DSB mobility on irradiation quality was found. This result is in line with earlier published results comparing IRIF mobility after X-ray and Ni ion irradiation (Jakob et al., 2009b). However, variations in the extent of mobility were found between individual experiments (Figure 26). The variations might be attributed to the used cell charge and cultivation time, as the experiments were executed over a longer time period. To reduce the influence of this variability on the interpretation of obtained results, only measurements of contiguous experiments were compared.

In experiments using depletion of ATP prior to charged particle irradiation a strong energy dependence of foci mobility could be shown (Figure 27). ATP serves as the main source of energy and cellular functions depend on its availability. In accordance with the observed results other studies have shown that mobility of PML bodies as well as of IRIF was reduced following depletion of ATP (Heun et al., 2001; Krawczyk et al., 2012). This goes along with a compaction of chromatin and reduced chromatin expansion after the induction of DSBs (Kruhlak et al., 2006). These chromatin related changes might be connected to missing chromatin remodeling as chromatin remodelers are ATP dependent (Clapier and Cairns, 2009). In addition to the shown dependency of mobility on the energy metabolism of the cell, the measurements validated the experimental setup and tracking mechanism and illustrated the range in which changes of DSB mobility can be reduced by disturbance of cellular integrity. Analyses of fixed samples complete the validation of the experimental setup, showing possible setup dependent variations in the msd curves in a range below $0.1 \mu\text{m}/\text{hour}$.

4.2. Role of repair proteins and chromatin modifiers on DSB mobility

4.2.1. Chromatin modifications

Mobility of DSBs is expected to go along with mobility of surrounding chromatin and the impact of DSB mediated chromatin alterations on the movement of damaged DNA was determined. Dense chromatin areas might act as a constricting environment and a local decondensation was shown upon induction of DSBs, possibly enhancing mobility of DSBs compared to undamaged chromatin (Goodarzi and Jeggo, 2012; Krawczyk et al., 2012). Several cellular proteins like chromatin remodelers are known to influence changes in chromatin structure after ionizing radiation and therefore serve as potential mediators of DSB mobility (Price and D'Andrea, 2013).

Chromatin remodelers are a class of proteins involved in the regulation of chromatin and act by histone rearrangements and exchanges or sliding and eviction of nucleosomes during the whole cell

cycle (Xu and Price, 2011). Essential cellular functions like gene regulation, transcription, cell division or DNA repair are maintained through this organized remodeling of chromatin (Clapier and Cairns, 2009). Remodelers are separated into 4 large families, each consisting of several proteins, acting solo or in complex on chromatin rearrangements (Bao and Shen, 2007). They consist of an ATP binding domain and utilize energy to mediate structural changes (Clapier and Cairns, 2009). The deficiency of chromatin remodeling by depletion of ATP might be one factor leading to a reduced mobility of DSBs (Figure 27). After the induction of DSBs several chromatin remodelers are recruited to the damage site and act in signaling cascades to mediate ongoing repair (Price and D'Andrea, 2013). The local relaxation of chromatin observed following induction of DSBs is only one action mediated by chromatin remodelers acting in DNA repair (Price and D'Andrea, 2013). The chromatin remodeler ACF1 is one of the mammalian remodelers known to have a direct role in DNA repair (Lan et al., 2010; Sánchez-Molina et al., 2011). It is recruited to DNA damage sites after laser irradiation and cells deficient of ACF1 show a higher sensitivity to ionizing irradiation, a compromised G2/M checkpoint and enhanced apoptosis (Sánchez-Molina et al., 2011). Besides its remodeling activity ACF1 was found to be involved in NHEJ repair as it is required for the accumulation of Ku70/80 at DSBs (Lan et al., 2010).

By knockdown of ACF1 the influence of DNA repair mediated chromatin remodeling on mobility of DSB containing chromatin was determined. Tracking of 53BP1 foci revealed a slight reduction in the slope of the msd curve after knockdown of ACF1, which however was not significantly below the wt (Figure 28). As multiple chromatin remodeler complexes are involved in the promotion of chromatin rearrangements during DNA repair (Price and D'Andrea, 2013), possibly working in part redundantly, it is likely that knockdown of a single remodeler is not sufficient to account for larger changes in chromatin structure, promoting DSB mobility. This is in line with findings that inhibition of the remodeler TIP60 alone did not lead to differences in mobility of IRIF (Krawczyk et al., 2012). Moreover, it can be assumed that the chromatin remodeler only mediates changes in chromatin structure in a range of few nucleosomes and does not affect the general chromatin organization to a larger extent. However, the drastic reduction of mobility observed after ATP depletion (Figure 27) might be at least partly related to multiple chromatin remodeling processes in the surrounding of DSBs and further studies depleting multiple chromatin remodeling complexes would be needed to determine remodeling dependent changes in DSB dynamics.

Enzymatic cascades of various proteins mediate changes in chromatin structure. In this context poly-ADP-ribosylation by PARP1 was expected to have a pronounced effect on chromatin structure as it is a mediator of DNA damage repair upstream of most remodeling complexes and several pathways are known in which PARP1 and its poly-ADP-ribosylation mediate changes in chromatin structure. PARP1 is one of the first proteins recruited to DNA damage sites (Haince et al., 2008). The attachment of

poly-ADP-ribose (PAR) moieties on PARP1 and other acceptor proteins like histones and DNA repair factors serves as a signaling instrument for the recruitment of repair factors as well as chromatin remodeling proteins to the damage site (Thomas and Tulin, 2013). Poly-ADP-ribose glycohydrolase (PARG) degrades the PAR chains afterwards and the dynamic turnover of PAR is needed for the proceeding of DNA repair, checkpoint control, apoptosis and the maintenance of genomic integrity (Gagné et al., 2008).

One of the earliest characterized effects of PARP1 on chromatin structure was poly-ADP-ribosylation of histones, leading to a destabilization of nucleosome interactions with DNA and a disruption of chromatin structure (Huletsky et al., 1989). Poly-ADP-ribose holds twice the negative charge of DNA, resulting in an electrorepulsive interaction with DNA. The negative charges of poly-ADP-ribose are thought to directly loosen interactions within nucleosomal arrays and promote a removal of histones from DNA (Thomas and Tulin, 2013). Moreover, it has been shown that active PARP1 modifies and removes histone H1 which facilitates local chromatin relaxation (Kim 2004). Changes in chromatin structure are not only mediated by PARP1 itself but also through a poly-ADP-ribose promoted recruitment of chromatin remodeling enzymes like the NuRD complex or ALC1 (Ahel et al., 2009; Chou et al., 2010). Price et al. recently presented the model of a PARP1 dependent transient formation of a repressive chromatin structure mediated by NuRD, ALC1 and the Kap1/HP1 complex. A subsequent opening of the chromatin structure after rapid release of these factors is thought to be mediated by the degradation of PAR through PARG (Price and D'Andrea, 2013). By those different mechanisms, PARP1 and PARG were shown to possess complex roles in the chromatin response after DNA damage.

Surprisingly inhibition of PARP as well as diminishing degradation of poly-ADP-ribose by knockdown of PARG had no significant influence on DSB mobility (Figure 30). The unaffected mobility can not be related to incomplete inhibition or knockdown as a high efficiency of both was observed by western blot and a functional immunofluorescence assay (Figure 29). This suggests that the resulting changes in chromatin structure by the radiation induced PARylation have either only minor effects on the compaction or act locally restricted and thus do not influence mobility of DSB containing chromatin in the observed range.

4.2.2. Tethering of DNA strands

A similar explanation might apply to the absence of a measurable increase in DSB mobility by the knockdown of SMC1 or MRE11 (Figure 36). Tethering of DNA strands is expected to stabilize DSBs in the surrounding chromatin (Dorsett and Ström, 2012; Thompson, 2012). The probed MRN and Cohesin complexes which have DNA tethering functions both also act in the DNA damage response and

are recruited to DSBs upon ionizing radiation. Therefore, stabilization of DNA by those complexes can be expected after the induction of DSBs. Especially following charged particle irradiation, known to induce high number of clustered DSBs in close proximity a stabilization of broken DNA strands might be of great relevance for correct repair.

The MRN complex tethers DNA strands by long coiled coil domains of RAD50 acting as a molecular clamp to connect broken chromosomes during recombination and repair (Hopfner et al., 2002; Lammens et al., 2011; Lobachev et al., 2004b). A MRE11 nuclease dimer and two RAD50 proteins build the ATP driven head domain of the complex (Figure 48A). Therefore, in mobility analyses studies knockdown of MRE11 as well as a RAD50 deficient cell line were used to prevent the formation of the tethering complex.

RAD50 contains a globular ATPase domain and long coiled-coil domains, important for binding of DNA which terminate in a Zn-hook motive (Hopfner et al., 2002). The Zn-hook of RAD50 acts as a dimerization domain that can either intramolecularly link two Rad50 monomers of the same complex or intermolecularly link two MRN complexes, creating bridges of DNA up to a distance of 1200 Å (Hopfner et al., 2002). Binding of RAD50 to DNA straightens the coiled-coils, favoring intermolecular Zn-hook dimers by which juxtaposed coiled-coils of RAD50 molecules were found to interact and tether DNA ends within a distance of 100 nm (Figure 48B) (Moreno-Herrero et al., 2005). This mechanism provides a long-range tethering of DNA by the MRN complex expected to transiently tether broken chromosomes (Lammens et al., 2011).

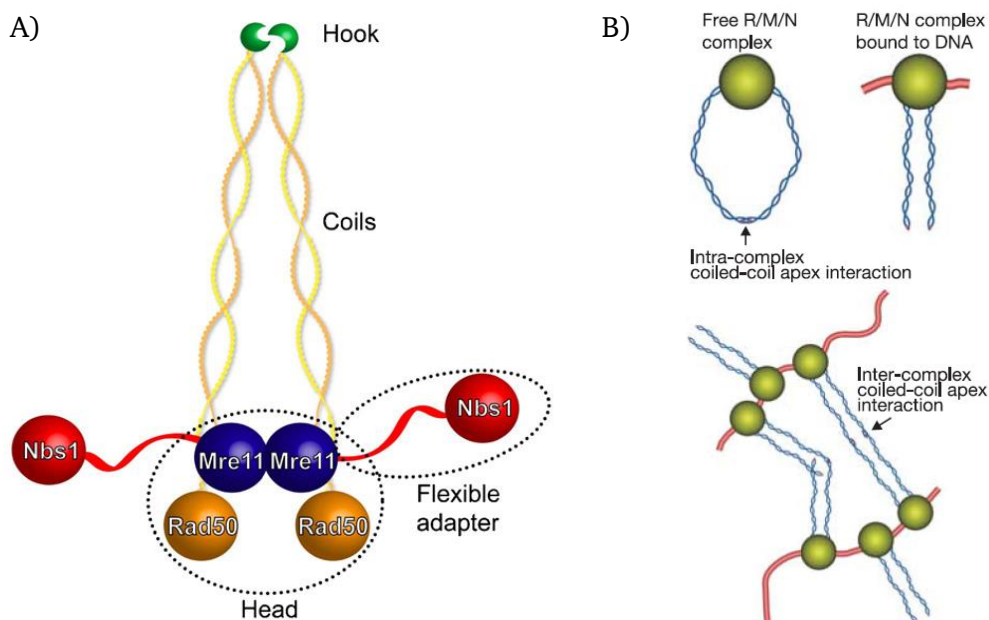


Figure 48 – Tethering of DNA strands by the MRN complex

A) Schematic structure of the MRN complex and its tethering function by Zn-hook and coiled coils of Rad50 (Williams et al., 2010). B) Schematic view of intra- or intermolecular tethering of DNA strands by the MRN complex (Moreno-Herrero et al., 2005).

Through its tethering properties the MRN complex is often referred to hold broken DNA strands in close proximity to facilitate repair (Van Gent and Van der Burg, 2007; Zha et al., 2009b) similar to Ku70/80. However, different structural properties underlie both complexes. While Ku70/80 forms a ring structure around broken DNA and two Ku70/80 proteins are thought to interact across the break site the MRN complex can also interact with surrounding DNA strands and stabilize the DSB within the chromatin.

Loss of Rad50 was expected to enhance DSB mobility, which could then be observed in fixed samples by a change in the ion induced DSB pattern over time. To visualize changes in the irradiation track a focal movement of few μm is needed. However, no changes in the distribution of repair foci could be observed in the Rad50 deficient cell line (Figure 18). Moreover, by life cell analyses no influence of MRE11 knockdown on DSB mobility in a range below one μm was found (Figure 36). Both results point to a positional stability of DSBs, independent on the MRN complex. In line with this result, also no dependency of the MRN complex on a distribution of free DNA ends was observed (Soutoglou et al., 2007). Stabilization of complex breaks or connections with sister chromatids during HR repair might not be sufficient to mediate mobility changes in a range observed by the applied approach. Moreover, different protein complexes like the analyzed Cohesin complex could work redundantly and reduce the effect expected from knockdown of the MRN complex.

Cohesin also consists of a similar structure like the MRN complex containing an ATPase domain and two coiled-coil stretches by which it tethers DNA strands like sister chromatids for HR repair (Dorsett and Ström, 2012; Wu and Yu, 2012). It was shown, that in yeast which utilized HR as the main repair pathway, Cohesin constrains the mobility of RAD52 foci (Dion et al., 2013), opening the question if a similar effect might affect mobility in mammalian cells as well.

The heterodimer of two SMC (structural maintenance of chromosomes) proteins SMC1/SMC3 displays the major subunit of the Cohesin complex forming a ring structure which entraps sister chromatids by ATP driven dimerization (Alberts et al., 2008). Loss of SMC1 would prevent the complex formation and was expected to destabilize DNA strands leading to an enhanced DSB mobility. Cohesin is maintained in different stably or dynamically bound pools in the nucleus (Gerlich et al., 2006) but for association with DNA NIPBL (nipped-B-like protein) is required to load Cohesin onto DNA (Bermudez et al., 2012). Knockdown of NIPBL prevents loading of the complex and tethering of DNA strands will be diminished. However, mobility of DSBs did not depend on complex formation or loading of the complex onto DNA as observed by knockdown of SMC1 or NIPBL (Figure 36, Figure 37).

The recruitment and binding of Cohesin to DSBs is limited to the S/G2 phase of the cell cycle (Sjögren and Ström, 2010; Wu and Yu, 2012). In S/G2 phase it is then expected to facilitate homology search and stabilization of sister chromatids during HR repair (Wu and Yu, 2012). As Cohesin acts in DNA damage response in a cell cycle dependent way, diminishing the Cohesin complex should affect mainly cells in S or G2 phase. A cell cycle distribution of 51 % G1, 26 % S and 23 % G2 phase was found in

U2OS cells 24 hours after seeding as used for live cell studies (Figure 20). Under these conditions around 50 % of the cells can be expected not to be influenced by tethering of Cohesin as they are in G1 phase during irradiation. However, it was not possible to distinguish two populations exhibiting different movement kinetics as expected if Cohesin would only influence mobility of S and G2 phase cells.

A different cell system of U2OS-G1/S-GFP NBS1-cherry cells was applied which allows to discriminate the cell cycle phases during live cell imaging. This cell system was tested by tracking of NBS1 foci. Using this cell line, the general small scale DSB mobility and the afore obtained results showing an independency of DSB mobility on DNA tethering complexes (Figure 36) were confirmed (Figure 39). As those cells express a GFP tagged cell cycle marker, cell cycle specific analyses of DSB mobility were performed to determine if tethering of DSBs is influencing mobility in dependency of cell cycle phases. Moreover, by this system a general influence on the cell cycle phases on DSB mobility was determined. By investigation of cell cycle phase dependent mobility after knockdown of SMC1 and NIPBL no trend of a dependency of mobility to a cell cycle phase could be revealed (Figure 40B). In wildtype cells a tendency of G2 cells to exhibit higher mobility than S/G1 cells could be observed (Figure 40A). An enhanced mobility during G2 phase could be related to a homology search or differences in the chromatin state. Krawczyk et al. showed a reduced DSB mobility in S-phase cells compared to G1 and G2 phase (Krawczyk et al., 2012) being in line with the observed effect of a lower mobility of S and G1 phase cells compared to G2 (Figure 40A). However, due to limitations in the numbers of observed cells the statistics are very low for these preliminary results and experiments need to be repeated. In general, the used cell system of U2OS-G1/S-GFP NBS1-cherry cells was found to provide a useful tool to investigate DSB mobility at different cell cycle phases, enabling future experiments to provide more detailed results.

4.2.3. Repair proteins Ku80 and ATM

The Ku heterodimer of Ku70 and Ku80 is one of the first proteins binding to DSBs and essential for NHEJ repair (Davis and Chen, 2013). By its ring structure it binds specifically to DNA ends where it is referred to hold ends in close proximity (Downs and Jackson, 2004; Walker et al., 2001). An enhanced mobility of free DNA ends was observed in cells deficient of Ku80 (Soutoglou et al., 2007) which might be related to missing stabilization of DNA ends by loss of Ku80. The exact mechanism by which Ku80 reduces mobility of DNA ends is still unknown but is expected to be mediated by the structural interaction of two Ku70/80 dimers binding to the two ends of a DSB (Soutoglou et al., 2007; Walker et al., 2001). To determine if Ku70/80 mediates DNA stability only at the break site or in addition in the

surrounding chromatin, the influence of Ku80 on mobility of DSB containing chromatin after charged particle irradiation was analyzed.

Retention of Ku80 at the break site depends on complexity of DNA damage. In simple DSBs Ku80 only remains at the break site around 20 min while it persists over several hours at complex lesions (Reynolds et al., 2012). A prolonged retention of Ku80 was expected following heavy ion irradiation, which induces multiple complex DSBs in close proximity, possibly enhancing stabilization of DNA. Loss of Ku80 would then result in a reduction of stability, leading to enhanced diffusion rates of DSBs in a μm range. However, by analyses of linear DSB patterns induced by ion traversals, a strong positional stability of the irradiation pattern could be observed, both in wildtype as well as in Ku80 deficient mouse cells 15 min after irradiation (Figure 14).

By labeling of individual DNA ends Soutoglou et al. have shown that loss of Ku80 enhanced mobility from an average of 50 nm/min to more than 80 nm/min and after 24 hours separation of broken ends was increased from 200 nm in wildtype to >500 nm in Ku80 deficient cells. However by a time scale of 2 hours no differences in mobility of free ends were observed between wildtype and cells deficient in Ku80 (Soutoglou et al., 2007). An increase in mobility on a 100 nm scale would be too small to detect differences in the irradiation pattern as multiple DSBs are marked by GFP, compared to a visualization of two breaks ends by different colors as used by Soutoglou et al. Changes in a μm range are needed to visualize mobility of DSBs from analyses of track structure. Loss of Ku80 was found not to cause this long scale movement of DSBs (Figure 14) indicating that stabilization of DNA breaks by Ku80 is limited to a smaller spatial scale. Longer observation times of several hours might reveal changes in diffusion patterns of DSBs if loss of Ku80 enhances the general diffusion of DSBs. To determine influences of Ku80 on diffusion kinetics of DSBs in a smaller spatial scale live cell imaging was performed in Ku80 deficient mouse cells. However, those cells exhibit strong movement and nuclear deformations after transient transfection with 53BP1-GFP. Tracking of individual repair foci was therefore nearly impossible using this approach. Future studies with other cells knocked down of Ku80 might be used for live cell analyses to elucidate a stabilization effect of Ku80 on DSB containing chromatin.

In earlier studies an enhanced spreading of DSBs over several hours was observed in a AT h-tert cell line (Figure 13) (unpublished results of B. Jakob). In this PhD thesis it was now determined if the effect was mediated by the absence of ATM. Usage of a different ATM deficient cell line did not replicate the observed results and no spreading of foci was observed even after several hours (Figure 16), proving that deficiency of ATM does not lead to an enhanced DSB mobility. To determine if deficiency of ATM induces smaller changes in DSB mobility live cell analyses were performed. By these experiments, a strong reduction in mobility of 53BP1 foci occurred due to inhibition of ATM (Figure 33). ATM is a major signaling protein in the DNA damage response, responsible for γH2AX formation

as well as recruitment of MDC1. Nevertheless, following induction of DSBs 53BP1 foci still form after inhibition of ATM activity. It was shown that phosphorylation of 53BP1 by ATM does influence repair capacity but is not required for the recruitment of 53BP1 (Goodarzi and Jeggo, 2013) which depends mainly on methylation of histone 4 (H4K20me2) (Botuyan et al., 2006).

A strong confinement of DSB mobility was found following inhibition of ATM (Figure 33). The msd was reduced from $1.0 \mu\text{m}^2$ in control to $0.53 \mu\text{m}^2$ in ATM inhibited cells after 100 min observation time following charged particle irradiation (Figure 33). As specific inhibition of the kinase function of ATM was applied, not the presence of ATM in the nucleus, but the phosphorylation of substrates by ATM accounts for the observed effect. The resulting confinement radii were discriminated being $1.05 \pm 0.07 \mu\text{m}$ in wildtype cells while ATM inhibition resulted in confinement to a much smaller radius of $0.73 \pm 0.01 \mu\text{m}$, leading to a reduction of the sampled nuclear volume by a factor of 3 ($4.85 \mu\text{m}^3$ vs $1.63 \mu\text{m}^3$). A visual comparison of both confinement radii is given in Figure 49. This reduction in the sampled volume is expected to be sufficient to change pairing and interaction events of DSB ends, leading to the formation of chromosomal aberrations as these formations not only dependent on chromosome size or gene density but moreover on proximity (Bickmore and Teague, 2002). In this context the roaming volume of DNA breaks is thought to strongly influence pairing events and aberration rates (Dion and Gasser, 2013; Krawczyk et al., 2012; Roukos et al., 2013).

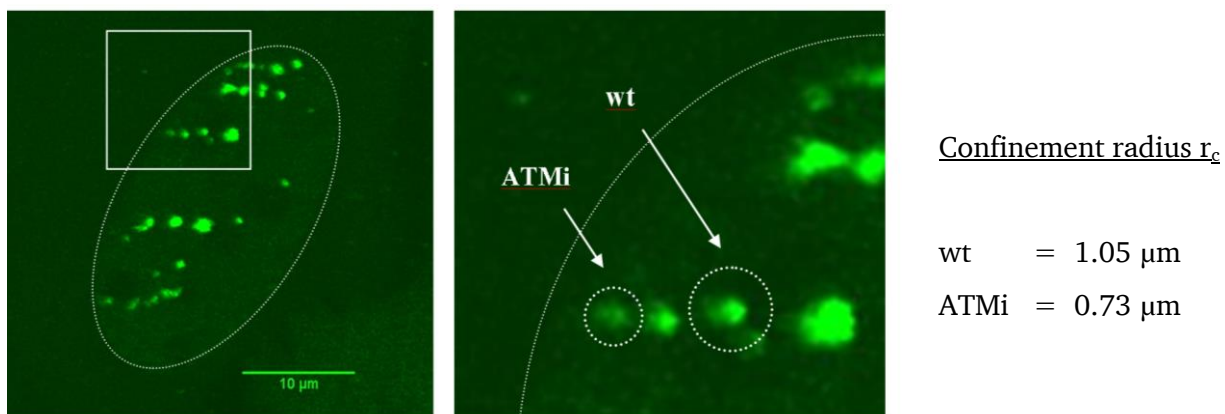


Figure 49 – The sampled volume of IRIF is reduced after inhibition of ATM.

A) U2OS-53BP1-GFP cell after low angle irradiation with C ($170 \text{ keV}/\mu\text{m}$). B) Magnification of the cell nucleus. Confinement radii are marked by dotted lines. For simplification, both radii are exemplarily shown in the same nucleus. 3D confinement volumes in ATM inhibited cells are decreased by a factor of 3 compared to the reference volumes of non-treated cells.

Moreover a strong disturbance of a random walk is seen by reduced α values using the subdiffusive model and a change of the diffusion coefficient D_c from $5.12 \times 10^{-5} \mu\text{m}^2/\text{s}$ for wildtype cells to $4.58 \times 10^{-5} \mu\text{m}^2/\text{s}$ in ATM inhibited cells. To examine if the confinement of mobility is mediated by the induction of high numbers of DSBs in close proximity from heavy ion irradiation further experiments

following X-ray irradiation were performed. The confinement of DSB mobility due to inhibition of ATM was confirmed by X-ray irradiation excluding that only high numbers of DSBs are responsible for ATM dependent changes in mobility. A hyperactivation of ATM was found to be induced by heavy ion irradiation (Meyer et al., 2013) possibly contributing to an enhanced effect of ATM after charged particle irradiation compared to X-ray induced DSBs.

Dense chromatin areas in the environment of DSB might be one cause of a confinement and suppression of mobility. A strong decondensation was observed after the induction of DSBs by charged particle irradiation (Jakob et al., 2011; Müller et al., 2013) as well as by γ -rays (Falk et al., 2007). This is assumed to facilitate recruitment of repair proteins and ongoing repair. ATM was proven to act in the local decondensation of heterochromatic areas upon induction of DSBs through phosphorylation of KAP1 (Geuting et al., 2013; Goodarzi and Jeggo, 2012; Goodarzi et al., 2008). Moreover, an ATM dependent decondensation was also observed after the induction of DSBs by X-rays (Ziv et al., 2006) proving that a missing chromatin relaxation due to inhibition of ATM can mediate chromatin mobility independent on irradiation quality. Also the enhancement of chromatin mobility after induction of DSBs (Krawczyk et al., 2012) was proposed to be caused by decondensation, leading to a reduction in the structural confinement of DSB mobility.

Deficiency of KAP1 mediated decondensation by inhibition of ATM would therefore constrain mobility of DSBs by structural properties of chromatin. A fraction of long persisting DSBs associated with heterochromatic regions arise by inhibition of ATM, both after X-rays as well as carbon ion irradiation (Goodarzi and Jeggo, 2012; Goodarzi et al., 2008; Jakob et al., 2011). For those heterochromatin associated breaks 24h after the DSB induction Krawczyk et al. described a decrease in mobility (Krawczyk et al., 2012). Even though in both experiments inhibition of ATM led to a reduced mobility different mechanisms ought to apply. At early time points 53BP1 foci can not be considered to belong mainly to heterochromatic areas, which comprises around 20 % of the chromatin, as seen at later time points due to differences in the repair kinetics (Goodarzi et al., 2008). In addition it was shown that 53BP1 can only penetrate into heterochromatic areas after their decondensation (Ježková et al., 2014). At later time points (24h), persisting foci as observed by Krawczyk et al. (Krawczyk et al., 2012) are expected to be mainly associated to heterochromatic areas due to slower repair kinetics (Goodarzi and Jeggo, 2012; Goodarzi et al., 2008). However, so far it is not known whether ATM only affects decondensation in heterochromatic areas or also in euchromatic areas as 80 % of the observed DSBs after irradiation are expected to belong to euchromatic areas (Goodarzi et al., 2008).

As there exist a plethora of phosphorylation substrates of ATM which act in cell-cycle arrest, apoptosis and DNA repair (Matsuoka et al., 2007) it will be not an easy task to find the effectors responsible for changes in chromatin and DNA mobility.

4.3. Interactions between the nuclear matrix and DSBs

4.3.1. Nuclear matrix proteins influence DSB mobility

The nuclear matrix acts in stabilizing the shape and internal organization of nuclei and contains anchoring sites for chromatin or DNA. The so called matrix attachment regions (MARs) in the DNA mediate interactions between DNA, chromatin and the nuclear matrix (Barboro et al., 2012) and are expected to constrict mobility of chromatin during interphase (Parada and Misteli, 2002).

The main components of the nuclear matrix are A-type and B-type Lamins acting together with other structural proteins like spectrins or NuMA (Simon and Wilson, 2011). Lamin filaments are distributed throughout the nucleoplasm but mainly concentrate at the inner nuclear membrane (INM) forming the lamina, a 15-20 nm thin meshwork exhibiting structural as well as important signaling and regulatory functions (Burke and Stewart, 2013). In the context of DNA repair mutations or loss of A-type Lamins, encoded by the *LMNA* gene, are leading to increased sensitivity to ionizing radiation and defects in DSB repair (Gonzalez-Suarez et al., 2009b; Liu et al., 2005; Singh et al., 2013). Moreover, an abnormal nuclear morphology, a rearranged organization of chromatin, loss of heterochromatic markers and proteasomal degradation of HP1a and b was found in Lamin A/C deficient cells (Broers et al., 2005; Chaturvedi et al., 2012).

By mobility analyses an enhancement in DSB mobility around 31 % could be seen after knockdown of NuMA which was even more pronounced (72 %) after knockdown of Lamin A/C (Figure 41). As the nuclear matrix is mediating nuclear stability, chromatin organization and chromosomal anchoring to the nuclear matrix, it was expected that chromatin mobility is restricted by functions of nuclear matrix proteins. A dependency of DSBs mobility on nuclear matrix proteins could moreover be suggested by interactions with repair mediating proteins and the observed influence of Lamins on DNA repair and the formation of chromosomal aberrations (Gonzalez-Suarez et al., 2009b; Redwood et al., 2011). The higher effect due to knockdown of Lamin A/C can result from the fact that Lamins constitute the main part of the nuclear matrix and lamina, providing binding sites for chromatin and regulatory molecules (Burke and Stewart, 2013). By disruption of these binding sites chromatin might be destabilized and exhibit enhanced mobility within the nucleus. Especially the strongly enhanced diffusion coefficient from $4.5 \pm 0.2 \times 10^{-5} \mu\text{m}^2/\text{s}$ in wt cells to $8.1 \pm 0.2 \times 10^{-5} \mu\text{m}^2/\text{s}$ after knockdown of Lamin A/C is remarkable and suggests a direct effect on chromatin mobility. The findings are confirmed by a recent publication of Mahen et al., showing an enhanced mobility of 53BP1 foci in *LMNA*^{-/-} mouse cells (Mahen et al., 2013).

NuMA plays a role in the maintenance of spindle poles during mitosis but by its coiled coil structure it assembles into filaments distributed throughout the nucleus during interphase (Harborth et al., 1999). There it has been proposed to be essential for the creation of chromosome domains either by

organizing chromatin, by interaction with MARs or by providing a substrate for intranuclear processes (Radulescu and Cleveland, 2010). MARs are 300–1000 bp long AT rich DNA regions promoting interactions between chromatin and the nuclear matrix. They function in the organization of chromatin loops, have potential roles in gene expression or replication and are specifically bound by Lamins and to a lesser amount by NuMA (Barboro et al., 2012; Ludérus et al., 1994). Through their interaction with MARs NuMA and A-type Lamins are expected to influence anchoring of chromatin to the nuclear matrix and thereby mediate chromatin stability. Both, the interaction with anchoring sites as well as the overall structural properties of the nuclear matrix, strongly influencing chromatin organization are suggested to explain the observed enhancement of mobility following knockdown of NuMA or Lamin A/C.

It needs to be determined if the knockdown mediated disruption of the nuclear matrix affects the overall mobility of chromatin or if the effect is restricted to DSB containing chromatin domains. By FRAP measurements a decrease in the mobile fraction of Lamin A was found after induction of DSBs together with an direct interaction between γ H2AX and Lamin A (Mahen et al., 2013). Even though Lamin A/C does not accumulate at sites of DSBs (Mahen et al., 2013) these findings as well as a repair defect in Lamin A/C deficient cells suggest an enhanced interaction between the nuclear matrix and DSBs compared to undamaged chromatin.

In dysfunctional telomeres a dependency of A-type Lamins was found on NHEJ mediated fusion rates which were reduced by a factor of four compared to wildtype cells (Gonzalez-Suarez et al., 2009b). The effect was pointed to a decreased 53BP1 level in Lamin deficient cells (Gonzalez-Suarez et al., 2009b) as 53BP1 depletion was shown to reduce mobility of uncapped telomeres and their fusion rates (Dimitrova et al., 2008). Mobility of deprotected telomeres was not determined in *LMNA*^{-/-} cells but a reduced mobility of telomeres due to loss of Lamin A/C would be contradictory to the observed enhanced mobility of IRIF. A determination of telomere mobility in Lamin A/C deficient cells would shed more light onto these questions, possibility revealing different mechanisms for mobility and fusion of DSBs and telomeres in dependence of Lamin A/C.

53BP1 protein levels are supposed to be stabilized by A-type Lamins preventing their degradation by the proteasome and this effect could be rescued by reconstitution of 53BP1 into Lamin A/C-depleted cells (Gonzalez-Suarez et al., 2009b). In the shown experiments, using knockdown of NuMA or Lamin A/C overexpression of 53BP1-GFP was used for mobility analyses explaining why no compromises in 53BP1 foci accumulations were observed.

The obtained results clearly show that mobility of DSBs is enhanced following depletion of nuclear matrix proteins. To address the mechanism by which the nuclear matrix acts on DSB repair and mobility, nuclear extractions were performed, visualizing direct interactions of repair proteins and nuclear matrix proteins.

4.3.2. Nuclear extractions reveal interactions of repair proteins with the nuclear matrix

Protocols adapted from nuclear skeleton preparation in electron microscopic studies (Nickerson et al., 1997) were used to extract DNA and proteins (Figure 41, Figure S 1, Figure S 2). Soluble proteins were extracted, cells were fixed by PFA and DNA was digested and extracted afterwards. Staining for DNA and RNA revealed a strong reduction of DNA signal following extraction while RNA remains inside the nucleoli. Extraction of DNA and proteins is depending on buffering conditions, DNase I concentration and time of digestion and small variations in the extraction occurred between individual experiments. However, only experiments in which the digestion of DNA was nearly completed, indicated by the absence of Dapi signal, were used for analyses. Extraction of proteins from the nucleus can be divided into three groups: soluble proteins which are easily extractable by detergents, the chromatin compartment from which components are released upon DNA digestion and the insoluble nuclear matrix, which is resistant to detergent extraction as well as DNA digestion (Abad et al., 2007). By the used nuclear extraction soluble as well as chromatin bound proteins are expected to be withdrawn from the nucleus.

In first experiments using nuclear extraction, the repair mediator protein MDC1 was found to be removed completely (Figure S 2) while a low background level of histone H3 and pATM remained in the nucleus (Figure 42). In early studies histones were shown to be removed by nuclear extraction and digestion of DNA (Nickerson et al., 1997). Possible explanations for the remaining H3 level are an incomplete extraction and DNA digestion as well as cross-linking of proteins by PFA fixation prior to digestion of DNA. DNA staining was almost completely removed, indicating a complete digestion of DNA and extraction pointing to an influence of PFA fixation prior to DNA extraction. To prevent fixation dependent influences further experiments were performed by extraction and digestion of DNA prior to cellular fixation. In those experiments, the complete extraction of histones could be visualized by staining for γ H2AX which is removed from the nucleus completely after nuclear extraction (Figure 44).

MDC1 is a repair mediator protein involved in signal amplification and checkpoint control following induction of DSBs (Coster and Goldberg, 2010). It mediates repair by protein interactions and does not contain a DNA binding motive itself (Jungmichel et al., 2012). No interaction with Lamins or other proteins of the nuclear matrix are known for MDC1. Binding of MDC1 to repair proteins or chromatin at sites of DSBs seems not to prevent extraction, explaining the complete removal from the nucleus. Similar results are obtained for pATM, which is extracted completely from the nucleus following nuclear extraction (Figure 43). Even by nuclear extraction using fixation with PFA prior to digestion of DNA pATM was removed to a great extent (Figure 42). The observed differences for pATM between both extraction protocols confirm an incomplete extraction due to protein cross-linking of PFA.

ATM binds to DNA and chromatin and interacts with several proteins like the MRN complex which is necessary for activation of ATM and its kinase function (Lee et al., 2013). In Lamin A/C deficient cells no differences in the expression of ATM was found. The same applies for other repair proteins like MDC1, DNA-PK, MRE11, NBS11, Ku70 or γ H2AX for which no detectable differences in the cellular levels could be observed (Gonzalez-Suarez et al., 2009b). Also ATM dependent phosphorylation of p53 was not altered in Lamin A/C deficient cells (Redwood et al., 2011). By complete extraction of pATM from the nucleus it can be concluded that no direct interaction between pATM and the nuclear matrix exists even though some nuclear matrix proteins like NuMA are phosphorylation substrates of ATM (Matsuoka et al., 2007).

By immunofluorescent staining of NuMA following nuclear extraction the remaining amount of NuMA was visualized serving as a control of the remaining nuclear matrix. A chromatin associated fraction of NuMA was shown in a different cell system, not involved in the formation of the stabilizing nuclear matrix (Abad et al., 2007). This fraction is removed from the nucleus by nuclear extraction as observed in experiments with U2OS cells (Figure 45). The fraction of NuMA which remains associated with the nuclear matrix after extractions depends on RNA as NuMA strongly interacts with RNA and combined extraction with RNase treatment was shown to cause a drastic reduction of NuMA levels while Lamins remain unaffected (Barboro et al., 2002). Therefore care has to be taken not to remove RNA by RNases.

In U2OS cells a homogenous distribution of NuMA could be seen in untreated cells, diminished in intensity following nuclear extraction (Figure 45). Experiments were also carried out with normal human fibroblasts revealing differences in the NuMA pattern in controls (Figure 46). AG cell showed either a strong and homogenous staining of NuMA as seen in U2OS cells, a weak homogenous signal or in few cases a distribution of NuMA in distinct foci. In the literature different distribution patterns of NuMA were described, mostly related to developmental stages, cell type dependent and sometimes coming along with altered chromatin organization (Abad et al., 2007). Independent on the NuMA pattern observed in U2OS and AG cells, after nuclear extraction a homogenous distribution of NuMA is found in the cell nucleus (Figure 45, Figure S 6) revealing parts of the nuclear matrix, which are not extracted by the used protocols.

Following PFA fixation and nuclear extraction of X-ray irradiated cells, the repair proteins 53BP1 and MRE11 showed a low background signal and in some cases focal accumulations (Figure S 1 and Figure S 2). Using nuclear extraction without PFA fixation prior to DNA digestion still revealed focal accumulations of MRE11 (Figure 44). 53BP1 was removed from the nucleus in most cases (Figure 43) but few exceptions were seen in which an inhomogenous pattern of 53BP1 maintained throughout the nucleus (Figure S 3). The remaining protein in few experiments can not be attributed to incomplete extraction as DNA and γ H2AX staining completely vanished (Figure S 3). By comparison with MDC1,

which is extracted completely it can be concluded that the extraction is protein dependent and most probably mediated by differences in nuclear matrix interactions. MRE11 foci were reduced in number but a subset remained visible after extraction, which was moreover confirmed by the use of a different cell line (Figure S 4). This finding suggests that MRE11 not only binds directly to DNA strands but moreover exhibits binding interactions with filamentous structures of the nuclear matrix. The detailed mechanism and purpose of these interactions is unknown and needs to be determined. It is yet unclear if the association is maintained through the MRN complex and associations of RAD50 coiled coils or by the MRE11 protein itself. Similar results of retention of repair proteins in the nuclear matrix fraction after extraction were shown by staining for XRCC1 and poly-ADP-ribose after treatment with H₂O₂ (Kubota et al., 2009). Cells were fixed by methanol/acetone in these experiments and retention of XRCC1 seems to be independent of treatment with H₂O₂.

Knockdown studies of Lamin A/C and NuMA were expected to reveal further insights in the interactions of repair proteins with the nuclear matrix. The cellular level and recruitment of 53BP1 to DSBs was shown to be reduced in cells deficient for Lamin A/C due to a proteasome mediated degradation of 53BP1 (Gonzalez-Suarez et al., 2009b). However, by experiments of this thesis, only a slight reduction in 53BP1 foci could be observed in cells knocked down in Lamin (Figure 47). This might be attributed to remaining levels of Lamin A/C following knockdown. Knockdown efficiency was around 89 % as determined by western blot analyses (Figure S 7). 53BP1 recruitment was not altered after knockdown of NuMA (Figure S 6) and foci formation of pATM was not impaired, neither by knockdown of NuMA nor of Lamin (Figure S 6 and Figure 47). As expected knockdown of NuMA or Lamin A/C did not reduce the extractability of repair proteins compared to wildtype cells (Figure 43). Further experiments are needed to determine the influence of nuclear matrix protein knockdowns on the interaction with MRE11. A direct interaction of MRE11 with nuclear matrix proteins is assumed and a reduced retention of MRE11 in the nucleus would be expected by knockdown of these nuclear matrix proteins. As it remains largely unknown what influences the extraction and retention of repair proteins further experiments are required. By the use of heavy ion irradiation defined tracks of DSBs are created in the cell nucleus at which repair proteins accumulate (Figure 21). Taking advantage of this irradiation combined with nuclear extractions more detailed analyses of repair protein interactions with the nuclear matrix can be maintained, as it can be determined if the retention of repair proteins is DSB dependent or found in the whole cell nucleus.

5. Conclusions and outlook

Proximity and movement of DSBs are considered to play an important role in the formation of chromosome aberrations, which favour the development of cancer (Dion and Gasser, 2013). Therefore in this PhD thesis mobility of DSBs was analyzed in a human cell system to address the influence of repair and chromatin related factors on the mobility of DSB containing chromatin.

Charged particle irradiation was used to induce multiple DSBs at a defined linear track. By analyses of irradiated and fixed cells no changes in the track structure of DSBs were obtained by depletion of selected repair proteins like Ku80, ATM or RAD50, pointing to a stable position of DSB over several hours, independent on the aforementioned repair factors. To visualize the temporal and spatial aspects of DSB mobility in more detail live cell microscopy of IRIF was applied.

Findings revealed that mobility of DSB containing chromatin domains is mostly independent against a series of small scale chromatin remodeling processes as seen by knockdown of ACF1, PARP and PARG. Even tethering of damaged DNA strands by the MRN complex or the Cohesin complex did not influence mobility of IRIF in the observed spatial scale. The confinement of mobility due to inhibition of ATM gives new hints into the regulation of mobility, possibly maintained by the organization of chromatin as ATM promotes local decondensation mechanisms (Geuting et al., 2013; Ziv et al., 2006). An enhancement in the diffusion coefficient and confinement radius of IRIF due to knockdown of Lamin A/C and NuMA provides important information about the interplay between the nuclear matrix, chromatin and DSB mobility. Additional nuclear extraction studies, revealing the insoluble nuclear matrix protein meshwork, moreover provided a useful method to determine direct interactions between repair proteins and the nuclear matrix. This opens up new opportunities for further investigations of DSB dependent matrix interactions and their role in maintaining positional stability of DSBs or influences on repair capacity and pathways. Future studies using charged particle irradiation, inducing a defined linear track of DSBs, will help determine a dependency of interactions between repair proteins and nuclear matrix proteins on DSBs.

Results obtaining changes in DSB mobility prove that by loss of individual proteins DSB mobility can be strongly affected and consequences on cell viability, repair capacity and genomic stability need to be determined. The findings also raise new questions regarding the mechanism by which ATM or Lamin A/C influence chromatin dynamics. Future experiments are expected to reveal details of these mechanisms and analyze further contributions of repair related proteins on IRIF dynamics. Moreover, extended studies should reveal an impact of the cell cycle phases on mobility of chromatin and DSBs using the introduced cell system of U2OS-G1/S-GFP NBS1-cherry cells. To detect a contribution of enhanced DSB mobility on the formation of chromosomal aberrations, translocation rates following irradiation should be determined in cells showing enhanced DSB mobility as seen by knockdown of Lamin A/C or NuMA.

Bibliography

- Abad, P.C., Lewis, J., Mian, I.S., Knowles, D.W., Sturgis, J., Badve, S., Xie, J., and Lelièvre, S.A. (2007). NuMA influences higher order chromatin organization in human mammary epithelium. *Molecular Biology of the Cell* 18, 348–361.
- Ahel, D., Horejsí, Z., Wiechens, N., Polo, S.E., Garcia-Wilson, E., Ahel, I., Flynn, H., Skehel, M., West, S.C., Jackson, S.P., et al. (2009). Poly(ADP-ribose)-dependent regulation of DNA repair by the chromatin remodeling enzyme ALC1. *Science* 325, 1240–1243.
- Alberts, B., Johnson, A., Lewis, J., Raff, M., Roberts, K., and Walter, P. (2008). *Molecular biology of the cell* (Garland Science).
- Alpen, E.L. (1990). *Radiation Biophysiks* (Englewood Cliffs).
- Asaithamby, A., and Chen, D.J. (2011). Mechanism of cluster DNA damage repair in response to high-atomic number and energy particles radiation. *Mutation Research* 711, 87–99.
- Aten, J. a, Stap, J., Krawczyk, P.M., Van Oven, C.H., Hoebe, R. a, Essers, J., and Kanaar, R. (2004). Dynamics of DNA double-strand breaks revealed by clustering of damaged chromosome domains. *Science (New York, N.Y.)* 303, 92–95.
- Bakkenist, C.J., and Kastan, M.B. (2003). DNA damage activates ATM through intermolecular autophosphorylation and dimer dissociation. *Nature* 421, 499–506.
- Bao, Y., and Shen, X. (2007). SnapShot: chromatin remodeling complexes. *Cell* 129, 632.
- Barboro, P., D'Arrigo, C., Diaspro, A., Mormino, M., Alberti, I., Parodi, S., Patrone, E., and Balbi, C. (2002). Unraveling the organization of the internal nuclear matrix: RNA-dependent anchoring of NuMA to a lamin scaffold. *Experimental Cell Research* 279, 202–218.
- Barboro, P., Repaci, E., D'Arrigo, C., and Balbi, C. (2012). The role of nuclear matrix proteins binding to matrix attachment regions (Mars) in prostate cancer cell differentiation. *PloS One* 7, e40617.
- Bartek, J., and Lukas, J. (2007). DNA damage checkpoints: from initiation to recovery or adaptation. *Current Opinion in Cell Biology* 19, 238–245.
- Bauerschmidt, C., Arrichiello, C., Burdak-Rothkamm, S., Woodcock, M., Hill, M. a, Stevens, D.L., and Rothkamm, K. (2010). Cohesin promotes the repair of ionizing radiation-induced DNA double-strand breaks in replicated chromatin. *Nucleic Acids Research* 38, 477–487.
- Becker, A., Durante, M., Taucher-Scholz, G., and Jakob, B. (2014). ATM Alters the Otherwise Robust Chromatin Mobility at Sites of DNA Double-Strand Breaks (DSBs) in Human Cells. *PloS One* 9, e92640.
- Bekker-Jensen, S., Lukas, C., Melander, F., Bartek, J., and Lukas, J. (2005). Dynamic assembly and sustained retention of 53BP1 at the sites of DNA damage are controlled by Mdc1/NFBD1. *The Journal of Cell Biology* 170, 201–211.
- Bermudez, V.P., Farina, A., Higashi, T.L., Du, F., Tappin, I., Takahashi, T.S., and Hurwitz, J. (2012). In vitro loading of human cohesin on DNA by the human Scc2-Scc4 loader complex. *Proceedings of the National Academy of Sciences of the United States of America* 109, 9366–9371.

Bethe, H. (1930). Zur Theorie des Durchgangs schneller Korpuskularstrahlen durch Materie. *Annalen Der Physik* 397, 324–400.

Bickmore, W. a, and Teague, P. (2002). Influences of chromosome size, gene density and nuclear position on the frequency of constitutional translocations in the human population. *Chromosome Research : an International Journal on the Molecular, Supramolecular and Evolutionary Aspects of Chromosome Biology* 10, 707–715.

Blenn, C., Althaus, F.R., and Malanga, M. (2006). Poly(ADP-ribose) glycohydrolase silencing protects against H₂O₂-induced cell death. *The Biochemical Journal* 396, 419–429.

Bloch, F. (1930). Zur Bremsung rasch bewegter Teilchen beim Durchgang durch die Materie. *Annalen Der Physik* 5, 285–320.

Botuyan, M.V., Lee, J., Ward, I.M., Kim, J., Thompson, J.R., Chen, J., and Mer, G. (2006). Structural basis for the methylation state-specific recognition of histone H4-K20 by 53BP1 and Crb2 in DNA repair. *Cell* 127, 1361–1373.

Brandsma, I., and Gent, D.C. (2012). Pathway choice in DNA double strand break repair: observations of a balancing act. *Genome Integrity* 3, 9.

Broers, J.L. V, Kuijpers, H.J.H., Ostlund, C., Worman, H.J., Endert, J., and Ramaekers, F.C.S. (2005). Both lamin A and lamin C mutations cause lamina instability as well as loss of internal nuclear lamin organization. *Experimental Cell Research* 304, 582–592.

Burke, B., and Stewart, C.L. (2013). The nuclear lamins: flexibility in function. *Nature Reviews. Molecular Cell Biology* 14, 13–24.

Bürkle, a, Chen, G., Küpper, J.H., Grube, K., and Zeller, W.J. (1993). Increased poly(ADP-ribosyl)ation in intact cells by cisplatin treatment. *Carcinogenesis* 14, 559–561.

Chapman, J.R., Taylor, M.R.G., and Boulton, S.J. (2012). Playing the end game: DNA double-strand break repair pathway choice. *Molecular Cell* 47, 497–510.

Chaturvedi, P., Khanna, R., and Parnaik, V.K. (2012). Ubiquitin ligase RNF123 mediates degradation of heterochromatin protein 1 α and β in lamin A/C knock-down cells. *PloS One* 7, e47558.

Chioda, M., Vengadasalam, S., Kremmer, E., Eberharter, A., and Becker, P.B. (2010). Developmental role for ACF1-containing nucleosome remodellers in chromatin organisation. *Development (Cambridge, England)* 137, 3513–3522.

Chou, D.M., Adamson, B., Dephoure, N.E., Tan, X., Nottke, A.C., Hurov, K.E., Gygi, S.P., Colaiácovo, M.P., and Elledge, S.J. (2010). A chromatin localization screen reveals poly (ADP ribose)-regulated recruitment of the repressive polycomb and NuRD complexes to sites of DNA damage. *Proceedings of the National Academy of Sciences of the United States of America* 107, 18475–18480.

Chubb, J.R., and Bickmore, W.A. (2003). Considering nuclear compartmentalization in the light of nuclear dynamics. *Cell* 112, 403–406.

Clapier, C.R., and Cairns, B.R. (2009). The biology of chromatin remodeling complexes. *Annual Review of Biochemistry* 78, 273–304.

Collins, N., Poot, R. a, Kukimoto, I., García-Jiménez, C., Dellaire, G., and Varga-Weisz, P.D. (2002). An ACF1-ISWI chromatin-remodeling complex is required for DNA replication through heterochromatin. *Nature Genetics* 32, 627–632.

Cortes, U., Tong, W.-M., Coyle, D.L., Meyer-Ficca, M.L., Meyer, R.G., Petrilli, V., Herceg, Z., Jacobson, E.L., Jacobson, M.K., and Wang, Z.-Q. (2004). Depletion of the 110-kilodalton isoform of poly(ADP-ribose) glycohydrolase increases sensitivity to genotoxic and endotoxic stress in mice. *Molecular and Cellular Biology* 24, 7163–7178.

Coster, G., and Goldberg, M. (2010). The cellular response to DNA damage: a focus on MDC1 and its interacting proteins. *Nucleus (Austin, Tex.)* 1, 166–178.

D'Amours, D., Desnoyers, S., D'Silva, I., and Poirier, G.G. (1999). Poly(ADP-ribosyl)ation reactions in the regulation of nuclear functions. *The Biochemical Journal* 342 (Pt 2), 249–268.

Davis, A.J., and Chen, D.J. (2013). DNA double strand break repair via non-homologous end-joining. *Translational Cancer Research* 2, 130–143.

Deckbar, D., Birraux, J., Krempler, A., Tchouandong, L., Beucher, A., Walker, S., Stiff, T., Jeggo, P., and Löbrich, M. (2007). Chromosome breakage after G2 checkpoint release. *The Journal of Cell Biology* 176, 749–755.

Desai-Mehta, A., Cerosaletti, K.M., and Concannon, P. (2001). Distinct functional domains of nibrin mediate Mre11 binding, focus formation, and nuclear localization. *Molecular and Cellular Biology* 21, 2184–2191.

Dimitrova, N., Chen, Y.-C.M., Spector, D.L., and De Lange, T. (2008). 53BP1 promotes non-homologous end joining of telomeres by increasing chromatin mobility. *Nature* 456, 524–528.

Dion, V., and Gasser, S.M. (2013). Chromatin movement in the maintenance of genome stability. *Cell* 152, 1355–1364.

Dion, V., Kalck, V., Horigome, C., Towbin, B.D., and Gasser, S.M. (2012). Increased mobility of double-strand breaks requires Mec1, Rad9 and the homologous recombination machinery. *Nature Cell Biology* 14, 502–509.

Dion, V., Kalck, V., Seeber, A., Schleker, T., and Gasser, S.M. (2013). Cohesin and the nucleolus constrain the mobility of spontaneous repair foci. *EMBO Reports* 14, 984–991.

Doil, C., Mailand, N., Bekker-Jensen, S., Menard, P., Larsen, D.H., Pepperkok, R., Ellenberg, J., Panier, S., Durocher, D., Bartek, J., et al. (2009). RNF168 binds and amplifies ubiquitin conjugates on damaged chromosomes to allow accumulation of repair proteins. *Cell* 136, 435–446.

Dorsett, D., and Ström, L. (2012). The ancient and evolving roles of cohesin in gene expression and DNA repair. *Current Biology* 22, R240–50.

Downs, J. a, and Jackson, S.P. (2004). A means to a DNA end: the many roles of Ku. *Nature Reviews. Molecular Cell Biology* 5, 367–378.

Durante, M., and Loeffler, J.S. (2010). Charged particles in radiation oncology. *Nature Reviews. Clinical Oncology* 7, 37–43.

- Elbashir, S.M., Harborth, J., Lendeckel, W., Yalcin, a, Weber, K., and Tuschl, T. (2001). Duplexes of 21-nucleotide RNAs mediate RNA interference in cultured mammalian cells. *Nature* 411, 494–498.
- Falk, M., Lukasova, E., Gabrielova, B., Ondrej, V., and Kozubek, S. (2007). Chromatin dynamics during DSB repair. *Biochimica Et Biophysica Acta* 1773, 1534–1545.
- Fournier, C., Wiese, C., and Taucher-Scholz, G. (2004). Accumulation of the cell cycle regulators TP53 and CDKN1A (p21) in human fibroblasts after exposure to low- and high-LET radiation. *Radiation Research* 161, 675–684.
- Fowler, J.F. (1989). The linear-quadratic formula and progress in fractionated radiotherapy. *The British Journal of Radiology* 62, 679–694.
- Gagné, J.-P., Isabelle, M., Lo, K.S., Bourassa, S., Hendzel, M.J., Dawson, V.L., Dawson, T.M., and Poirier, G.G. (2008). Proteome-wide identification of poly(ADP-ribose) binding proteins and poly(ADP-ribose)-associated protein complexes. *Nucleic Acids Research* 36, 6959–6976.
- Garcia Soriano F, Virág, L., Jagtap, P., Szabó, E., Mabley, J.G., Liaudet, L., Marton, a, Hoyt, D.G., Murthy, K.G., Salzman, a L., et al. (2001). Diabetic endothelial dysfunction: the role of poly(ADP-ribose) polymerase activation. *Nature Medicine* 7, 108–113.
- Van Gent, D.C., and Van der Burg, M. (2007). Non-homologous end-joining, a sticky affair. *Oncogene* 26, 7731–7740.
- Gerlich, D., Koch, B., Dupeux, F., Peters, J.-M., and Ellenberg, J. (2006). Live-cell imaging reveals a stable cohesin-chromatin interaction after but not before DNA replication. *Current Biology : CB* 16, 1571–1578.
- Geuting, V., Reul, C., and Löbrich, M. (2013). ATM Release at Resected Double-Strand Breaks Provides Heterochromatin Reconstitution to Facilitate Homologous Recombination. *PLoS Genetics* 9, e1003667.
- Girst, S., Hable, V., Drexler, G. a, Greubel, C., Siebenwirth, C., Haum, M., Friedl, a a, and Dollinger, G. (2013). Subdiffusion supports joining of correct ends during repair of DNA double-strand breaks. *Scientific Reports* 3, 2511.
- Gontijo, A.M. de M.C., Green, C.M., and Almouzni, G. (2003). Repairing DNA damage in chromatin. *Biochimie* 85, 1133–1147.
- Gonzalez-Suarez, I., Redwood, A.B., and Gonzalo, S. (2009a). Loss of A-type lamins and genomic instability. *Cell Cycle (Georgetown, Tex.)* 8, 3860–3865.
- Gonzalez-Suarez, I., Redwood, A.B., Perkins, S.M., Vermolen, B., Lichtensztejin, D., Grotzky, D. a, Morgado-Palacin, L., Gapud, E.J., Sleckman, B.P., Sullivan, T., et al. (2009b). Novel roles for A-type lamins in telomere biology and the DNA damage response pathway. *The EMBO Journal* 28, 2414–2427.
- Goodarzi, A. a, and Jeggo, P. a (2012). The heterochromatic barrier to DNA double strand break repair: how to get the entry visa. *International Journal of Molecular Sciences* 13, 11844–11860.
- Goodarzi, A. a, and Jeggo, P. a (2013). The repair and signaling responses to DNA double-strand breaks. (Elsevier Inc.).

-
- Goodarzi, A. a, Noon, A.T., Deckbar, D., Ziv, Y., Shiloh, Y., Löbrich, M., and Jeggo, P. a (2008). ATM signaling facilitates repair of DNA double-strand breaks associated with heterochromatin. *Molecular Cell* 31, 167–177.
- Goodarzi, A. a, Jeggo, P., and Lobrich, M. (2010). The influence of heterochromatin on DNA double strand break repair: Getting the strong, silent type to relax. *DNA Repair* 9, 1273–1282.
- Görisch, S.M., Wachsmuth, M., Ittrich, C., Bacher, C.P., Rippe, K., and Lichter, P. (2004). Nuclear body movement is determined by chromatin accessibility and dynamics. *Proceedings of the National Academy of Sciences of the United States of America* 101, 13221–13226.
- Gu, J., Xia, X., Yan, P., Liu, H., Podust, V.N., Reynolds, A.B., and Fanning, E. (2004). Cell cycle-dependent regulation of a human DNA helicase that localizes in DNA damage foci. *Molecular Biology of the Cell* 15, 3320–3332.
- Guigas, G., Kalla, C., and Weiss, M. (2007). The degree of macromolecular crowding in the cytoplasm and nucleoplasm of mammalian cells is conserved. *FEBS Letters* 581, 5094–5098.
- Hagstrom, K. a, and Meyer, B.J. (2003). Condensin and cohesin: more than chromosome compactor and glue. *Nature Reviews. Genetics* 4, 520–534.
- Haince, J.-F., McDonald, D., Rodrigue, A., Déry, U., Masson, J.-Y., Hendzel, M.J., and Poirier, G.G. (2008). PARP1-dependent kinetics of recruitment of MRE11 and NBS1 proteins to multiple DNA damage sites. *The Journal of Biological Chemistry* 283, 1197–1208.
- Hall, E.J., and Giaccia, A.J. (2006). *Radiobiology for the Radiologist* (LIPPINCOTT WILLIAMS & WILKINS).
- Harborth, J., Wang, J., Gueth-Hallonet, C., Weber, K., and Osborn, M. (1999). Self assembly of NuMA: multiarm oligomers as structural units of a nuclear lattice. *The EMBO Journal* 18, 1689–1700.
- Haren, L., Gnadt, N., Wright, M., and Merdes, A. (2009). NuMA is required for proper spindle assembly and chromosome alignment in prometaphase. *BMC Research Notes* 2, 64.
- Heun, P., Laroche, T., Shimada, K., Furrer, P., and Gasser, S.M. (2001). Chromosome dynamics in the yeast interphase nucleus. *Science* 294, 2181–2186.
- Hickson, I., Zhao, Y., Richardson, C.J., Green, S.J., Martin, N.M.B., Orr, A.I., Reaper, P.M., Jackson, S.P., Curtin, N.J., and Smith, G.C.M. (2004). Identification and characterization of a novel and specific inhibitor of the ataxia-telangiectasia mutated kinase ATM. *Cancer Research* 64, 9152–9159.
- Hirayama, R., Ito, A., Tomita, M., Tsukada, T., Yatagai, F., Noguchi, M., Matsumoto, Y., Kase, Y., Ando, K., Okayasu, R., et al. (2009). Contributions of direct and indirect actions in cell killing by high-LET radiations. *Radiation Research* 171, 212–218.
- Hochegger, H., Dejsuphong, D., Fukushima, T., Morrison, C., Sonoda, E., Schreiber, V., Zhao, G.Y., Saberi, A., Masutani, M., Adachi, N., et al. (2006). Parp-1 protects homologous recombination from interference by Ku and Ligase IV in vertebrate cells. *The EMBO Journal* 25, 1305–1314.
- Hopfner, K.-P., Craig, L., Moncalian, G., Zinkel, R. a, Usui, T., Owen, B. a L., Karcher, A., Henderson, B., Bodmer, J.-L., McMurray, C.T., et al. (2002). The Rad50 zinc-hook is a structure joining Mre11 complexes in DNA recombination and repair. *Nature* 418, 562–566.

-
- Huletsky, A., De Murcia, G., Muller, S., Hengartner, M., Ménard, L., Lamarre, D., and Poirier, G.G. (1989). The effect of poly(ADP-ribosyl)ation on native and H1-depleted chromatin. A role of poly(ADP-ribosyl)ation on core nucleosome structure. *The Journal of Biological Chemistry* 264, 8878–8886.
- Ito, T., Levenstein, M.E., Fyodorov, D. V, Kutach, A.K., Kobayashi, R., and Kadonaga, J.T. (1999). ACF consists of two subunits, Acf1 and ISWI, that function cooperatively in the ATP-dependent catalysis of chromatin assembly. *Genes & Development* 13, 1529–1539.
- Jakob, B., Scholz, M., and Taucher-Scholz, G. (2003). Biological imaging of heavy charged-particle tracks. *Radiation Research* 159, 676–684.
- Jakob, B., Splinter, J., and Taucher-Scholz, G. (2009a). Positional stability of damaged chromatin domains along radiation tracks in mammalian cells. *Radiation Research* 171, 405–418.
- Jakob, B., Splinter, J., Durante, M., and Taucher-Scholz, G. (2009b). Live cell microscopy analysis of radiation-induced DNA double-strand break motion. *Proceedings of the National Academy of Sciences of the United States of America* 106, 3172–3177.
- Jakob, B., Splinter, J., Conrad, S., Voss, K.-O., Zink, D., Durante, M., Löbrich, M., and Taucher-Scholz, G. (2011). DNA double-strand breaks in heterochromatin elicit fast repair protein recruitment, histone H2AX phosphorylation and relocation to euchromatin. *Nucleic Acids Research* 39, 6489–6499.
- Jegou, T., Chung, I., Heuvelman, G., Wachsmuth, M., Görisch, S.M., Greulich-Bode, K.M., Boukamp, P., Lichter, P., and Rippe, K. (2009). Dynamics of telomeres and promyelocytic leukemia nuclear bodies in a telomerase-negative human cell line. *Molecular Biology of the Cell* 20, 2070–2082.
- Ježková, L., Falk, M., Falková, I., Davidková, M., Bačková, A., Stefančková, L., Vachelová, J., Michaelidesová, A., Lukášová, E., Boreyko, A., et al. (2014). Function of chromatin structure and dynamics in DNA damage, repair and misrepair: γ rays and protons in action. *Applied Radiation and Isotopes : Including Data, Instrumentation and Methods for Use in Agriculture, Industry and Medicine* 83 Pt B, 128–136.
- Jungmichel, S., Clapperton, J. a, Lloyd, J., Hari, F.J., Spycher, C., Pavic, L., Li, J., Haire, L.F., Bonalli, M., Larsen, D.H., et al. (2012). The molecular basis of ATM-dependent dimerization of the Mdc1 DNA damage checkpoint mediator. *Nucleic Acids Research* 40, 3913–3928.
- Kakarougkas, A., Ismail, A., Klement, K., Goodarzi, A. a, Conrad, S., Freire, R., Shibata, A., Lobrich, M., and Jeggo, P. a (2013). Opposing roles for 53BP1 during homologous recombination. *Nucleic Acids Research* 41, 9719–9731.
- Kase, Y., Kanai, T., Matsufuji, N., Furusawa, Y., Elsässer, T., and Scholz, M. (2008). Biophysical calculation of cell survival probabilities using amorphous track structure models for heavy-ion irradiation. *Physics in Medicine and Biology* 53, 37–59.
- Kiefer, J., and Kiefer, I. (2003). *Allgemeine Radiologie*. (Parey Verlag).
- Kim, M.Y., Mauro, S., Gévry, N., Lis, J.T., and Kraus, W.L. (2004). NAD⁺-dependent modulation of chromatin structure and transcription by nucleosome binding properties of PARP-1. *Cell* 119, 803–814.
- Kim, M.Y., Zhang, T., and Kraus, W.L. (2005). Poly(ADP-ribosyl)ation by PARP-1: “PAR-laying” NAD⁺ into a nuclear signal. *Genes & Development* 19, 1951–1967.

-
- Kraft, G. (GSI) (2008). Tumortherapie mit schweren Ionen (Verein zur Förderung der Tumortherapie mit schweren Ionen e.V.).
- Krawczyk, P.M., Borovski, T., Stap, J., Cijssouw, T., Ten Cate, R., Medema, J.P., Kanaar, R., Franken, N. a P., and Aten, J. a (2012). Chromatin mobility is increased at sites of DNA double-strand breaks. *Journal of Cell Science* 125, 2127–2133.
- Kruhlak, M.J., Celeste, A., Dellaire, G., Fernandez-Capetillo, O., Müller, W.G., McNally, J.G., Bazett-Jones, D.P., and Nussenzweig, A. (2006). Changes in chromatin structure and mobility in living cells at sites of DNA double-strand breaks. *The Journal of Cell Biology* 172, 823–834.
- Kubota, Y., Takanami, T., Higashitani, A., and Horiuchi, S. (2009). Localization of X-ray cross complementing gene 1 protein in the nuclear matrix is controlled by casein kinase II-dependent phosphorylation in response to oxidative damage. *DNA Repair* 8, 953–960.
- Lamarque, B.J., Orazio, N.I., and Weitzman, M.D. (2010). The MRN complex in double-strand break repair and telomere maintenance. *FEBS Letters* 584, 3682–3695.
- Lammens, K., Bemeleit, D.J., Möckel, C., Clausing, E., Schele, A., Hartung, S., Schiller, C.B., Lucas, M., Angermüller, C., Söding, J., et al. (2011). The Mre11:Rad50 structure shows an ATP-dependent molecular clamp in DNA double-strand break repair. *Cell* 145, 54–66.
- Lan, L., Ui, A., Nakajima, S., Hatakeyama, K., Hoshi, M., Watanabe, R., Janicki, S.M., Ogiwara, H., Kohno, T., Kanno, S.-I., et al. (2010). The ACF1 complex is required for DNA double-strand break repair in human cells. *Molecular Cell* 40, 976–987.
- De Lange, T. (2005). Shelterin: the protein complex that shapes and safeguards human telomeres. *Genes & Development* 19, 2100–2110.
- Lee, J.-H., Mand, M.R., Deshpande, R.A., Kinoshita, E., Yang, S.-H., Wyman, C., and Paull, T.T. (2013). Ataxia telangiectasia-mutated (ATM) kinase activity is regulated by ATP-driven conformational changes in the Mre11/Rad50/Nbs1 (MRN) complex. *The Journal of Biological Chemistry* 288, 12840–12851.
- Lever, E., and Sheer, D. (2010). The role of nuclear organization in cancer. *The Journal of Pathology* 220, 114–125.
- Liao, H., Winkfein, R.J., Mack, G., Rattner, J.B., and Yen, T.J. (1995). CENP-F is a protein of the nuclear matrix that assembles onto kinetochores at late G2 and is rapidly degraded after mitosis. *The Journal of Cell Biology* 130, 507–518.
- Lieber, M.R. (2010). The mechanism of double-strand DNA break repair by the nonhomologous DNA end-joining pathway. *Annual Review of Biochemistry* 79, 181–211.
- Linnemann, A.K., and Krawetz, S.A. (2009). Maintenance of a functional higher order chromatin structure: The role of the nuclear matrix in normal and disease states. *Gene Therapy & Molecular Biology* 13, 231–243.
- Lisby, M., Mortensen, U.H., and Rothstein, R. (2003). Colocalization of multiple DNA double-strand breaks at a single Rad52 repair centre. *Nature Cell Biology* 5, 572–577.

-
- Liu, B., Wang, J., Chan, K.M., Tjia, W.M., Deng, W., Guan, X., Huang, J., Li, K.M., Chau, P.Y., Chen, D.J., et al. (2005). Genomic instability in laminopathy-based premature aging. *Nature Medicine* *11*, 780–785.
- Lobachev, K., Vitriol, E., Stemple, J., Resnick, M.A., and Bloom, K. (2004a). Chromosome fragmentation after induction of a double-strand break is an active process prevented by the RMX repair complex. *Current Biology : CB* *14*, 2107–2112.
- Lobachev, K., Vitriol, E., Stemple, J., Resnick, M.A., and Bloom, K. (2004b). Chromosome fragmentation after induction of a double-strand break is an active process prevented by the RMX repair complex. *Current Biology* *14*, 2107–2112.
- Löbrich, M., Shibata, A., Beucher, A., Fisher, A., Ensminger, M., Goodarzi, A.A., Barton, O., and Jeggo, P.A. (2010). gammaH2AX foci analysis for monitoring DNA double-strand break repair: strengths, limitations and optimization. *Cell Cycle (Georgetown, Tex.)* *9*, 662–669.
- LOWRY, O.H., ROSEBROUGH, N.J., FARR, A.L., and RANDALL, R.J. (1951). Protein measurement with the Folin phenol reagent. *The Journal of Biological Chemistry* *193*, 265–275.
- Ludérus, M.E., Den Blaauwen, J.L., De Smit, O.J., Compton, D. a, and Van Driel, R. (1994). Binding of matrix attachment regions to lamin polymers involves single-stranded regions and the minor groove. *Molecular and Cellular Biology* *14*, 6297–6305.
- Luger, K., Mäder, A.W., Richmond, R.K., Sargent, D.F., and Richmond, T.J. (1997). Crystal structure of the nucleosome core particle at 2.8 Å resolution. *Nature* *389*, 251–260.
- Lukacs, G.L., Haggie, P., Seksek, O., Lechardeur, D., Freedman, N., and Verkman, A.S. (2000). Size-dependent DNA mobility in cytoplasm and nucleus. *The Journal of Biological Chemistry* *275*, 1625–1629.
- Lukas, C., Falck, J., Bartkova, J., Bartek, J., and Lukas, J. (2003). Distinct spatiotemporal dynamics of mammalian checkpoint regulators induced by DNA damage. *Nature Cell Biology* *5*, 255–260.
- Lukas, C., Melander, F., Stucki, M., Falck, J., Bekker-Jensen, S., Goldberg, M., Lerenthal, Y., Jackson, S.P., Bartek, J., and Lukas, J. (2004). Mdc1 couples DNA double-strand break recognition by Nbs1 with its H2AX-dependent chromatin retention. *The EMBO Journal* *23*, 2674–2683.
- Lukas, C., Savic, V., Bekker-Jensen, S., Doil, C., Neumann, B., Pedersen, R.S., Grøfte, M., Chan, K.L., Hickson, I.D., Bartek, J., et al. (2011a). 53BP1 nuclear bodies form around DNA lesions generated by mitotic transmission of chromosomes under replication stress. *Nature Cell Biology* *13*, 243–253.
- Lukas, J., Lukas, C., and Bartek, J. (2011b). More than just a focus: The chromatin response to DNA damage and its role in genome integrity maintenance. *Nature Cell Biology* *13*, 1161–1169.
- Mahen, R., Hattori, H., Lee, M., Sharma, P., Jeyasekharan, A.D., and Venkitaraman, A.R. (2013). A-type lamins maintain the positional stability of DNA damage repair foci in Mammalian nuclei. *PloS One* *8*, e61893.
- Mansour, W.Y., Rhein, T., and Dahm-Daphi, J. (2010). The alternative end-joining pathway for repair of DNA double-strand breaks requires PARP1 but is not dependent upon microhomologies. *Nucleic Acids Research* *38*, 6065–6077.

-
- Marshall, W.F., Straight, A., Marko, J.F., Swedlow, J., Dernburg, A., Belmont, A., Murray, a W., Agard, D. a, and Sedat, J.W. (1997). Interphase chromosomes undergo constrained diffusional motion in living cells. *Current Biology* 7, 930–939.
- Masutani, M., and Fujimori, H. (2013). Poly(ADP-ribosyl)ation in carcinogenesis. *Molecular Aspects of Medicine* 1–15.
- Matsuoka, S., Ballif, B.A., Smogorzewska, A., McDonald, E.R., Hurov, K.E., Luo, J., Bakalarski, C.E., Zhao, Z., Solimini, N., Lerenthal, Y., et al. (2007). ATM and ATR substrate analysis reveals extensive protein networks responsive to DNA damage. *Science* 316, 1160–1166.
- Meaburn, K.J., Misteli, T., and Soutoglou, E. (2007). Spatial genome organization in the formation of chromosomal translocations. *Seminars in Cancer Biology* 17, 80–90.
- Meijering, E., Dzyubachyk, O., and Smal, I. (2012). Methods for cell and particle tracking. *Methods in Enzymology* 504, 183–200.
- Meyer, B., Voss, K.-O., Tobias, F., Jakob, B., Durante, M., and Taucher-Scholz, G. (2013). Clustered DNA damage induces pan-nuclear H2AX phosphorylation mediated by ATM and DNA-PK. *Nucleic Acids Research* 41, 6109–6118.
- Mika, S., and Rost, B. (2005). NMPdb: Database of Nuclear Matrix Proteins. *Nucleic Acids Research* 33, D160–3.
- Miné-Hattab, J., and Rothstein, R. (2012). Increased chromosome mobility facilitates homology search during recombination. *Nature Cell Biology* 14, 510–517.
- Miné-Hattab, J., and Rothstein, R. (2013). DNA in motion during double-strand break repair. *Trends in Cell Biology* 23, 529–536.
- Misteli, T., and Soutoglou, E. (2009). The emerging role of nuclear architecture in DNA repair and genome maintenance. *Nature Reviews. Molecular Cell Biology* 10, 243–254.
- Moreno-Herrero, F., De Jager, M., Dekker, N.H., Kanaar, R., Wyman, C., and Dekker, C. (2005). Mesoscale conformational changes in the DNA-repair complex Rad50/Mre11/Nbs1 upon binding DNA. *Nature* 437, 440–443.
- Müller, I., Merk, B., Voss, K.-O., Aeverbeck, N., Jakob, B., Durante, M., and Taucher-Scholz, G. (2013). Species conserved DNA damage response at the inactive human X chromosome. *Mutation Research* 756, 30–36.
- Nagai, S., Dubrana, K., Tsai-Pflugfelder, M., Davidson, M.B., Roberts, T.M., Brown, G.W., Varela, E., Hediger, F., Gasser, S.M., and Krogan, N.J. (2008). Functional targeting of DNA damage to a nuclear pore-associated SUMO-dependent ubiquitin ligase. *Science (New York, N.Y.)* 322, 597–602.
- Neri, L.M., Raymond, Y., Giordano, A., Capitani, S., and Martelli, A.M. (1999). Lamin A is part of the internal nucleoskeleton of human erythroleukemia cells. *Journal of Cellular Physiology* 178, 284–295.
- Nickerson, J. a, Krockmalnic, G., Wan, K.M., and Penman, S. (1997). The nuclear matrix revealed by eluting chromatin from a cross-linked nucleus. *Proceedings of the National Academy of Sciences of the United States of America* 94, 4446–4450.

-
- Noon, A.T., and Goodarzi, A. a (2011). 53BP1-mediated DNA double strand break repair: insert bad pun here. *DNA Repair* 10, 1071–1076.
- Olins, a L., and Olins, D.E. (1974). Spheroid chromatin units (v bodies). *Science (New York, N.Y.)* 183, 330–332.
- Oza, P., Jaspersen, S.L., Miele, A., Dekker, J., and Peterson, C.L. (2009). Mechanisms that regulate localization of a DNA double-strand break to the nuclear periphery. *Genes & Development* 23, 912–927.
- Parada, L., and Misteli, T. (2002). Chromosome positioning in the interphase nucleus. *Trends in Cell Biology* 12, 425–432.
- Paull, T.T., and Gellert, M. (1998). The 3' to 5' exonuclease activity of Mre 11 facilitates repair of DNA double-strand breaks. *Molecular Cell* 1, 969–979.
- Paull, T.T., and Gellert, M. (1999). unwinding and endonuclease cleavage by the Mre11 / Rad50 complex. 1276–1288.
- Platani, M., Goldberg, I., Lamond, A.I., and Swedlow, J.R. (2002). Cajal body dynamics and association with chromatin are ATP-dependent. *Nature Cell Biology* 4, 502–508.
- Price, B.D., and D'Andrea, A.D. (2013). Chromatin remodeling at DNA double-strand breaks. *Cell* 152, 1344–1354.
- Radulescu, A.E., and Cleveland, D.W. (2010). NuMA after 30 years: the matrix revisited. *Trends in Cell Biology* 20, 214–222.
- Redwood, A.B., Perkins, S.M., Vanderwaal, R.P., Feng, Z., Biehl, K.J., Gonzalez-Suarez, I., Morgado-Palacin, L., Shi, W., Sage, J., Roti-Roti, J.L., et al. (2011). A dual role for A-type lamins in DNA double-strand break repair. *Cell Cycle (Georgetown, Tex.)* 10, 2549–2560.
- Reynolds, P., Anderson, J. a, Harper, J. V, Hill, M. a, Botchway, S.W., Parker, A.W., and O'Neill, P. (2012). The dynamics of Ku70/80 and DNA-PKcs at DSBs induced by ionizing radiation is dependent on the complexity of damage. *Nucleic Acids Research* 40, 10821–10831.
- Riballo, E., Kühne, M., Rief, N., Doherty, A., Smith, G.C.M., Recio, M.-J., Reis, C., Dahm, K., Fricke, A., Krempler, A., et al. (2004). A pathway of double-strand break rejoining dependent upon ATM, Artemis, and proteins locating to gamma-H2AX foci. *Molecular Cell* 16, 715–724.
- Rogakou, E.P., Boon, C., Redon, C., and Bonner, W.M. (1999). Megabase chromatin domains involved in DNA double-strand breaks in vivo. *The Journal of Cell Biology* 146, 905–916.
- Rothkamm, K., and Horn, S. (2009). gamma-H2AX as protein biomarker for radiation exposure. *Annali dell'Istituto Superiore Di Sanità* 45, 265–271.
- Rothkamm, K., and Löbrich, M. (2003). Evidence for a lack of DNA double-strand break repair in human cells exposed to very low x-ray doses. *Proceedings of the National Academy of Sciences of the United States of America* 100, 5057–5062.
- Roukos, V., Voss, T.C., Schmidt, C.K., Lee, S., Wangsa, D., and Misteli, T. (2013). Spatial dynamics of chromosome translocations in living cells. *Science* 341, 660–664.

-
- Rudra, S., and Skibbens, R. V (2013). Cohesin codes - interpreting chromatin architecture and the many facets of cohesin function. *Journal of Cell Science* 126, 31–41.
- Sánchez-Molina, S., Mortusewicz, O., Bieber, B., Auer, S., Eckey, M., Leonhardt, H., Friedl, A. a, and Becker, P.B. (2011). Role for hACF1 in the G2/M damage checkpoint. *Nucleic Acids Research* 39, 8445–8456.
- Sarkaria, J.N., Busby, E.C., Tibbetts, R.S., Roos, P., Taya, Y., Karnitz, L.M., and Abraham, R.T. (1999). Inhibition of ATM and ATR kinase activities by the radiosensitizing agent, caffeine. *Cancer Research* 59, 4375–4382.
- Schär, P., Fäsi, M., and Jessberger, R. (2004). SMC1 coordinates DNA double-strand break repair pathways. *Nucleic Acids Research* 32, 3921–3929.
- Schardt, D., Elsässer, T., and Schulz-Ertner, D. (2010). Heavy-ion tumor therapy: Physical and radiobiological benefits. *Reviews of Modern Physics* 82, 383–425.
- Scholz, M. (GSI) (2003). Effects of Ion Radiation on Cells and Tissues. In *Radiation Effects on Polymers for Biological Use*, (Advances in Polymer Science, Vol. 162), pp. 95–155.
- Schreiber, V., Dantzer, F., Ame, J.-C., and De Murcia, G. (2006). Poly(ADP-ribose): novel functions for an old molecule. *Nature Reviews. Molecular Cell Biology* 7, 517–528.
- Shi, L., and Oberdoerffer, P. (2012). Chromatin dynamics in DNA double-strand break repair. *Biochimica Et Biophysica Acta* 1819, 811–819.
- Shiloh, Y. (2003). ATM and related protein kinases: safeguarding genome integrity. *Nature Reviews. Cancer* 3, 155–168.
- Simon, D.N., and Wilson, K.L. (2011). The nucleoskeleton as a genome-associated dynamic “network of networks”. *Nature Reviews. Molecular Cell Biology* 12, 695–708.
- Singh, M., Hunt, C.R., Pandita, R.K., Kumar, R., Yang, C.-R., Horikoshi, N., Bachoo, R., Serag, S., Story, M.D., Shay, J.W., et al. (2013). Lamin A/C depletion enhances DNA damage-induced stalled replication fork arrest. *Molecular and Cellular Biology* 33, 1210–1222.
- Sjögren, C., and Ström, L. (2010). S-phase and DNA damage activated establishment of sister chromatid cohesion--importance for DNA repair. *Experimental Cell Research* 316, 1445–1453.
- Slade, D., Dunstan, M.S., Barkauskaite, E., Weston, R., Lafite, P., Dixon, N., Ahel, M., Leys, D., and Ahel, I. (2011). The structure and catalytic mechanism of a poly(ADP-ribose) glycohydrolase. *Nature* 477, 616–620.
- Smetana, K., Steele, W.J., and Busch, H. (1963). A nuclear ribonucleoprotein network. *Experimental Cell Research* 31, 198–201.
- Soutoglou, E., Dorn, J.F., Sengupta, K., Jasin, M., Nussenzweig, A., Ried, T., Danuser, G., and Misteli, T. (2007). Positional stability of single double-strand breaks in mammalian cells. *Nature Cell Biology* 9, 675–682.
- Stabin, M.G. (2007a). *Radiation protection and dosimetry* (Springer).

Stabin, M.G. (2007b). Radiation protection and dosimetry (Springer).

Stracker, T.H., Roig, I., Knobel, P. a, and Marjanović M. (2013). The ATM signaling network in development and disease. *Frontiers in Genetics* 4, 37.

Sulli, G., Di Micco, R., and d'Adda di Fagagna, F. (2012). Crosstalk between chromatin state and DNA damage response in cellular senescence and cancer. *Nature Reviews. Cancer* 12, 709–720.

Surova, O., and Zhivotovsky, B. (2013). Various modes of cell death induced by DNA damage. *Oncogene* 32, 3789–3797.

Thomas, C., and Tulin, A. V (2013). Poly-ADP-ribose polymerase: machinery for nuclear processes. *Molecular Aspects of Medicine* 34, 1124–1137.

Thompson, L.H. (2012). Recognition, signaling, and repair of DNA double-strand breaks produced by ionizing radiation in mammalian cells: the molecular choreography. *Mutation Research* 751, 158–246.

Tommasino, F., Friedrich, T., Scholz, U., Taucher-Scholz, G., Durante, M., and Scholz, M. (2013). A DNA double-strand break kinetic rejoining model based on the local effect model. *Radiation Research* 180, 524–538.

Vidi, P.-A., Chandramouly, G., Gray, M., Wang, L., Liu, E., Kim, J.J., Roukos, V., Bissell, M.J., Moghe, P. V, and Lelièvre, S. a (2012). Interconnected contribution of tissue morphogenesis and the nuclear protein NuMA to the DNA damage response. *Journal of Cell Science* 125, 350–361.

Walker, J.R., Corpina, R. a, and Goldberg, J. (2001). Structure of the Ku heterodimer bound to DNA and its implications for double-strand break repair. *Nature* 412, 607–614.

Ward, I.M., Minn, K., Van Deursen, J., and Chen, J. (2003). p53 Binding protein 53BP1 is required for DNA damage responses and tumor suppression in mice. *Molecular and Cellular Biology* 23, 2556–2563.

Williams, G.J., Lees-Miller, S.P., and Tainer, J. a (2010). Mre11-Rad50-Nbs1 conformations and the control of sensing, signaling, and effector responses at DNA double-strand breaks. *DNA Repair* 9, 1299–1306.

Williams, R.S., Moncalian, G., Williams, J.S., Yamada, Y., Limbo, O., Shin, D.S., Grocock, L.M., Cahill, D., Hitomi, C., Guenther, G., et al. (2008). Mre11 dimers coordinate DNA end bridging and nuclease processing in double-strand-break repair. *Cell* 135, 97–109.

Woodcock, C.L., and Ghosh, R.P. (2010). Chromatin higher-order structure and dynamics. *Cold Spring Harbor Perspectives in Biology* 2, a000596.

Worman, H.J., Ostlund, C., and Wang, Y. (2010). Diseases of the nuclear envelope. *Cold Spring Harbor Perspectives in Biology* 2, a000760.

Wu, N., and Yu, H. (2012). The Smc complexes in DNA damage response. *Cell & Bioscience* 2, 5.

Xu, Y., and Price, B.D. (2011). Chromatin dynamics and the repair of DNA double strand breaks. *Cell Cycle* 10, 261–267.

Yuan, J., and Chen, J. (2010). MRE11-RAD50-NBS1 complex dictates DNA repair independent of H2AX. *The Journal of Biological Chemistry* 285, 1097–1104.

Yun, M.H., and Hiom, K. (2009). CtIP-BRCA1 modulates the choice of DNA double-strand-break repair pathway throughout the cell cycle. *Nature* 459, 460–463.

Zha, S., Boboila, C., and Alt, F.W. (2009a). Mre11: roles in DNA repair beyond homologous recombination. *Nature Structural & Molecular Biology* 16, 798–800.

Zha, S., Boboila, C., and Alt, F.W. (2009b). Mre11: roles in DNA repair beyond homologous recombination. *Nature Structural & Molecular Biology* 16, 798–800.

Zimmermann, M., and De Lange, T. (2013). 53BP1: pro choice in DNA repair. *Trends in Cell Biology* 1–10.

Ziv, Y., Bielopolski, D., Galanty, Y., Lukas, C., Taya, Y., Schultz, D.C., Lukas, J., Bekker-Jensen, S., Bartek, J., and Shiloh, Y. (2006). Chromatin relaxation in response to DNA double-strand breaks is modulated by a novel ATM- and KAP-1 dependent pathway. *Nature Cell Biology* 8, 870–876.

Supplementary Figures

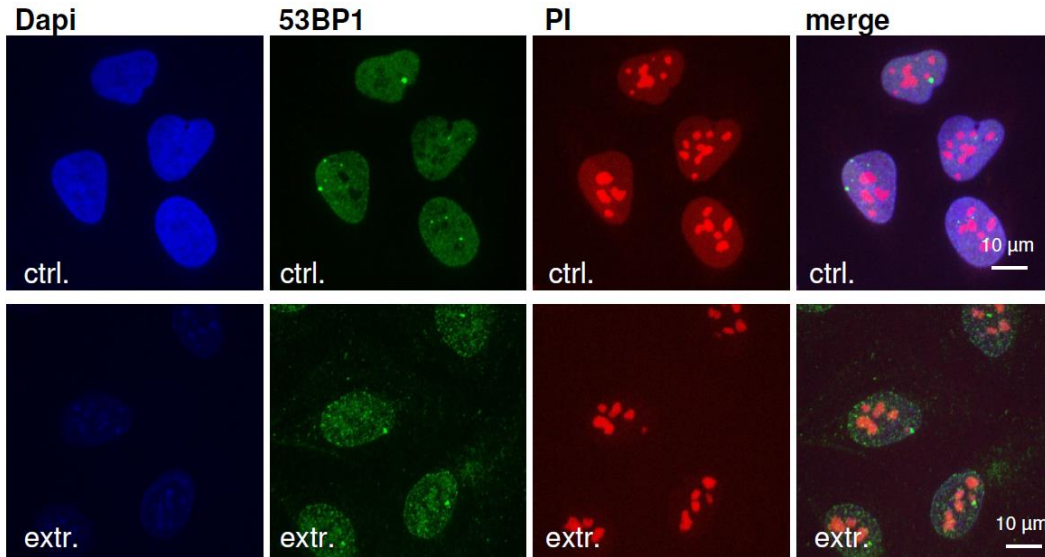


Figure S 1 – 53BP1 persists in nuclei after nuclear extraction

U2OS cells after nuclear extraction (extr.) and controls without DNase I digestion (ctrl.). Cells are fixed by PFA prior to DNase I digestion and extraction. Staining of DNA by Dapi (blue), 53BP1 (green), PI (red) reveals complete extraction and a retention of 53BP1 in the nucleus following extraction.

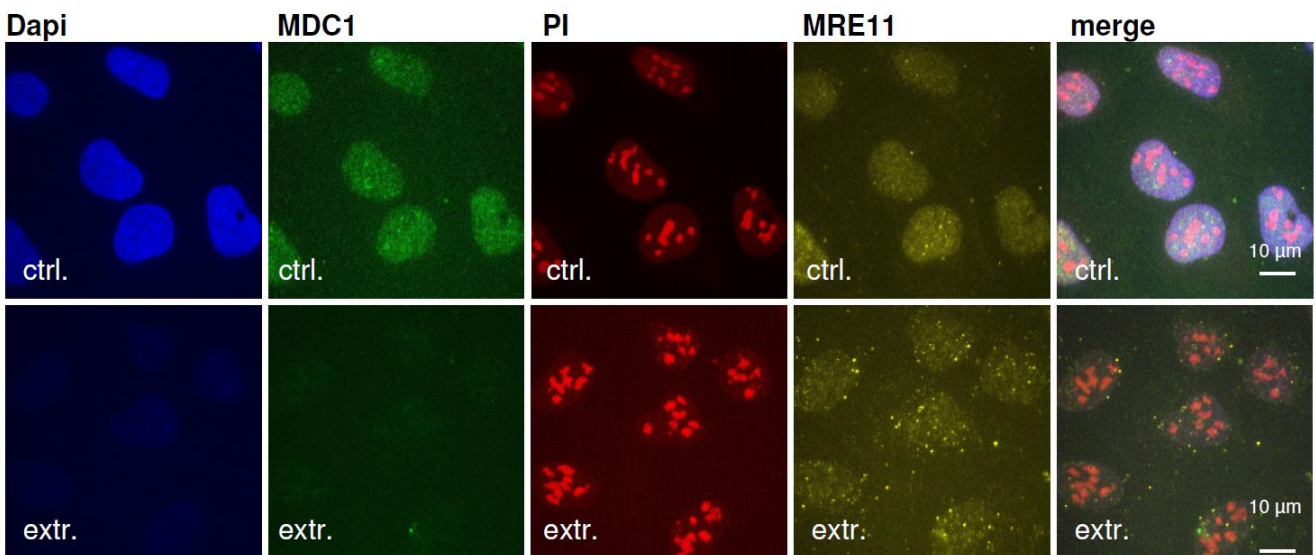


Figure S 2 – Nuclear extraction is protein specific

U2OS cells after nuclear extraction (extr.) and controls without DNase I digestion (ctrl.). Cells are fixed by PFA prior to extraction. Cells are stained for Dapi (blue), MDC1 (green), PI (red) and MRE11 (yellow). Complete extraction of MDC1 is seen while MRE11 foci and background signal remain following extraction.

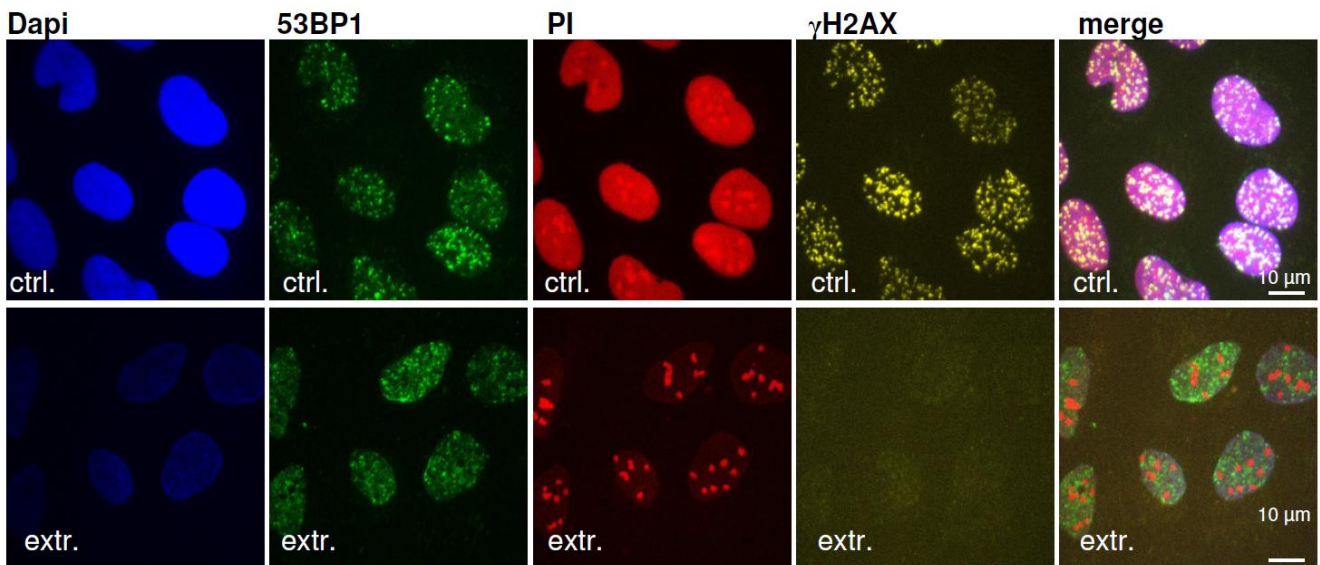


Figure S 3 – Nuclear extraction of U2OS cells shows incomplete removal of 53BP1

U2OS cells after nuclear extraction (extr.) and controls without DNase I digestion (ctrl.). Cells are stained for Dapi (blue), 53BP1 (green), PI (red) and γ H2AX (yellow). While extraction removes γ H2AX from the nucleus 53BP1 signal remains.

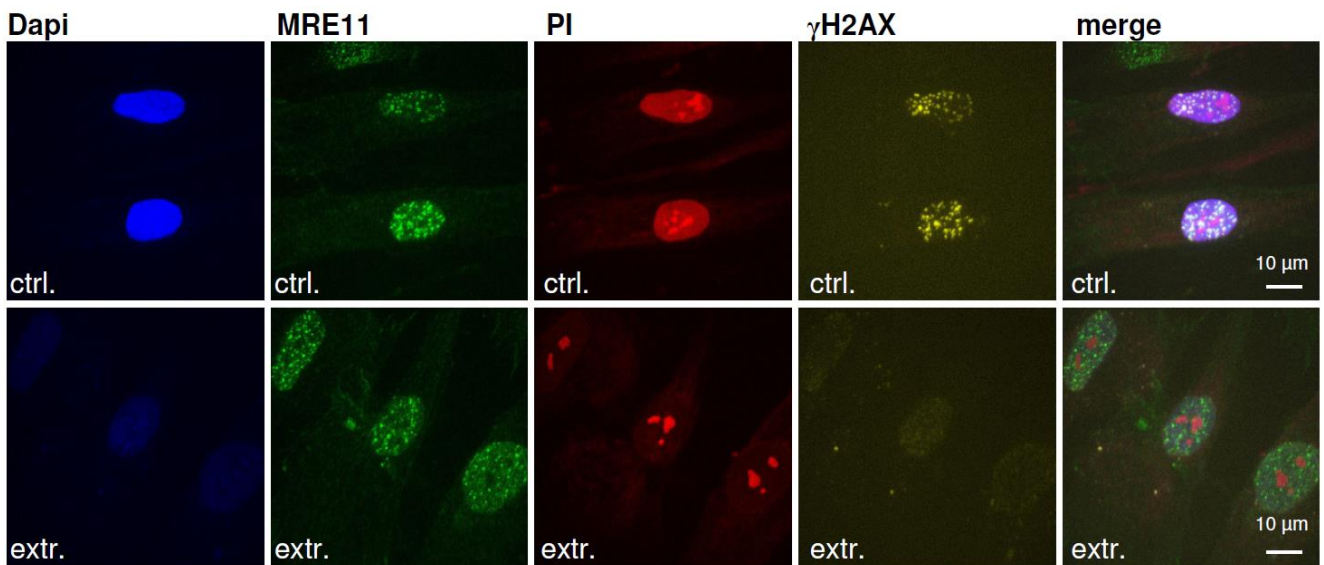


Figure S 4 – Nuclear extraction of AG cells after 2 Gy X-rays

AG cells irradiated with 2 Gy and extracted 20 min afterwards. By nuclear extraction (extr.) γ H2AX is removed from the nucleus while MRE11 remains in focal accumulations. Cells extracted and controls without DNase I digestion (ctrl.) are stained for Dapi (blue), MRE11 (green), PI (red) and γ H2AX (yellow).

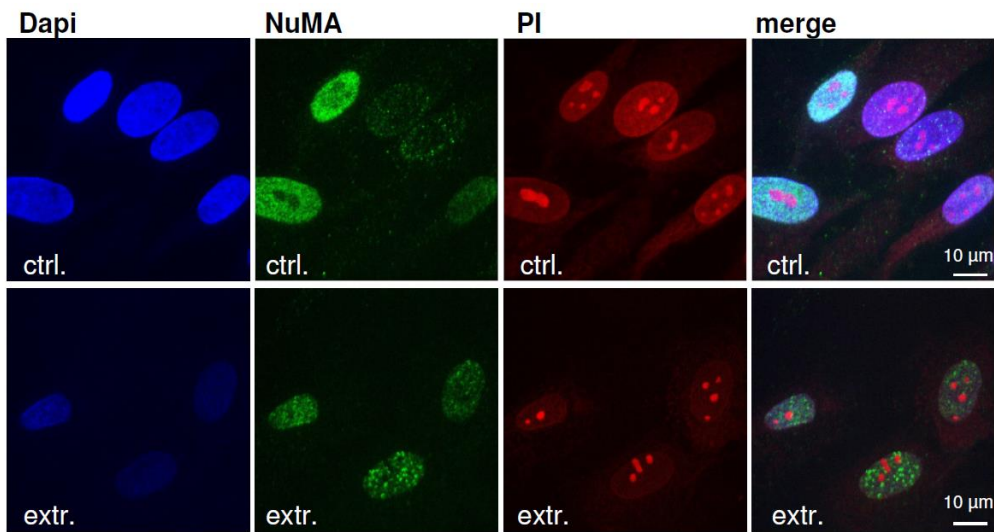


Figure S 5 – Distribution of NuMA in AG cells after nuclear extraction

AG cells after nuclear extraction (extr.) and controls without DNase I digestion (ctrl.). Cells are stained for Dapi (blue), NuMA (green) and PI (red). While NuMA shows cell specific distribution pattern in control cells most cells show a homogenous background of NuMA following nuclear extraction.

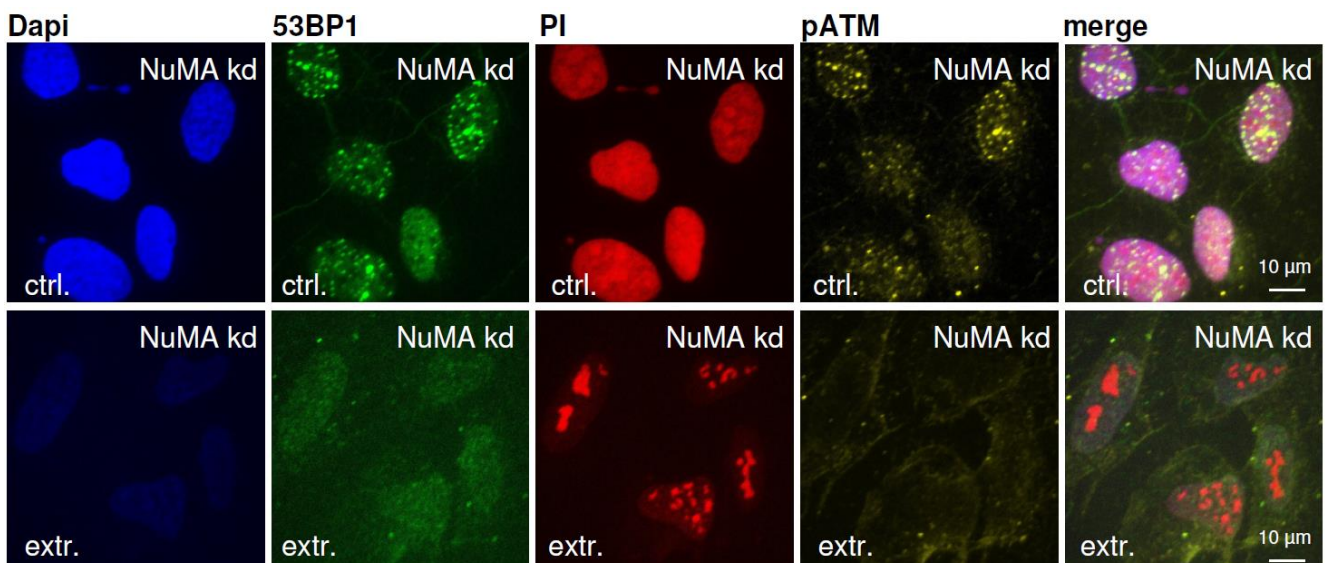


Figure S 6 – Nuclear extraction of U2OS cells knocked down of NuMA

U2OS cells knocked down of NuMA were irradiated with 2 Gy X-rays and incubated for 20 minutes. Nuclear extraction was applied (extr.) and controls treated without DNase I digestion (ctrl.). Cells are stained for Dapi (blue), 53BP1 (green), PI (red) and pATM (yellow). 53BP1 and pATM accumulate in foci at sites of DSBs in controls and signal is absent after extraction.

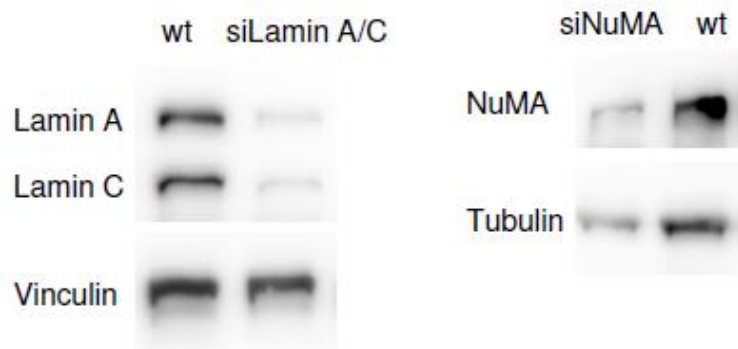


Figure S 7 – Western blot revealing knockdown efficiency of NuMA and Lamin A/C

Knockdown of U2OS cells treated with siRNA against NuMA or Lamin A/C for 48 hours. Analyses reveals 89 % knockdown efficiency for Lamin A/C and 87 % knockdown efficiency for NuMA (compared to wildtype).

List of Figures

Figure 1 – Physical interaction processes of photons with matter.	11
Figure 2 – Dose distribution of X-rays and carbon ions of different energies.....	12
Figure 3 – Depth dose profiles of particles and photon irradiation at different energies in water.	13
Figure 4 – Track structures of protons and carbon ions of different energies in water.	13
Figure 5 – Direct and indirect effects of ionizing radiation on DNA	14
Figure 6 – RBE measurement of carbon ions compared to X-rays	15
Figure 7 – NHEJ and HR, two mayor DNA repair pathways in mammals.....	18
Figure 8 – Functions of the MRN complex in DNA repair	21
Figure 9 – MRE11 and RAD50 acting as an ATP driven molecular clamp	21
Figure 10 – Chemical structure of a poly-ADP-ribose chain	22
Figure 11 – The Cohesin complex in maintaining sister chromatid cohesion.....	24
Figure 12 – Nuclear structure and components	25
Figure 13 – Positional stability and spreading of DSBs after charged particle irradiation	35
Figure 14 – Influence of Ku80 on chromatin mobility after charged particle irradiation	36
Figure 15 – Positional stability of irradiation induced repair proteins in human fibroblasts	37
Figure 16 – ATM deficiency does not induce a spreading of IRIF.....	37
Figure 17 – Schematic view of DNA tethering by the MRN complex.....	38
Figure 18 – Positional stability of repair proteins in RAD50 deficient cells	38
Figure 19 – Cell cycle distribution of U2OS-53BP1-GFP cells.....	39
Figure 20 – CENPF marked cell cycle phases of U2OS 53BP1-GFP cells.....	40
Figure 21 – Irradiation pattern in U2OS-53BP1-GFP cells	40
Figure 22 – Mobility measurement of 53BP1 IRIF in U2OS-cells.	42
Figure 23 – Comparison of two particle tracking programs.	42
Figure 24 – Tracking of DSB in fixed samples	42
Figure 25 – 53BP1 and NBS1 foci exhibit similar mobility characteristics.....	43
Figure 26 – Mobility of DSBs can be described by the model of confined diffusion or subdiffusion.....	45
Figure 27 – ATP depletion causes drastic reduction of foci mobility	47
Figure 28 – Knockdown of ACF1 does not change mobility of IRIF.....	48
Figure 29 – Functional essay of inhibition of PARP and knockdown of PARG after H ₂ O ₂ treatment	50
Figure 30 – Influence of poly-ADP-ribosylation on DSB mobility	51
Figure 31 – Caffeine confines mobility of IRIF.....	52
Figure 32 – ATM inhibition observed by immunofluorescent staining of U2OS-53BP1-GFP cells	52
Figure 33 – Influence of ATM on DSB mobility after charged particle irradiation	53

Figure 34 – Mobility of X-ray induced damage is reduced after inhibition of ATM.....	54
Figure 35 – Knockdown of MRE11 hampers recruitment of MRE11 to DSBs	55
Figure 36 – Tethering of DNA strands does not influence DSB mobility.....	56
Figure 37 – Knockdown of NIPBL does not increase the msd of radiation induced 53BP1 foci	57
Figure 38 – Simultaneous determination of cell cycle phase and DSB sites.....	58
Figure 39 – DSB mobility in U2OS G1/S-GFP NBS1-cherry cells.....	58
Figure 40 – Cell cycle specific determination of foci mobility	59
Figure 41 – Influence of nuclear matrix proteins on DSB mobility	60
Figure 42 – Nuclear extraction of U2OS cells	61
Figure 43 – Labeling of 53BP1 and pATM after nuclear extraction.	62
Figure 44 – Immunofluorescent labeling of repair proteins after nuclear extraction.	63
Figure 45 – NuMA signal is reduced after nuclear extraction of U2OS cells.....	64
Figure 46 – Distribution of NuMA in U2OS compared to AG cells.....	65
Figure 47 – Extraction of U2OS cells following knockdown of Lamin A/C.....	65
Figure 48 – Tethering of DNA strands by the MRN complex.....	74
Figure 49 – The sampled volume of IRIF is reduced after inhibition of ATM.....	78

List of Tables

Table 1 – used siRNAs for protein knockdown	28
Table 2 – UNILAC accelerated ions and corresponding energies and LET values.....	30
Table 3 – used primary antibodies	31
Table 4 – used secondary antibodies.	32

Danksagung

Ich möchte mich bei Herrn Prof. Dr. Marco Durante bedanken der es mir ermöglichte meine Doktorarbeit in der Abteilung Biophysik der GSI durchführen zu können und für die Unterstützung meiner Arbeit.

Herrn Prof. Dr. Gerhard Thiel danke ich für die Übernahme des zweiten Gutachtens und für viele hilfreiche Diskussionen und Anregungen während GRK Treffen die ich sehr zu schätzen weiß.

Bei meinem Betreuer Dr. Burkhard Jakob bedanke ich mich sehr herzlich für die Zusammenarbeit in den letzten 3 Jahren, für das interessante Thema, das ich bearbeiten durfte und für stetige Hilfsbereitschaft, Geduld, Unterstützung und Kreativität bei neuen Ideen. Ich habe es sehr genossen mit dir zu arbeiten!

Bei Frau Prof. Dr. Gisela Taucher-Scholz möchte ich mich ebenfalls für die Betreuung und Unterstützung bedanken sowie für die immer sehr gute Organisation von z.B. Strahlzeiten und hilfreichen Diskussionen im „Palaver“.

Bei meiner „DNA Gruppe“ mit wechselnden Mitgliedern möchte ich mich ganz herzlich für die tolle gemeinsame Arbeit bedanken und die gute Arbeitsatmosphäre. Vor allem danke ich Gudrun Becker und Anna Lena Leifke für die perfekte Organisation des Labors. Danke an alle für eure Hilfsbereitschaft, gute Zusammenarbeit und Spaß im Labor. Ich habe mich bei euch sehr wohl gefühlt.

Ein großes Dankeschön auch an meine „Physiker Gruppe“ und Büro Kollegen, die jeden Tag zu einer Freude gemacht haben und mir in den letzten 3 Jahren zu sehr guten Freunden wurden.

Für die technische Unterstützung bei der UNILAC- Bestrahlung möchte ich Rayees Khan, Wolfgang Becher, Günter Lenz und Michael Scholz danken, sowie vielen weiteren Mitgliedern der GSI Biophysik.

Für mein GRK Stipendium danke ich der TU-Darmstadt und DFG. Allen Mitgliedern des GRK 1657 danke ich für die konstruktiven Austausche in Seminaren und Kursen, vielen wichtigen Gesprächen und neuen Ideen und speziell Britta für die gemeinsame Organisation der GRK-Kurse.

Meiner Familie möchte ich für die jahrelange Unterstützung danken die es mir erst ermöglichte diese Doktorarbeit zu verfassen. Ihr wart immer für mich da und werdet es immer bleiben, wofür ich euch unendlich dankbar bin!

Danke auch an meinen Freund, der mein Leben während dieser Zeit bereichert hat und mir immer wieder neue Motivation und Energie gegeben hat!

Zudem danke ich auch allen Freunden, die ein wichtiger Teil meines Lebens sind und mich durch das Studium und die Promotion begleitet haben.

Lebenslauf

Persönliche Daten:

Name	Linda Carmen Annabelle Becker
Geburtsdatum	23.04.1986
Geburtsort	Darmstadt

Universitäre Ausbildung

2011 – 2014	Promotion an der Technischen Universität Darmstadt, durchgeführt am GSI Helmholzzentrum für Schwerionenforschung, Abteilung Biophysik Stipendium der DFG (GRK 1657)
2005 – 2010	Studium der Biologie an der Technischen Universität Darmstadt
2010	Diplomarbeit am MPI für Biophysik in Frankfurt, Abteilung Strukturbiologie Thema: Entwicklung eines lichtgesteuerten Kanalproteins und phänotypische Analyse der nativen Funktion von OmpG Abschluss Diplom Biologie
2007	Vordiplom Biologie

Schulische Ausbildung

1996 – 2005	Dreieich-Gymnasium Langen
2005	Abschluss Abitur
1992 – 1996	Grundschule Langen

Ehrenwörtliche Erklärung:

Ich erkläre hiermit ehrenwörtlich, dass ich die vorliegende Arbeit entsprechend den Regeln guter wissenschaftlicher Praxis selbstständig und ohne unzulässige Hilfe Dritter angefertigt habe.

Sämtliche aus fremden Quellen direkt oder indirekt übernommenen Gedanken sowie sämtliche von Anderen direkt oder indirekt übernommenen Daten, Techniken und Materialien sind als solche kenntlich gemacht. Die Arbeit wurde bisher bei keiner anderen Hochschule zu Prüfungszwecken eingereicht.

Darmstadt, 28.03.2014

.....

Linda Carmen Annabelle Becker

